UNIVERSITY OF CALIFORNIA, SAN DIEGO

Transcriptional Responses of Insulin Resistance and Mechanisms of Drug Action

A dissertation submitted in partial satisfaction of the
requirements for the degree of Doctor of Philosophy

in

Bioengineering

by

Gene Hsiao

Committee in charge:

Professor Shankar Subramaniam, Chair
Professor Dorothy D. Sears, Co-Chair
Professor Alexander Hoffmann
Professor Marcos Intaglietta
Professor Richard Lieber
Professor Gabriel A. Silva

2010

The Dissertation of Gene Hsiao is approved, and it is acceptable in quality and form for publication on microfilm and electronically:

_____

_____

_____

_____

_____
Co-Chair

_____
Chair

University of California, San Diego

2010

DEDICATION

to
my
parents
and
my
brother

EPIGRAPH

Not everything that can be counted counts,
and not everything that counts can be counted.

Albert Einstein

TABLE OF CONTENTS

LIST OF FIGURES

LIST OF TABLES

ACKNOWLEDGEMENTS

I would first like to acknowledge my advisor, Dr. Shankar Subramaniam, for his unequivocal support, his encouragement, and the opportunities which he has given me. I would also like to thank my co-advisor, Dr. Dorothy Sears, for her instrumental support, expertise, and patience as we engaged in research problems through marathon meetings. I would like to thank all members of my dissertation committee for their time and support.

I would also like to acknowledge Dr. Mark Kamps and the HHMI Med-into-Grad initiative for instilling in me new perspectives in clinical research. I also would like to thank Dr. Stephen Jenks and Dr. Gary Huber for originally inspiring me to join the field of research.

Chapter 2, in part, is currently being prepared for submission for publication of the material. Hsiao, Gene; Subramaniam, Shankar, "Variance estimation based on global modeling of gene expression array data increases sensitivity for detecting differentially expressed genes." The dissertation author was the primary investigator and sole first author of this paper.

Chapter 3, in full, is a reprint of the material as it appears in Proceedings of the National Academy of Sciences of the United States of America 2009. Sears, Dorothy D.; Hsiao, Gene; Hsiao, Albert; Yu, J.G.; Courtney, C.H.; Ofrecio, Jachelle M.; Chapman, Justin; Subramaniam, Shankar. "Mechanisms of human insulin resistance and thiazolidinedione-mediated insulin sensitization", Proc. Natl. Acad. Sci. USA 2009 Nov 3;106(44):18745-50. Epub 2009 Oct 19. The dissertation author was the second author on

this work, responsible for developing the statistical methodology, data analysis and curation, pathway and network analyses and manuscript preparation.

Chapter 4, in full, has been submitted for publication of the material as it may appear in American Journal of Physiology Endocrinology and Metabolism, 2010, Hsiao, Gene; Chapman, Justin; Ofrecio, Jachelle M.; Wilkes, Jason; Resnik, Jamie L.; Thapar, Divya; Subramaniam, Shankar; Sears, Dorothy D. "Multi-tissue, selective PPARγ modulation of insulin sensitivity and metabolic pathways in obese rats." The dissertation author was the sole first author on this paper.

VITA

2004 Bachelor of Science, University of California, Irvine

2006 Master of Science, University of California, San Diego

2010 Doctor of Philosophy, University of California, San Diego

PUBLICATIONS

G Hsiao, J Chapman, JM Ofrecio, J Wilkes, JL Resnik, D Thapar, S Subramaniam, DD Sears. Multi-tissue, selective PPARγ modulation of insulin sensitivity and metabolic pathways in obese rats. *Submitted.*

DD Sears, G Hsiao, A Hsiao, JG Yu, CH Courtney, JM Ofrecio, J Chapman, S Subramaniam. (2009) Mechanisms of human insulin resistance and thiazolidinedione-mediated insulin sensitization. Proc Natl Acad Sci U S A, vol. 106, no. 44, pp. 18745-18750.

S Sugii, P Olson, DD Sears, M Saberi, A Atkins, G Barish, S Hong, G Castro, Y Yin, M Nelson, G Hsiao, D Greaves, M Downes, R Yu, J Olefsky, R Evans. (2009) PPARγ activation in adipocytes is sufficient for systemic insulin sensitization. Proc Natl Acad Sci U S A, vol 106, no. 52, pp. 22504-22509.

CE Green, T Liu, V Montel, G Hsiao, RD Lester, S Subramaniam, SL Gonias, RL Klemke. (2009) Chemoattractant signaling between tumor cells and macrophages regulates cancer cell migration, Metastasis and Neovascularization. PLoS ONE, 4(8): e6713.

AE Hill-Baskin, MM Markiewski, DA Buchner, H Shao, D DeSantis, G Hsiao, S Subramaniam, NA Berger, C Croniger, JD Lambris, JH Nadeau. (2009) Diet-induced hepatocellular carcinoma in genetically predisposed mice. Hum Mol Genet, 18(16):2975-88.

BM Stack, G Hsiao, SF Jenks. (2005) A middleware architecture to facilitate distributed programming. Future Generation Computer Systems, vol. 22, no. 1-2, pp. 88-101.

FIELDS OF STUDY

Major Field: Bioengineering

Studies in Bioinformatics
Professor Shankar Subramaniam

Studies in Energy Minimization
Professor Gary A. Huber

Studies in Computer Engineering and High Performance Computing
Professor Stephen Jenks

ABSTRACT OF THE DISSERTATION

Transcriptional Responses of Insulin Resistance

and Mechanisms of Drug Action

by

Gene Hsiao

Doctor of Philosophy in Bioengineering

University of California, San Diego, 2010

Professor Shankar Subramaniam, Chair

Professor Dorothy D. Sears, Co-Chair

Insulin resistance is the defining feature of the metabolic syndrome and the primary defect leading to type 2 diabetes. Insulin resistance is a pathological state in

which the normal physiological function of insulin is impaired in target tissues including skeletal muscle, adipose tissue, and liver. Thiazolidinediones, synthetic ligands of the PPARγ nuclear receptor, are clinically potent insulin sensitizing drugs; however, not all individuals respond to treatment. Although PPARγ-mediated gene regulation is the predominant mode of thiazolidinedione-enhanced insulin sensitivity, the exact mechanisms by which PPARγ activation leads to insulin sensitization or by which insulin sensitization is prevented are poorly understood.

Addressing these expansive but fundamental questions concerning multi-tissue insulin resistance and PPARγ ligand-mediated insulin sensitization necessitates a comprehensive system-wide approach. The advent and maturation of the gene expression microarray allows for high-throughput transcript measurements. The massively parallel nature of microarrays, though, requires robust statistical analysis in order to obtain sensitive, accurate, and reliable results. With these tools, we characterize human subjects whom range in insulin sensitivity and relate their clinical phenotypes with functional pathway alterations. Multi-tissue gene expression profiles are further interrogated for distinctions between thiazolidinedione treatment responder and non-responder subjects. We further characterize the insulin sensitivity and multi-tissue gene expression profiles of lean and insulin resistant, obese Zucker rats treated with one of four PPARγ ligands, in order to identify functional pathways which are necessary for effective insulin sensitization.

A robust statistical approach is formulated, through which sensitivity analysis of leading microarray statistical testers on various controlled datasets demonstrates that a global variance modeling methodology is advantageous towards increased sensitivity for

the detection of true differential expression. With this devised approach, we identify pathway alterations in multiple tissues which are characteristic of insulin resistance, TZD-induced insulin sensitization, and potential TZD responsiveness. We also identify transcriptional biomarkers of insulin resistance and response signatures of PPARγ ligand treatment. These new insights suggest new targets for the therapy of type 2 diabetes, and measures to decrease risk for existing treatments.

I.

Introduction

A. Insulin resistance and PPARγ ligand treatment

Insulin resistance is a pathological state in which the normal physiological function of insulin is impaired in target tissues including liver, skeletal muscle, and adipose tissue. Although insulin resistance is associated with numerous conditions such as polycystic ovary syndrome (PCOS), Donohue syndrome, and various lipodystrophies, its most common association is with the metabolic syndrome and type 2 diabetes [1]. In fact, insulin resistance is the defining feature of the metabolic syndrome and the primary defect leading to type 2 diabetes [2, 3]. Incidence of diabetes is increasing in epidemic proportions worldwide. In the United States, nearly 8% of the population has diabetes with type 2 diabetes accounting for 90-95% of the cases. It is projected that 1 in 3 of Americans will develop the disease. In the U.S., diabetes continues to be the leading cause of blindness, non-traumatic amputation, end-stage renal disease, and the sixth leading cause of death [4].

Insulin resistance is classically characterized by impaired insulin-stimulated glucose uptake in skeletal muscle, impaired suppression of glucose production in liver, and impaired suppression of lipolysis in adipose tissue. Together, tissue-specific insulin resistances contribute to whole-body insulin resistance. The gold standard method to measure insulin resistance, specifically insulin-mediated glucose disposal, is the hyperinsulinemic-euglycemic clamp technique. This is performed by constant intravenous insulin infusion and *variable* intravenous glucose infusion in order to maintain constant plasma glucose. The average glucose infusion rate during the last stage

of the clamp is typically used as the summary measure of whole-body insulin resistance. This measure is representative of the nearly 90% of the insulin-induced glucose disposal that occurs in skeletal muscle. Insulin resistance in the liver can also be approximated by the clamp, but using a tracer technique which isolates the fraction of glucose production from liver gluconeogenesis. Furthermore, a proxy of insulin resistance in the adipose tissue can be approximated by insulin-induced suppression of plasma free fatty acids (FFA).

While nutritional therapy and exercise may alleviate metabolic abnormalities associated with type 2 diabetes, maintaining that regimen for many individuals is difficult and oftentimes simply insufficient. Various oral antidiabetic agents are available for the treatment of type 2 diabetes, including biguanides (e.g. metformin), sulfonylureas (e.g. glyburide), alpha-glucosidase inhibitors, dipeptidyl peptidase-4 inhibitors (DPP-4 inhibitors, e.g. sitagliptin), and thiazolidinediones (TZDs, e.g. rosiglitazone, pioglitazone). Each agent has different pharmacokinetics, potency, adverse effects, and mechanisms of action. Biguanides act by suppressing hepatic glucose production; sulfonylureas trigger pancreatic beta cell insulin secretion; alpha-glucosidase inhibitors prevent intestinal absorption of carbohydrates; DPP-4 inhibitors increase incretin levels thereby promoting insulin secretion; and TZDs reduce insulin resistance in various tissues. Although there is evidence that biguanides too increase sensitivity in skeletal muscle, TZDs are the prominent insulin sensitizing agents.

Thiazolidinediones are ligands of the nuclear receptor peroxisome proliferator-activated receptor gamma (PPARγ) through which they alter the expression of hundreds of genes in skeletal muscle, adipocytes, liver, and macrophages. Ordinarily, PPARγ,

tissue-specific endogenous ligands, and transcriptional regulators coordinately maintain whole body insulin sensitivity and normal metabolic homeostasis. Binding of various ligands induces ligand-specific 3-dimensional structures to PPARγ, which confer ligand-specific interactions of PPARγ to transcriptional regulators and DNA, thereby orchestrating ligand-specific transcriptional activity [5-8]. Although PPARγ-mediated gene regulation is the predominant mode of TZD-enhanced insulin sensitivity, the exact mechanisms by which PPARγ activation leads to insulin sensitization are poorly understood.

Thiazolidinediones are clinically potent insulin sensitizing drugs. The High A1C Study demonstrated that rosiglitazone improved type 2 diabetics HbA_{1c} levels by 3% with 40% of the patients reaching the glycemic control target HbA_{1c}<7% [9]. In the A Diabetes Outcome Progression Trial (ADOPT), rosiglitazone as a monotherapy resulted in significantly better long-term glycemic control and insulin-sensitization compared to metformin and glyburide [10, 11]. However, TZDs are associated with weight gain, edema, and increased risk for congestive heart failure. Furthermore, ~30% of diabetic subjects do not respond to TZD treatment [12, 13]. In order to develop new therapies or to decrease risk for existing drugs, it is necessary to clarify the pathophysiology of insulin resistance, isolate the fundamental mechanisms by which PPARγ activation leads to insulin sensitization, and define the mechanisms by which TZD-induced insulin sensitization is prevented.

B. Gene expression microarray technology and analysis

These expansive but fundamental questions concerning multi-tissue insulin resistance and PPARγ ligand-mediated insulin sensitization necessitate a comprehensive system-wide approach. Although high-throughput DNA and protein measurement technologies are developing, RNA microarray technology is preferred for various reasons. First, since gene expression is a tightly regulated process, the cellular responses to stimuli are represented dynamically in the mRNA. Second, large scale mRNA measurements are more feasible than protein, since proteins have complex 3-dimensional structure and readily denature. Third, microarray technology has matured greatly across the over 15 years since its inception [14-16]. The early substandard quality self-spotted arrays have developed into reproducible quality-controlled commercial platforms.

Generally, thousands to millions of oligonucleotide probes are placed on a solid surface. With the Affymetrix microarray technology, 25-mer nucleotide probes are synthesized on a silicon chip via photolithographic process. A set of probes constitute a probeset, which target a region along the mRNA sequence. In the Agilent Technologies process, 60-mer oligonucleotide probes are printed on glass slides, with each probe representing a single gene. In the Illumina process, 50-mer oligonucleotides are bound to bead arrays. Although the platforms differ in manufacturing process, probe length, and probe design, a recent study showed high intra-platform reproducibility and inter-platform concordance [17].

In addition to the manufacturing process, lab protocols have largely been optimized and standardized. After the biological experiment has been performed, samples are obtained and RNA isolated. In the Affymetrix lab process, RNA is checked for

quality, then reverse transcribed to cDNA. The more stable cDNA is then used as a template for an *in vitro* transcription reaction which produces amplified biotin-labeled cRNA. cRNA is fragmented and then hybridized to the chip. The chip is then imaged using a confocal microscope and commercial software is used to obtain intensity measurements for each probe.

Due to the many sources of variation and the massively parallel nature of microarray experiments, data preparation and statistical analysis are necessary to obtain accurate and reliable results. A countless number of preprocessing algorithms exist aimed to remove technical sources of variation; however, no one preprocessing method best fits all types of experiments. This is due to both the heterogeneity of experiments, and the assumptions that are made with each method. Statistical analysis is also crucial to ascertain reliable results with proper control over false positive rates. The fold change method was the first method adopted to determine differential expression. This method essentially determines differential expression by an absolute value of the ratio of means exceeding a value of two. This is now widely considered to be inadequate because it does not incorporate variance and therefore no control over error rates. Additionally, at low expression levels where the signal-to-noise ratio is also low, 2-fold changes can occur at random for many genes. At high levels of expression, smaller changes in gene expression may be real, but are rejected. Various statistical methods have since emerged, each incorporating some form of variance approximation for each gene. However, due to the low sample size nature of typical microarray experiments, variance estimation can be unstable therefore leading to inaccurate detection of differentially expressed genes. This is evidenced by the increasingly divergent results between statistical methods as sample

size decreases. Although there are numerous statistical testers, there is now limited consensus that methods which "borrow" information across genes towards the approximation of variance are preferred [18].

C. Organization of dissertation

In this introductory chapter we have described insulin resistance as the defining feature of type 2 diabetes and the implications of the disease worldwide. Manifestations of insulin resistance in multiple tissues are detailed along with methods to measure the degree of resistance in those tissues. Oral drug treatments for type 2 diabetes are overviewed; with emphasis on thiazolidinediones, as their mode of action is insulin sensitization of peripheral tissues. We then describe high throughput gene expression microarrays: the various but concordant commercial array platforms, the limited consensus on array data analysis, and the need for a defined analysis pipeline that is sensitive and robust.

In Chapter 2, we formulate a sensitive and robust statistical approach for the detection of differentially expressed genes in gene expression microarray experiments. We conduct sensitivity analysis of leading microarray statistical testers with receiver operating characteristic (ROC) curves on various controlled datasets where the true changes are known in advance. We determine that a global variance modeling approach towards a more stable estimation of individual gene variances increases detection sensitivity. With this defined approach, increased sensitivity is exhibited across the range of expression and fold-change levels. This sensitivity is consistent across the various controlled datasets, commercial platforms, and experimental designs tested.

In Chapter 3, we characterize 72 human subjects whom range in insulin sensitivity and relate their clinical phenotypes with functional pathway alterations. Multi-tissue gene expression profiles before and after hyperinsulinemic-euglycemic clamp studies, before and after TZD treatment, are interrogated for distinctions between TZD treatment responder and non-responder subjects. We identify pathway alterations in skeletal muscle and adipose tissue which are characteristic of insulin resistance, TZD-induced insulin sensitization, and potential TZD responsiveness. We also identify candidate genes in insulin resistant subjects which were linearly predictive of post-TZD insulin sensitization.

In Chapter 4, we further investigate functional pathways which are necessary and sufficient for effective insulin sensitization. We characterize the insulin sensitivity and multi-tissue gene expression profiles of lean and insulin resistant, obese Zucker rats untreated or treated with one of four PPARγ ligands (pioglitazone, rosiglitazone, troglitazone, and AG035029). Although all ligand treatments improved insulin sensitivity in obese rats, they did so to varying degrees. We analyze the transcriptional profiles of adipose tissue, skeletal muscle, and liver and determine whether ligand insulin-sensitizing potency was related to ligand-induced alteration of functional pathways. We determine that treatment potency correlated with the modulation of adipose tissue inflammatory and branched chain amino acid (BCAA) metabolic pathways, suggesting a functional relationship between these pathways and whole-body insulin sensitivity. Other ligand-induced pathway changes were detected in adipose tissue, skeletal muscle and liver profiles but were not related to degree of insulin sensitization, suggesting pathways which may be necessary but not sufficient for effective insulin-sensitization.

In Chapter 5, we conclude with a review of our devised statistical methodology towards the analysis of gene expression microarray data. We then summarize our findings from our systematic mechanistic analysis approach to insulin resistance and PPARγ ligand-mediated insulin sensitization. Finally, we discuss future directions in gene expression analysis, treatments for insulin resistance, and implications of emerging high throughput biological technologies.

II.

Variance estimation based on global modeling of gene expression array data increases sensitivity for detecting differentially expressed genes

A. Abstract

Background: Low sample size remains a characteristic feature of microarray experiments. The low sample size leads to unstable estimates of gene variances, leading to inaccurate detection of differentially expressed genes. Statistical methods which "borrow" information from genes across the array have been shown to generally perform better than standard statistical tests. However, as sample size decreases, results from these methods nonetheless increasingly diverge. This discordance is mainly attributed to differing approaches towards estimating gene level variance. We perform a comprehensive sensitivity analysis of statistical methodologies which differ in variance estimation in the context of a multitude of controlled datasets, arrayed on various array platforms (Affymetrix, Illumina, Agilent), and representing various experimental designs (two-class unpaired, two-class paired, multi-class). *Results:* Although methods based on a moderated t-statistic (i.e. CyberT, Limma, SAM), and a method based on global variance modeling (i.e. VAMPIRE), performed better than standard statistical tests, VAMPIRE's global variance modeling approach was consistently more sensitive than other methods while maintaining control over false positive rates. Increased sensitivity was especially observed at the low fold-change and low expression regions. Sensitivity gains were consistent across various controlled datasets, commercial array types, and experimental designs. *Conclusion:* For microarray experiments with low sample size, stable gene level

variance estimation through a global variance modeling approach results in improved sensitivity towards the detection of differentially expressed genes.

B. Background

Despite the decreasing cost of gene expression microarray platforms as a consequence of wide adoption and maturation, low sample size remains a characteristic feature of microarray experiments. This is mainly due to other costs of conducting the experiment, such as minimal availability of sample RNA. The low sample size leads to unstable estimates of gene variances, therefore leading to inaccurate detection of differentially expressed genes. This is evidenced by the increasingly divergent results between statistical methods as sample size decreases. For the t-test, the low sample size is especially debilitating as it leads to a low powered test statistic.

In order to offset the typically poor estimation of variance and to increase statistical power, investigators have developed methods which "borrow" information from genes across the array. This strategy is largely agreed upon [18], and has been implemented into many software packages by many groups, including but not limited to the following: SAM (significance analysis of microarrays) [19], CyberT [20], Limma (linear models for microarray data) [21], and VAMPIRE (variance-modeled posterior inference with regional exponentials) [22]. SAM augments standard deviation estimates with an estimated positive constant, such that variances closer to zero are proportionately penalized. CyberT uses a posterior variance estimate which combines sample variance and a background pooling of variances from neighboring genes contained in a window size defined by the user. Another hyper-parameter is defined which weights the strength

of the variance determined from the neighborhood. Limma instead uses a posterior variance which represents a weighted combination of sample variance and a more stable grand variance estimate that is approximated from all data on the array [23]. VAMPIRE uses variance estimates derived from a global model of the intrinsic variance structure of microarray data [24, 25], as previously reported and modeled by several groups [26-28].

Although these methods all borrow information from other genes on the array in order to improve variance estimation, they differ in theory and implementation and therefore may differ in performance for the detection of differentially expressed genes. A number of studies have conducted performance evaluations of significance testers using real experimental datasets, but this approach is limited since the true positives are not known in advance. Other studies use simulated data, but this too is limited since it is unclear if they accurately reflect the signal and noise behavior of real microarray experiments. In a different approach, Choe *et al* [29] introduced an innovative "Golden spike" dataset in which ~1300 cRNAs were spiked in at known differing concentrations between two groups of triplicates. Since this set includes not only a large number of true changes which are known in advance, but also features which span low fold concentration differences, detection sensitivity across fold-change levels can be evaluated among the significance testers. Detecting low fold changes is especially important since microarrays characteristically underestimate fold-change levels compared to other quantitative means (e.g. RT-PCR) [29]. Additionally, even small changes in gene expression can have large phenotypic consequences. Although there is criticism regarding the use of the Golden spike dataset, it still remains an important benchmarking tool for the characterization of microarray analysis methods [30]. Complimentary to the

Golden spike study are mixed-sample controlled datasets, whereby mixtures of tissue types [31] or references samples [17] are assayed with various commercial microarray platforms. These designs allow for defined target ratios of transcript measurements and therefore can be utilized for performance evaluations at variable fold-change levels across various commercial array types.

Performance can be evaluated on several levels: rank ordering of differentially expressed genes, proportion of true positives for a fixed number of false positives, and proportion of true positives for a given significance threshold. Receiver operating characteristic (ROC) curves plot true positive rate (TPR) against false positive rate (FPR), representing sensitivity and 1-specificity, respectively. Perfect performance is represented by a singular point at the top left of the plot, whereas performance that is no better than chance is represented by a line fitted to the diagonal. While these plots are useful in performance comparisons regarding to the rank ordering of differentially expressed genes, they neglect the influence of p-value assignment and realistic significance cutoffs. In controlled datasets the false positives are known in advance; however, in real experiments the false positives are not known and therefore FPR must be approximated by significance cutoffs such as false discovery rate (FDR) or Bonferroni thresholds. Choe *et al* have thus used a slight modification of the ROC curve such that false discovery rate (FDR) is used in place of FPR. In addition, although ROC curves which span the full range of data are informative, the region that is of most interest is that which precedes a false positive toleration level, such as 5% or 10%. ROC curves can be summarized into a scalar measure by calculating the area under the ROC curve (AUC). The AUC in this context represents the probability that the statistical tester will rank a

true positive instance higher than a randomly chosen negative instance. All these metrics allow for performance comparisons of microarray methods in regards to sensitivity for the detection of differentially expressed genes with control over error rates.

Here we present an assessment of sensitivity with proper error control for the detection of differentially expressed genes with leading microarray significance testers. These testers differ in variance estimation, which range from penalized variance (SAM), moderated variance (Limma), local variance pooling (CyberT), and global variance modeling (VAMPIRE) approaches. Sensitivity is assessed across the spectrum of expression level and fold-change with specific focus at the low expression, low fold, and higher sample variance regions. Sensitivity analysis is conducted on various controlled datasets, array platforms, and experimental designs.

C. Results

The global variance modeling approach leads to increased sensitivity to detect true changes in gene expression while maintaining proper false positive error control

Plotting Choe *et al*'s "Golden spike" dataset [29] as a function of log-transformed fold-change and normalized sample variance (Figure 1) shows that features represented on the microarray (all points) are present across all levels of variance. Since the cRNA spikes are known in advance, the true positives are also known (non-gray points). These spikes are also distributed across the range of sample variance. The spikes at the high fold-change and low variance region are easy to detect, even by the Student's T-test after Bonferroni multiple comparisons correction (α_{Bonf}=0.5) (blue points). The spikes at higher variances, however, are more difficult to detect since estimated noise level

oftentimes outweighs signal. VAMPIRE, a Bayesian statistic which models the global variance structure to acquire more stable variance estimates, is able to detect not only the spikes found by the t-test but significantly more spikes which are present at higher sample variances (red points, and points outlined in red). The t-test's ability to detect only 2% of the spikes is largely due to its lack of power for small sample sizes. When compared to CyberT (Figure 1, green points), a Bayesian regularized t-statistic whose variance estimates are combined with variances from neighboring genes, VAMPIRE still detects these spikes plus significantly more (39.5% detected by CyberT, 52.4% detected by VAMPIRE at α_{Bonf}=0.5). However, at this threshold the 13% gain in sensitivity by VAMPIRE over CyberT is at the expense of specificity, in which VAMPIRE finds 2.5% more false positives.

To better characterize sensitivity as a function of specificity for each of the statistical testers', ROC curves are computed (Figure 2a). ROC curves are generated by plotting true positive rate (TPR, representing sensitivity) versus false positive rate (FPR, representing 1-specificity). Perfect sensitivity and specificity is represented by a point at (0, 1), while random chance would result in a diagonal line from the origin to (1, 1) (Figure 2a, dashed line). Figure 2a displays ROC curves generated from the t-test (blue), SAM (orange), CyberT (green), Limma (purple), and VAMPIRE (red) statistical testers on "Choe-preferred" preprocessed Golden spike data. The curves, which are truncated to an FPR=0.1, demonstrate that CyberT and VAMPIRE perform similarly well and both methods exceeding the performance of Limma, SAM, and the t-test. VAMPIRE detects 65.3%, while CyberT detects 63.9% of the spikes before reaching an FPR=0.1 (Table 1).

From the ROC curves, Area Under the ROC curve (AUC) summary scores are computed by trapezoidal approximation across the full false positive rate range (FPR=1) as well as a partial range (pAUC, FPR=0.1). Perfect performance is represented when AUC and pAUC is equal to one. Performance by random chance alone for the full range is represented as AUC=0.5. For the partial range, performance by random chance is pAUC=0.1, since this is the length of the range evaluated. Table 1 lists AUCs for the various statistical testers with VAMPIRE showing the greatest score at 0.858. Among the partial AUCs, VAMPIRE and CyberT consistently outperform the other evaluated statistical testers (Table 1 and in graphical form, Figure 1b). SAM has little improvement over the t-test, adding only 0.012 AUC points. Since false positive rates are not known in real experiments, they are approximated by significance thresholds based on p-values. Using a Benjamini-Hochberg [32] implementation of false discovery rate (FDR) at the 10% threshold level, the difference in sensitivity is slight between VAMPIRE and CyberT. However, FDR is widely considered to be a lenient multiple comparison correction procedure compared to the Bonferroni family wise error correction method. At the more conservative Bonferroni threshold, the differences in sensitivity are much more apparent as the difference in pAUC goes from 0.055 to 0.142. For Limma and the t-test, the Bonferroni correction affects statistical power to the extent at which pAUCs are no better than random chance. SAM's performance for these metrics is unavailable since p-values are not easily attained in the software used.

VAMPIRE demonstrates increased sensitivity at low-fold and low-intensity regions

Since relative concentrations of each of the cRNAs in the Golden spike experiment are known, detection sensitivity at these specific fold-changes can be determined with respect to FPR, FDR, and Bonferroni thresholds. The defined target ratios span 1.2- , 1.5- , 1.7- , 2- , 2.5- , 3- , 3.5- , and 4-fold changes. Similar to the analysis done in Choe *et al*. [29] and Murie *et al*. [33], ROC curves are generated as a function of fold-change for different statistical testers. With respect to FDR, VAMPIRE can detect more than 90% of spikes whose fold-change is greater or equal to 2 (Figure 3). For spikes whose fold-change is less than 2, detection ranges between 74% for 1.7-fold and 18% for 1.5-fold features, but still consistently more sensitive than other testers. Partial AUCs for VAMPIRE as a function of fold with respect to FDR are listed in Figure 4, alongside other microarray statistical methods. CyberT, Limma, and the t-test, in that succession, have decreased sensitivity for nearly all folds, especially when compared to VAMPIRE. Furthermore, CyberT, Limma, and the T-test perform worse than random chance for 1.5- and 1.2-fold detection. While all methods suffer loss in sensitivity for features below 2-fold, as observed by Choe *et al*., VAMPIRE forestalls the sharp drop until 1.5-fold and still performs better across all fold-change levels. Increased sensitivity at the low-fold region is important since even small changes in gene expression can have significant biological consequences.

Accurate detection is difficult not only for low-fold fold features, but also for features with low levels of expression. At low levels of expression, expression-independent background variance dominates and leads to unstable variance estimates. In Figure 5, log-transformed baseline expression is plotted against fold-change. Spiked features (non-gray dots) are present across the range of expression. Spikes at high levels

of expression and high fold changes are generally easier to detect, as was accomplished by the Student's T-test (blue-filled dots) after Bonferroni correction (Figure 5) (α_{Bonf} = 0.1). CyberT detects all spikes that were found by the t-test plus significantly more spikes which are dispersed at lower expression levels (green-filled dots). At the same significance threshold, VAMPIRE further improves sensitivity at low expression levels (red filled and red outlined dots).

In order to assess performance at the low-fold and low-intensity region while controlling for false positive rates, spikes which are restricted to two-fold or less and are expressed at the lowest intensity levels are counted. Proportions of detected spikes at the various significance thresholds at the 10% level are listed in Table 2. In the lowest bin of expression, VAMPIRE and CyberT perform equally well at the false discovery rate threshold, both detecting more than 60% of the low-fold spikes. For the more stringent Bonferroni threshold though, VAMPIRE is clearly more sensitive than the other significance testers, gaining more than 20% in sensitivity. When comparing the ranked list of genes, VAMPIRE still finds more low-fold, low-expressed true positives before reaching a false positive rate of 10%. Increased sensitivity in this characteristically noisy region is important because even small changes among low expressors can have significant biological consequences.

Variance modeling improves sensitivity across various datasets, commercial array types, and experimental designs

Thompson *et al.*, [31] developed a Mixed Tissue RNA Reference Material (MTRRM) dataset which has shown its use in performance analysis of microarray

methods [34, 35]. This set serves complimentary to the Golden spike dataset as the latter has been argued to not accurately represent typical microarray experiments, as the arrays are not hybridized to a complex background and the spikes are uni-directional. The MTRRM is not characterized by these issues as rat tissue mixtures were hybridized to the arrays. The MTRRM constitutes two samples with known differing mixtures of RNA from rat four tissue types: testis, brain, liver, and kidney. Therefore, four target ratios of 4-, 2-, 1.5, and 1-fold features are defined in which true positives are considered to be the subset of transcripts predominately expressed in one of the four tissues [31]. In a log-transformed fold-change versus normalized sample variance plot (Figure 6a), the true positives (non-gray dots) are also distributed across all levels of variance as seen in the Golden spike dataset. Detection by the t-test is limited to higher fold-changes and lower variance features (blue-filled dots), whereas VAMPIRE detects these plus more (red dots) (α_{Bonf}=0.1). The additional features detected by VAMPIRE are distributed across lower fold changes and higher variance regions. VAMPIRE's increased sensitivity at higher variance regions allows it to detect three highlighted genes: fibrinogen beta chain (**Fgb**), serine peptidase inhibitor clade A member 3K (**Serpina3k**), and inter-alpha trypsin inhibitor heavy chain 3 (**Itih3**). Although characterized by higher variance, these biologically important genes are detected by VAMPIRE and are left undetected by the t-test. Sensitivity for each tester was quantified by AUCs and percent detection at various thresholds, as shown in Figure 6b. At all thresholds, VAMPIRE leads in sensitivity. At the Bonferroni threshold of 10%, VAMPIRE is 32% more likely than CyberT to detect a true positive as represented by respective AUCs. Separating sensitivity by specific fold-

changes reveals that VAMPIRE is the only statistical method to detect 1.5-fold genes, and is nearly 45% more likely to detect 2-fold genes compared to CyberT (Table 3).

In addition to the MTRRM dataset, the four titration pools dataset produced by the MicroArray Quality Control (MAQC) consortium [17] are used for performance evaluation. Four pools of RNA were created from two universal reference samples: Stratagene's Universal Human Reference RNA, which was derived from ten human cell lines, and Ambion's Human Brain Reference RNA, which represents a mixture of human brain tissue from several brain regions from multiple donors. The four pools were assayed on multiple arraytypes, including Affymetrix, Illumina, Agilent, and Applied Biosystems TaqMan arrays. As defined in [35], "true positives" were considered to be the selectively expressed genes in each of the two reference samples determined from Applied Biosystems TaqMan alternative arrays. AUCs for each statistical tester were generated from the Affymetrix (Figure 7a) and Illumina (Figure 7a) arrayed datasets. VAMPIRE consistently detects more true positives -- between 5-9% more than the next leading tester -- before reaching a false positive rate of 10%. This result demonstrates that the sensitivity gain by VAMPIRE is not only consistent among various datasets, but also for various array types.

Two-channel arrays necessitate a different statistical approach which accounts for dye bias. The MAQC samples were hybridized to Agilent's two-channel arrays and these were used to compare an assortment of paired analysis methods. AUCs were generated for the following statistical testers: paired t-test, paired SAM, Limma with dye as a factor, paired CyberT, and paired VAMPIRE (Figure 7c). VAMPIRE in the paired experimental design again emerges as the leader in sensitivity before reaching a false

positive rate of 10%, detecting 66% of the true positives. The next leading statistical method, paired CyberT, found only 32% of the true positives. Although this dataset shows VAMPIRE's sensitivity gain to be more than 30%, in the MTRRM dataset assayed on Agilent arrays, VAMPIRE's sensitivity gain is near 7% (data not shown).

Various statistical methods in the multi-class experimental design setting were also evaluated using MAQC's four titration pools. Four methods designed for microarrays, VAMPIRE, CyberT, Limma, and SAM, are compared together with three other standard multi-class statistical tests including the canonical ANOVA F-test, Levene's test, and Brown-Forsythe test. AUCs were computed for each method and displayed in Figure 7d. The traditional multi-class statistical methods, F-test, Levene's test, and Brown-Forsythe test, all rank last in sensitivity. The weak performances of these tests are attributed to the poor estimation of within-group variability for low sample size. The Levene's and Brown-Forsythe tests' also suffer from lack of power as they both require fewer assumptions, namely not requiring normality of the data. In contrast, CyberT and VAMPIRE, which have improved variance estimation by borrowing information across genes, perform markedly well. CyberT detects 55% of the true positives, while VAMPIRE detects 63% before reaching a false positive rate of 10%.

D. Discussion

Low sample size remains a characteristic feature of microarray experiments and this leads to unstable estimates of gene level variance. The unstable variance estimates ultimately result in inaccurate detection of differentially expressed genes, low statistical power, and particularly low sensitivity for small fold changes. Although "borrowing"

information from genes across the array generally improves detection of differentially expressed genes [18], the microarray methods which exercise this paradigm differ in variance estimation methodology and thus differ in performance. Comparisons among microarray methods have been extensively performed [29, 33], but none have evaluated a global variance modeling approach with reference to other methods on various controlled datasets, commercial platforms, and experimental designs. In this study, we demonstrate that the global variance modeling approach, as implemented in VAMPIRE [22], improves sensitivity towards the detection of differentially expressed genes with proper control over false positive rates. We demonstrate this through detailed sensitivity analysis of assorted statistical methods applied to a multitude of spike-in and mixed-tissue controlled datasets which represent various commercial array platforms and experimental designs.

Our results show that VAMPIRE, with CyberT not far behind, consistently outperform other statistical testers across the evaluated controlled datasets, commercial platforms, and experimental designs. Despite the diverse testing scenarios, the global variance modeling approach and CyberT's local pooling of variances consistently estimate gene level variance with greater stability. Oppositely, the standard statistical testers, including the Student's t-test and ANOVA, perform poorly due to their lack of power and inaccurate estimation of variability. VAMPIRE's increased sensitivity is more differentiable at realistic cutoffs. Since false positive rates are not known beforehand in real microarray experiments, cutoffs such as false discovery rate and the Bonferroni threshold are used to approximate these rates. For Limma and the t-test, the Bonferroni threshold dramatically decreases statistical power.

All statistical testers suffer at low fold-change detection, but VAMPIRE forestalls the steep drop in sensitivity for low fold-change genes. In fact, the variance modeling approach detects 1.5-fold genes while the other statistical approaches could not, as evidenced in the MTRRM dataset. Furthermore, when low intensity levels are taken into account, VAMPIRE detects more low fold-change spikes. The increased sensitivity at the low end is owed to the more stable estimates of variance, where variance would otherwise be underestimated (leading to increased false positive rates) or overestimated (leading to non-detection). The implications of detecting subtle changes in gene expression are important because these genes can have real biological significance, especially since microarrays systematically underestimate fold change levels compared to other quantitative means (e.g. RT-PCR) [29].

The main distinctive property of VAMPIRE is its use of a parameterized global variance model, which assumes a strong correlation between variance and expression level. CyberT and Limma instead employ a weighting scheme between sample variance and an additional variance estimate based on the array data. SAM, a non-parametric method, penalizes the sample variance with an estimated constant. VAMPIRE's increased statistical power is owed to its reliance on an explicit variance structure – one that is evident among various controlled datasets and array platforms. However, if this error structure is altered by vigorous normalization methods such that the strong correlation between variance and expression is confounded, VAMPIRE will become incompatible. In these cases, the performance will shift among the statistical methods which require fewer assumptions on the data structure.

As sample size increases, variance estimates become more stable and thus lead to a convergence of results among statistical testers. Nevertheless, increasing sample size is costly and oftentimes unfeasible. We demonstrate here the effectiveness of the global variance modeling approach towards the sensitive detection of differentially expressed genes.

E. Methods

Datasets

Golden Spike dataset

As described in [29], but briefly, "control" and "spike" samples were hybridized in triplicate to Affymetrix DrosGenome1 GeneChips. The spike sample contains the same cRNAs as the control sample in addition to ~1300 cRNAs, which were spiked in at known differing concentrations ranging from 1.2- to 4-fold between the samples. The "Choe-preferred" preprocessing algorithm [29] was conducted on the raw Affymetrix CEL data and this served as the basis for statistical method comparisons. Preprocessing was applied using the R statistical software [36] and Bioconductor's *affy* package [37].

MAQC 4 titration pools dataset

The MicroArray Quality Control (MAQC) Consortium assayed four titration pools from two different reference samples across multiple platforms and testing sites, as described in [17]. Briefly, four mixtures were made from Stratagene's Human Reference RNA and Ambion's Human Brain Reference RNA, in ratios of 100:0 (sample A), 0:100 (sample B), 75:25 (sample C), and 25:75 (sample D). These pools were hybridized to

various commercial microarray platforms, including Affymetrix HGU133plus2.0 GeneChip, Agilent Technologies Whole Human Genome Oligo Microarray G4112A, and Illumina Human-6 BeadChip 48Kv1.0. The pools were also tested on various alternative gene expression platforms, including the Applied Biosystems TaqMan Gene Expression Assay. Exhaustive probe mapping across platforms are available [17]. MAS 5.0, Feature Extraction software 8.5, and Beadstudio algorithms were used to preprocess Affymetrix, Agilent, and Illumina raw array data, respectively.

Mixed-tissue RNA reference material (MTRRM) dataset

As described in [31], but briefly, two samples with differing mixtures of RNA from various rat tissue types were hybridized to multiple microarray platforms and testing sites. One sample ("Mix1") consists of 10% rat testis, 40% brain, 30% liver, and 20% kidney RNA. The other sample ("Mix2") consists of 40% rat testis, 20% brain, 20% liver, and 20% kidney RNA. The samples were hybridized to Affymetrix RAE230A, CodeLink UniSet Rat I, and Agilent G4130A arrays. MAS 5.0 and Feature Extraction software 8.5 algorithms were used to preprocess Affymetrix and Agilent raw array data, respectively.

Pre-processing algorithms

The **MAS 5.0**, **RMA**, and **PLIER** pre-processing algorithms were conducted on Affymetrix CEL data using the Affymetrix Expression Console with default parameters: MAS 5.0 scaling to TGT=500, RMA using quantile normalization with global background correction, and PLIER using quantile normalization with PM-MM probe

level measurements. Choe et al.'s [29] preferred pre-processing method (**CP-MLMR**) was conducted on Affymetrix CEL data using the R statistical software [36] and Bioconductor's *affy* package [37]. The **GCRMA** and **PLM** pre-processing algorithms were conducted on Affymetrix CEL data using Bioconductor's *gcrma* and *affyPLM* packages.

Statistical testers

We evaluated various test statistics including the *Student's t-test*, *Welch's t-test*, *1-way ANOVA*, *Brown-Forsythe test*, *Levene's test* as well as other sophisticated methods designed specifically for microarrays, detailed below. Correction for multiple comparisons was done by the *Bonferroni* family-wise error correction, or the *Benjamini-Hochberg false discovery rate* procedure [32], unless otherwise specified.

Significance Analysis for Microarrays (SAM)

A permutation-based penalized *t*-statistic, developed by [19], which addresses the poor estimation of sample standard deviation from small sample sizes typical of microarray experiments by adding to it a 'fudge factor' stabilizing constant. SAM uses an FDR procedure developed in [38]. The method can be used for various experimental designs, including unpaired two-class, paired two-class, and multi-class designs. SAM was applied using the Microsoft Excel Add-in (v3.09) with default values: 100 permutations, k=10-nearest neighbors imputer.

CyberT

A Bayesian regularized *t*-statistic, developed by [20, 39], whereby posterior variance estimates are used in place of standard sample variances. The posterior variance estimate is computed from a conjugate prior and a pooling of the variances from neighboring genes. The neighboring genes are contained in a window size defined by the user. The user must also define a confidence weighting parameter which weights background variance over empirical variance. CyberT has other implementations which accommodate unpaired two-class, paired two-class, and multi-class designs. CyberT was applied using default values: window size=101, confidence value=10.

Linear Models for Microarray Data (Limma)

A moderated *t*-statistic, developed by [23], in which standard error is 'shrunk' using an empirical Bayes approach. Posterior variance is a weighted combination of sample variance and a grand variance estimate whose hyperparameters are stably estimated from the data. The statistical framework incorporates a linear model which accommodates a wide range of experimental designs. Limma is implemented as an R computing environment package [21, 40, 41].

Variance Modeled Posterior Inference with Regional Exponentials (VAMPIRE)

A Bayesian statistic, developed by [24, 25], whereby variance estimates are extrapolated from a global two-component model of the microarray variance structure. Stable parameters of the global variance model are computed by systematically drawing an expression level cutoff and employing computational fitting procedures on the data.

The variance models and corresponding posterior means are integrated in a Bayesian statistical framework. VAMPIRE is implemented as a web-based platform [22], accessible at http://genome.ucsd.edu/microarray.

F. Acknowledgements

This chapter, in part, is currently being prepared for submission for publication of the material. Hsiao, Gene; Subramaniam, Shankar, "Variance estimation based on global modeling of gene expression array data increases sensitivity for detecting differentially expressed genes." The dissertation author was the primary investigator and sole first author of this paper.

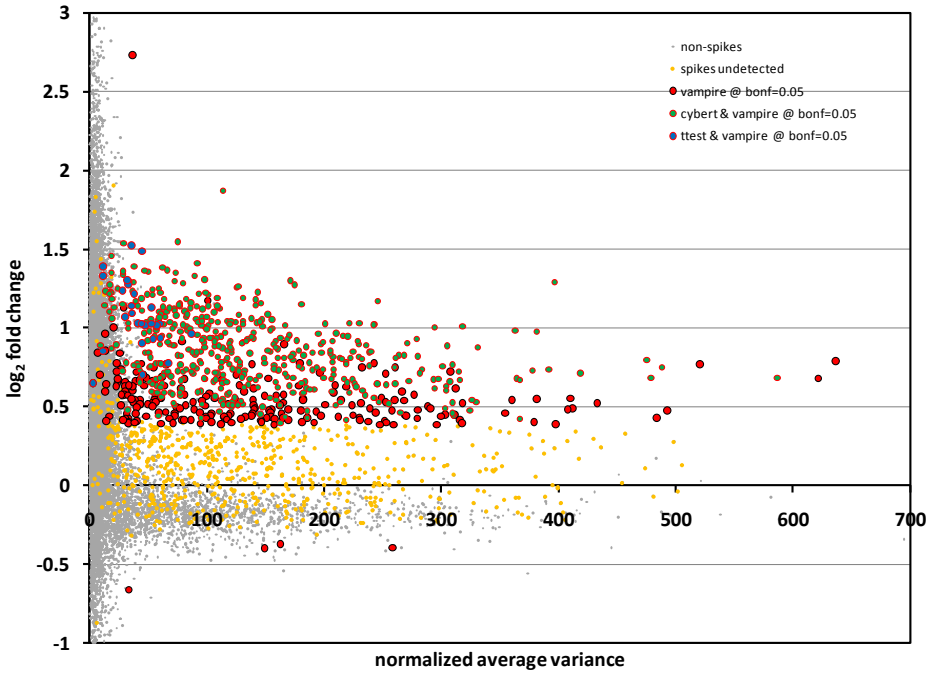

Figure 1: Spikes are distributed across variance levels

Golden spike data preprocessed with "Choe-preferred" summarization algorithm are variably detected by the Student's t-test, CyberT, and VAMPIRE. Before reaching a Bonferroni-corrected family wise error rate of 5% (α_{Bonf} = 0.05), the Student's t-test detects spikes in the high-fold, low-variance region (blue filled dots). CyberT detects all spikes found by the t-test, plus significantly more along higher variance levels (green filled dots). VAMPIRE detects all spikes found by the t-test and CyberT (red outlined dots), plus significantly more along higher variance levels and lower fold-changes (red dots). Gray = non-spiked features, blue filled = spikes detected by t-test, CyberT, and VAMPIRE, green-filled = spikes detected by CyberT and VAMPIRE, red-filled = spikes detected only by VAMPIRE, orange = spikes undetected.

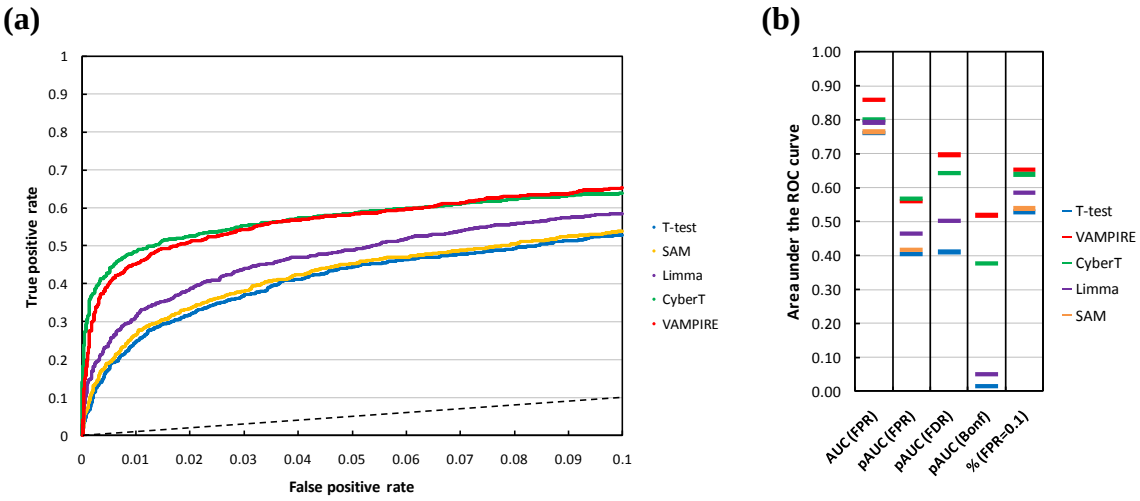

Figure 2: ROC curves and AUC summary scores at various significance thresholds
(a) Partial ROC curves shows VAMPIRE and CyberT have similar performance in sensitivity and specificity. (b) Graphical portrayal of Table 1 shows that VAMPIRE and CyberT consistently rank better at performance for various significance thresholds than the other methods tested. Difference in performance between VAMPIRE and CyberT grows as threshold stringency increases. Red = VAMPIRE, green = CyberT, purple = Limma, orange = SAM, blue = Student's t-test

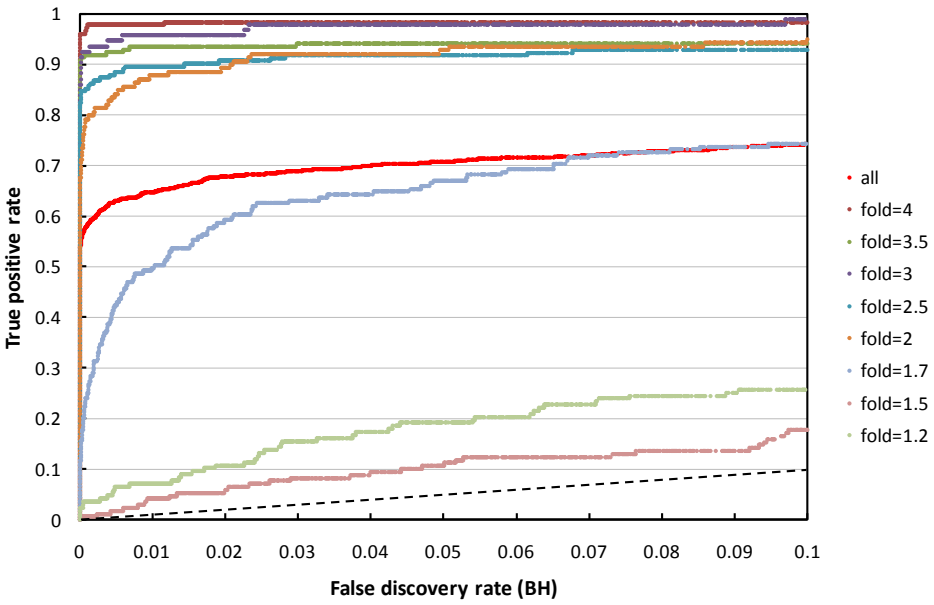

Figure 3: VAMPIRE ROC curves stratified by specific fold-change
ROC curves with respect to false discovery rate (FDR) shows that the VAMPIRE method can detect more than 90% of spikes whose fold-change is greater or equal to two. VAMPIRE can also detect 1.2- , 1.5-, 1.7-fold features better than random chance alone.

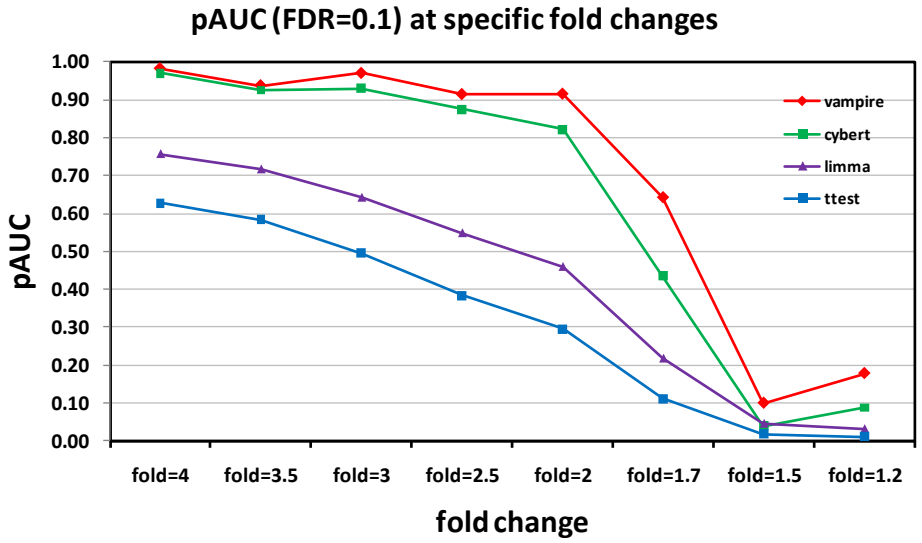

	fold=4	fold=3.5	fold=3	fold=2.5	fold=2	fold=1.7	fold=1.5	fold=1.2
VAMPIRE	0.982	0.937	0.970	0.914	0.915	0.642	0.099	0.178
CyberT	0.971	0.925	0.930	0.874	0.822	0.435	0.039	0.088
Limma	0.757	0.717	0.642	0.548	0.459	0.218	0.046	0.032
T-test	0.627	0.584	0.495	0.383	0.295	0.111	0.019	0.011

Figure 4: pAUCs as a function of specific fold-change with respect to FDR
All methods suffer loss in sensitivity for features below 2-fold, but VAMPIRE forestalls the sharp drop until 1.5-fold and consistently performs better across all fold-change levels.

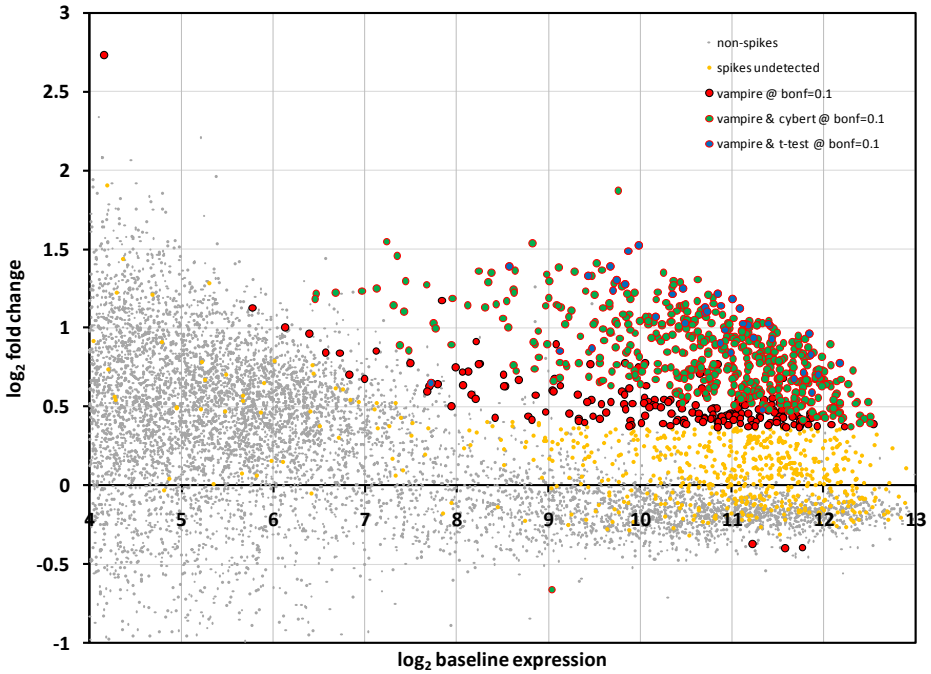

Figure 5: MA-like plot of the Golden spike data
Feature expression plotted versus fold change shows spikes span across all levels of expression. Spiked features are variably detected by the Student's t-test, CyberT, and VAMPIRE. Before reaching a Bonferroni-corrected family wise error rate of 10% (α_{Bonf} = 0.1), the Student's t-test detects spikes in the higher expression level, higher fold-change region (blue filled dots). CyberT detects all spikes found by the t-test, plus significantly more at lower expression (green filled dots). VAMPIRE detects all spikes found by the t-test and CyberT (red outlined dots), plus significantly more along low expression levels and lower fold-changes (red dots). Gray = non-spiked features, blue filled = spikes detected by t-test, CyberT, and VAMPIRE, green-filled = spikes detected by CyberT and VAMPIRE, red-filled = spikes detected only by VAMPIRE, orange = spikes undetected.

(a) **(b)**

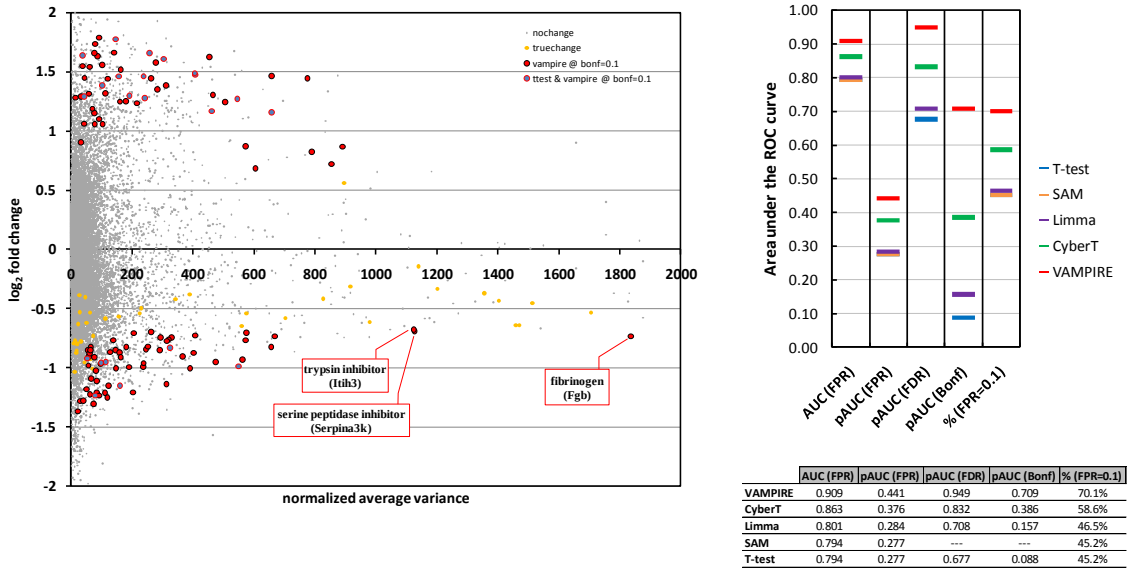

	AUC (FPR)	pAUC (FPR)	pAUC (FDR)	pAUC (Bonf)	% (FPR=0.1)
VAMPIRE	0.909	0.441	0.949	0.709	70.1%
CyberT	0.863	0.376	0.832	0.386	58.6%
Limma	0.801	0.284	0.708	0.157	46.5%
SAM	0.794	0.277	---	---	45.2%
T-test	0.794	0.277	0.677	0.088	45.2%

Figure 6: Thompson *et al*.'s MTRRM dataset is used for performance analysis
(a) MTRRM features are plotted by fold-change versus normalized sample variance. True positives are distributed across all levels of variance (non-gray dots). T-test detects features at high fold regions, but lacks power to detect features at higher variance. VAMPIRE detects true features found by the t-test, plus more at lower fold and higher variance regions (α_{Bonf}=0.1). Three genes (Itih3, Serpina3k, Fgb) are highlighted which demonstrate biologically significant features detected by VAMPIRE but not by the t-test. (b) AUCs of various statistical methods for various significance thresholds are listed and displayed in graphical form. VAMPIRE and CyberT consistently rank best among other methods tested.

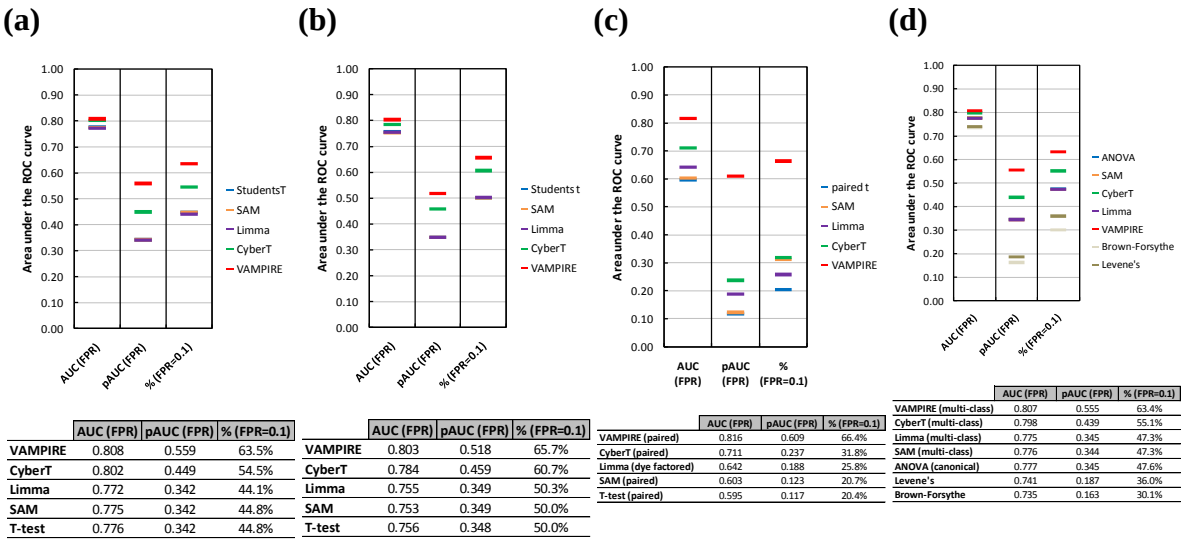

	AUC (FPR)	pAUC (FPR)	% (FPR=0.1)
VAMPIRE	0.808	0.559	63.5%
CyberT	0.802	0.449	54.5%
Limma	0.772	0.342	44.1%
SAM	0.775	0.342	44.8%
T-test	0.776	0.342	44.8%

	AUC (FPR)	pAUC (FPR)	% (FPR=0.1)
VAMPIRE	0.803	0.518	65.7%
CyberT	0.784	0.459	60.7%
Limma	0.755	0.349	50.3%
SAM	0.753	0.349	50.0%
T-test	0.756	0.348	50.0%

	AUC (FPR)	pAUC (FPR)	% (FPR=0.1)
VAMPIRE (paired)	0.816	0.609	66.4%
CyberT (paired)	0.711	0.237	31.8%
Limma (dye factored)	0.642	0.188	25.8%
SAM (paired)	0.603	0.123	20.7%
T-test (paired)	0.595	0.117	20.4%

	AUC (FPR)	pAUC (FPR)	% (FPR=0.1)
VAMPIRE (multi-class)	0.807	0.555	63.4%
CyberT (multi-class)	0.798	0.439	55.1%
Limma (multi-class)	0.775	0.345	47.3%
SAM (multi-class)	0.776	0.344	47.3%
ANOVA (canonical)	0.777	0.345	47.6%
Levene's	0.741	0.187	36.0%
Brown-Forsythe	0.735	0.163	30.1%

Figure 7: AUCs and percent detection of true positives for various statistical testers on the MAQC four titration pools dataset

Sensitivity analysis using the MAQC dataset demonstrates that VAMPIRE is consistently more sensitive than other leading testers across multiple array types and experimental designs: (a) Affymetrix, 2-class unpaired design, (b) Illumina, 2-class unpaired design, (c) Two-color Agilent, paired design, (d) Affymetrix, multi-class design.

Table 1: Golden spike dataset Area Under ROC Curve (AUC) summary scores, and percentage of true positives detected

Methods are sorted in descending order by AUC. pAUCs are calculated at the 10% threshold. pAUC scores for SAM at FDR and Bonferroni thresholds are unavailable since p-values are not easily attained from the software used.

	AUC (FPR)	pAUC (FPR)	pAUC (FDR)	pAUC (Bonf)	% (FPR=0.1)
VAMPIRE	0.858	0.560	0.697	0.518	65.29%
CyberT	0.800	0.567	0.642	0.376	63.86%
Limma	0.792	0.465	0.502	0.050	58.45%
SAM	0.765	0.417	---	---	53.87%
T-test	0.761	0.405	0.411	0.014	52.82%

Table 2: Proportion of true positives detected by various methods at low-expression, low-fold levels for the Golden spike dataset

Spikes are restricted to two- or lower fold-change and binned at the lowest end of expression. VAMPIRE demonstrates increased sensitivity for low-fold and low-expressed features with respect to various significance thresholds at the 10% level.

expression level bin →	250			500		
significance threshold →	FPR=0.1	FDR=0.1	Bonf=0.1	FPR=0.1	FDR=0.1	Bonf=0.1
VAMPIRE	47.9%	60.4%	25.0%	72.7%	87.9%	33.3%
CyberT	39.6%	60.4%	4.2%	54.5%	69.7%	12.1%
Limma	29.2%	41.7%	2.1%	51.5%	57.6%	0.0%
T-test	22.9%	29.2%	2.1%	39.4%	54.5%	0.0%

Table 3: MTRRM dataset pAUCs as a function of specific fold-change with respect to Bonferroni cutoff of 10%
While all methods lose sensitivity for features below 2-fold, VAMPIRE is the only method that can detect 1.5-fold features.

	fold=4	fold=2	fold=1.5
VAMPIRE	0.962	0.780	0.358
CyberT	0.797	0.334	0.000
Limma	0.294	0.173	0.000
T-test	0.156	0.105	0.000

III.

Mechanisms of human insulin resistance and thiazolidinedione-mediated insulin sensitization

A. Abstract

Cellular and tissue defects associated with insulin resistance are coincident with transcriptional abnormalities and are improved after insulin sensitization with thiazolidinedione (TZD) PPARγ ligands. We characterized 72 human subjects by relating their clinical phenotypes with functional pathway alterations. We transcriptionally profiled 364 biopsies harvested before and after hyperinsulinemic-euglycemic clamp studies, at baseline and after three-month TZD treatment. We have identified molecular and functional characteristics of insulin resistant subjects and distinctions between TZD treatment responder and non-responder subjects. Insulin resistant subjects exhibited alterations in skeletal muscle (e.g., glycolytic flux and intra-muscular adipocytes) and adipose tissue (e.g., mitochondrial metabolism and inflammation) that improved relative to TZD-induced insulin sensitization. Pre-TZD treatment expression of MLXIP in muscle and HLA-DRB1 in adipose tissue from insulin resistant subjects was linearly predictive of post-TZD insulin sensitization. We have uniquely characterized coordinated cellular and tissue functional pathways that are characteristic of insulin resistance, TZD-induced insulin sensitization, and potential TZD responsiveness.

B. Introduction

Insulin resistance is a pathological state in which insulin action is impaired in target tissues including liver, skeletal muscle, and adipose tissue. Insulin resistance is a defining feature of the metabolic syndrome and the primary defect leading to type 2 diabetes [2, 3]. Impaired insulin-stimulated glucose uptake in skeletal muscle and lipid metabolism in adipocytes are central characteristics of insulin-resistance. Other manifestations of the condition include elevated intramuscular fat content [42], dysregulation of adipokine secretion, and chronic low-grade inflammation in adipose tissue [43]. Macrophage infiltration in adipose tissue activates inflammatory pathways that induce insulin resistance and modulate the effects of adipose tissue on whole-body metabolism [44]. Several studies have shown that decreased mitochondrial protein and oxidative phosphorylation (OXPHOS) in skeletal muscle and adipocytes are also underlying factors of insulin resistance [45, 46].

Thiazolidinediones (TZDs) are insulin-sensitizing drugs used to treat type 2 diabetes. TZDs enhance insulin sensitivity by improving glucose and lipid metabolism, altering adipokine secretion, and reducing adipose tissue inflammation [43, 47]. Although TZDs improve insulin sensitivity and the glycemic, lipid, and inflammatory profiles of most patients, ~30% of diabetic subjects do not respond to TZD treatment, as gauged by fasting plasma glucose or HbA1c levels [12, 13]. TZDs are ligands of peroxisome proliferator-activated receptor gamma (PPARγ) through which they alter the expression of hundreds of genes in skeletal muscle, adipocytes, and macrophages. PPARγ-mediated gene regulation is the predominant mode of TZD-enhanced insulin sensitivity and metabolism. However, the mechanisms by which TZD-induced gene

expression changes lead to insulin sensitization or by which TZD-induced insulin sensitization is prevented are poorly understood.

We have conducted a mechanistic analysis of the gene expression profiles of adipose tissue (AT) and skeletal muscle (SM) from 72 subjects ranging from insulin-sensitive to insulin-resistant. The subjects underwent multiple SM and AT biopsies, hyperinsulinemic-euglycemic clamps, three month treatment with an insulin-sensitizing TZD, and clinical characterization. We have measured the transcriptional alterations associated with insulin-resistance in AT and SM in the fasting state and SM in the insulin-stimulated (post-clamp) state. Insulin resistant subjects responded to TZD treatment with varied improvements in insulin sensitivity. Thus, we characterized transcriptional alterations in AT and SM associated with TZD-induced insulin-sensitization. We ranked the insulin resistant subjects by their degree of TZD response (i.e., increased insulin sensitivity based on rate of glucose disposal during the hyperinsulinemic-euglycemic clamp) to define responder and non-responder subgroups. Based on our analysis of SM and AT from these subjects, we have defined pathways and key mechanisms of disease that distinguish the responder and non-responder subgroups.

C. Results

Characterization of insulin sensitive subjects and insulin resistant TZD-responder and non-responder subjects

We generated tissue gene expression profiles from 72 subjects with a broad range of insulin sensitivity, before and after TZD treatment, to identify transcriptional and

biochemical pathway signatures that characterize insulin sensitivity, insulin resistance, and pharmacological insulin sensitization. Each subject underwent a hyperinsulinemic-euglycemic clamp at the start of the study and a second hyperinsulinemic-euglycemic clamp after three months treatment with one of three TZDs: rosiglitazone, pioglitazone, or troglitazone. Vastus lateralus SM biopsies were harvested immediately before (basal) and after each clamp (post-clamp); abdominal subcutaneous AT biopsies were harvested immediately before each clamp (Figure 8a). AT biopsies were harvested only from the pioglitazone and rosiglitazone study groups (44 subjects). Dataset S1 shows selected clinical characteristics of the subjects measured before and after TZD treatment. We gauged the insulin sensitivity of each subject by their rate of glucose disposal (R_d) during the clamp. Individuals were divided into two major groups, based on their rate of glucose disposal during the first hyperinsulinemic-euglycemic clamp (R_d1). Subjects with R_d1 values greater than 8 mg/kg/min were classified as insulin sensitive (normal R_d, NR_d), and the remaining subjects were classified as insulin resistant (impaired R_d, IR_d). From each AT and SM biopsy, we generated gene expression profiles using genome-spanning microarrays and, with these, conducted biochemical pathway analyses (see Methods). We compared our results from NR_d subjects, IR_d subjects, and IR_d subject subgroups, described below.

Figure 8b shows the TZD-induced fractional R_d change [(R_d2-R_d1)/R_d1] for each subject correlated with their starting R_d (R_d1). TZD treatment did not increase the insulin sensitivity (R_d) of most NR_d subjects (see also Dataset S1). As expected, most IR_d subjects responded to TZD treatment, demonstrating improved insulin sensitivity ($R_d2 > R_d1$). Insulin-sensitizing efficacy was not significantly different between the three TZDs.

Approximately 25% of the IR_d subjects did not respond to TZD treatment, demonstrating minimal or no improvement in insulin-sensitivity. In order to contrast the expression profiles of IR_d TZD-responders (those having the best insulin sensitization response) with IR_d TZD-non-responders (those having the worst insulin sensitization response), all the IR_d subjects (referred to below as IR_d^{all}) were ranked by their fractional R_d change and divided into quartile subgroups. IR_d subjects in the top quartile of fractional change in R_d (>83% increase in R_d) were classified as IR_d responders (IR_d+). IR_d+ subjects not only had the largest fractional R_d change but also had the greatest improvement in plasma insulin levels (Dataset S1). IR_d subjects in the bottom quartile of fractional R_d change (<13% increase in R_d) were classified as IR_d non-responders (IR_d^-). IR_d subjects in the middle two quartiles of fractional R_d change (13-83% increase in R_d) were classified as IR_d mid-responders (IR_d^{mid}). Figure 8b shows the distribution of these IR_d subgroups. Thus, the IR_d^{all} subject group refers to the sum of the IR_d+, IR_d^-, IR_d^{mid} subject groups.

Insulin resistance is associated with impaired insulin-induced metabolic gene expression changes in skeletal muscle which are largely normalized after TZD treatment

We analyzed SM gene expression profiles from the subject groups and identified ~150 genes whose pre-TZD, basal and/or post-clamp expression levels were significantly different in IR_d^{all} subjects (α_{Bonf}=0.05) compared to NR_d subjects (Dataset S2). Among these genes were critical regulators of lipid metabolism. For example, expression of lipoprotein lipase (LPL), a critical regulator of SM lipid metabolism [48] and a target gene of PPARγ [49], was 48% lower in IR_d^{all} subjects in the pre-TZD fasting state

(α_{Bonf}=0.05), was fully rescued by TZD treatment, and was positively correlated with R_d (r = 0.53). All genes with baseline expression values that correlate with R_d are shown in Dataset S3. We also identified 237 insulin-target genes, i.e., genes suppressed or activated in the insulin-stimulated (post-clamp) state in NR_d subjects. 116 insulin-target genes were functionally involved with metabolism (Dataset S2). The insulin-induced response of 42 genes was significantly altered in the IR_d^{all} subjects, of which 19 genes were functionally involved with metabolism. IR_d^{all} subjects exhibited impaired insulin-induced expression changes in hexokinase 2 (HK2) and pyruvate dehydrogenase kinase 4 (PDK4) compared to NR_d subjects. HK2 expression is normally induced by insulin, but this induction was blunted in IR_d^{all} subjects (Figure 9a). Consequently, the post-clamp HK2 expression level in IR_d^{all} subjects was 50% lower (α_{Bonf}=0.05) than in NR_d subjects. Insulin activation of HK2 commits glucose to the intracellular compartment in muscle, facilitating glucose metabolism in the fed state. PDK4 expression is normally suppressed by insulin, but this effect was blunted in IR_d^{all} subjects (Figure 9b). As a result, the post-clamp PDK4 expression level in IR_d^{all} subjects was seven-fold higher than in NR_d subjects. PDK4, in its active state, inhibits pyruvate dehydrogenase complex conversion of pyruvate into acetyl-CoA, effectively disrupting glucose utilization. The schematic in Figure 9c shows how defective insulin-induced regulation of HK2 and PDK4 in insulin resistant subjects would reduce glycolytic flux. Additional genes involved in the glycolytic pathway (PFKFB3 and PKM2) exhibited defective insulin-induced regulation in IR_d^{all} subjects, also shown in Figure 9c. We observed insulin-induced, transcriptionally coordinated repression of the insulin signaling pathway (Fig. S1). Following TZD treatment, IR_d^{all} subjects exhibited improved insulin-induced HK2 and

PDK4 expression changes and post-clamp HK2 and PDK4 expression levels compared to NR_d subjects (red and blue bars, respectively, in Figure 9a,b). We contrasted these HK2 and PDK4 expression patterns with those from the responder (IR_d+) and non-responder (IR_d^-) subgroups (pink and yellow bars, respectively, in Figure 9a,b). Interestingly, post-TZD improvements in the expression of HK2 and PDK4 were more robust in the IR_d+ subject subgroup compared to the IR_d^{all} subject group and absent in the IR_d^- subject subgroup (Figure 9a,b). Thus, TZD-improved insulin-regulation of HK2 and PDK4, and presumably glycolytic flux, is related to the degree of TZD-improved insulin sensitization.

Insulin resistance is associated with elevated adipocyte markers in the skeletal muscle which are increased after TZD treatment

Despite the gross exclusion of perimuscular fat from SM biopsies, SM from IR_d subjects had higher levels of adipocyte-predominant transcripts (Dataset S2) compared to SM from NR_d subjects. Several of these genes are interesting to note, including leptin (LEP), adiponectin (ADIPOQ), and retinol-binding protein 4 (RBP4). Leptin was over-expressed >5-fold in IR_d^{all} subjects at baseline and in IR_d+ subjects before and after insulin-stimulation and/or TZD treatment. Leptin expression in IR_d^- subjects was not significantly different from that in NR_d subjects in any condition. Both ADIPOQ and RBP4 were over-expressed in IR_d^{all} and IR_d+ subjects and were significantly further elevated after TZD treatment. ADIPOQ and RBP4 were over-expressed in IR_d^- subjects only after TZD treatment and this pattern was significantly blunted compared to the over-expression we observed in IR_d+ subjects. Leptin, adiponectin, and RBP4 are principally

secreted by adipocytes [50] and have paracrine effects on glucose uptake, fatty acid uptake, and fatty acid oxidation in peripheral tissues [51-54]. Thus, altered expression of these genes suggests that the insulin-sensitizing effects of TZDs involve increased adipocyte-myocyte crosstalk.

Genes involved in other aspects of adipocyte biology were differentially expressed in SM from the subject groups. IR_d^{all} and IR_d+ subjects had higher basal and post-TZD expression of genes that regulate lipid uptake and storage, compared to NR_d subjects. Perilipin (PLIN), fatty acid binding protein (FABP4), stearoyl-CoA desaturase (SCD), cell death-inducing DFFA-like effector c (CIDEC) are among these genes. Over-expression of these genes was increased after TZD treatment. Overall, these over-expression patterns were more pronounced in IR_d+ subjects and weakest in IR_d^- subjects suggesting that elevated lipid uptake and storage is related to insulin sensitization. In fact, fractional CIDEC expression change correlated with fractional R_d change (r=0.57). We observed significant over-expression of genes involved in adipogenesis in SM of IR_d subjects, including CCAAT/enhancer binding protein α (CEBPA), sterol regulatory element binding transcription factor (SREBF1), and early growth response 2 (EGR2). CEBPA over-expression and SREBF1 expression each increased significantly after insulin infusion in IR_d^{all} subjects. Interestingly, only the IR_d+ subjects exhibited significant up-regulation of EGR2 (8.6-fold) after TZD treatment (α_{Bonf}=0.05). Together, these findings suggest that TZD-induced insulin-sensitization is mediated, in part, by stimulation of intramuscular adipocyte differentiation (see Discussion).

Insulin resistance is associated with increased inflammatory markers in adipose tissue which are coordinately decreased after TZD treatment

We identified 588 AT genes that were differentially regulated between NR_d and IR_d subjects before TZD treatment (Dataset S4). The genes in this set were generally distinct from those we identified in our SM profiling (Compare gene expression profiles in Dataset S5). We used functional analysis [22, 36] to identify enriched function and pathway annotations within this gene set (Dataset S6). We identified statistical enrichment of several inflammation-related ontology categories, including immune system process, extracellular matrix, and MHC class II receptor activity. Several immune system pathways were also significantly enriched, including antigen processing and presentation and leukocyte transendothelial migration. Thirty-four percent of the adipose tissue genes differentially expressed IR_d^{all} subjects were associated with inflammation and virtually all of these (192 of 202) were over-expressed. This is shown schematically in Figure 10 for genes involved in the antigen processing and presentation pathway (panel a) and leukocyte transendothelial migration pathway (panel c), two critical pathways regulating tissue inflammation and immune cell infiltration. AT is a heterogeneous mixture of cell types. The enriched functional ontology and pathway annotations, of the differentially expressed genes, associated with the immune system are evidence of increased antigen-presenting cells in AT from the IR_d^{all} subjects.

Over-expression of inflammatory markers was universally decreased in IR_d+ subjects after TZD treatment. Interestingly, most genes over-expressed in IR_d^{all} subjects and subsequently down-regulated after TZD treatment were macrophage-specific (Dataset S4). Several facilitate macrophage chemotaxis, including matrix remodeling

genes (MMP7, MMP9) and osteopontin (SPP1). Post-TZD repression of over-expressed genes in IR_d+ subjects is shown schematically in Figure 10 for antigen processing and presentation (compare panels a,b) and leukocyte transendothelial migration pathways (compare panels c,d). A significantly smaller percentage of inflammatory markers were normalized in IR_d^- subjects compared to IR_d+ subjects (Chi square test, $p<0.05$) (shown schematically in Fig. S2). Genes still over-expressed in IR_d^- but not IR_d+ subjects after TZD treatment are shown in Dataset S4. Over-expression of CD74, a MHC class II invariant chain gene, was significantly repressed 46% in IR_d+ subjects but not in IR_d^- subjects after TZD treatment (Figure 10e). In fact, CD74 expression was inversely correlated with R_d ($r = ^-0.60$) (Figure 10f).

Gene expression signatures that correlate with insulin resistance and TZD-induced insulin sensitization

To further elucidate relationships between expression and insulin sensitivity in AT, we determined the correlations between genome-wide gene expression and R_d values (Dataset S7 shows all correlations with $|r|>0.45$). As expected, a set of 319 genes with robust negative correlations between R_d and expression ($r< -0.5$) was enriched for genes functionally annotated with immune response ($\alpha_{Bonf}=0.05$) (Dataset S6), including >60% of the genes shown in Figure 10a,c. We used statistical regression test (Methods) to identify AT expression patterns that significantly correlate with R_d. Expression of CD14 molecule (CD14) ($r = ^-0.71$), cathepsin S (CTSS) ($r = ^-0.51$), neutrophil cytosolic factor 4 (NCF4) ($r = ^-0.65$), MHC class II DM beta (HLA-DMB) ($r= ^-0.70$), and 28 other genes was inversely correlated with insulin sensitivity (R_d) (Dataset S7). CD14, CTSS, NCF4

and HLA-DMB were also differentially expressed between NR_d and IR_d^{all} subjects before TZD treatment (Dataset S4), represented in Figure 10a,c. These results suggest that insulin resistance is functionally related to elevated AT expression of CD74, CD14, CTSS, NCF4 and HLA-DMB and indicate that these genes are transcriptional markers of insulin resistance. Negative correlations between insulin sensitivity and expression levels of these and the other genes associated with leukocyte transendothelial migration show the association of AT macrophages and insulin resistance. TZD-induced insulin-sensitization (observed in IR_d+ subjects but not IR_d^- subjects) correlated with normalization of these coordinated pathway systems, perhaps as a result of attenuated immune cell residency and recruitment.

We observed robust positive correlations ($r>0.5$) between R_d and the pre- and post-TZD expression of 315 genes. This positively correlated gene set was statistically enriched for genes annotated with mitochondria functional pathways (Dataset S6). Expression of the majority of genes involved in mitochondrial β-oxidation of fatty acids (even-, odd-, mono-, and poly-unsaturated and saturated fatty acids) and TCA cycle was correlated with insulin sensitivity (Figure 11a), including hydroxyacyl-Coenzyme A dehydrogenase (HADH, $r = 0.73$), dodecenoyl-Coenzyme A delta isomerase (DCI, $r = 0.64$), and succinate-CoA ligase (SUCLG2, $r = 0.68$). Expression of genes encoding subunits from all five complexes in the oxidative phosphorylation pathway was correlated with insulin sensitivity (Figure 11b), including NADH dehydrogenase (NDUFB5, $r = 0.62$), electron-transfer-flavoprotein alpha (ETFA, $r = 0.69$), and cytochrome c reductase (UQCRC2, $r = 0.66$). Expression of genes involved in branched chain amino acid (BCAA) metabolism (several also involved in TCA cycle) is also

correlated with insulin sensitivity (Fig. 4a). Importantly, this set includes all the genes that regulate the initial, rate-limiting steps of BCAA metabolism (BCAT2, DBT, DLD, BCKDHA and BCKDHB). Overall, these results indicate that impaired fatty acid and BCAA metabolism and oxidative phosphorylation are proportional to the degree of insulin resistance.

Several published studies have attempted to identify plasma components and other clinical parameters that predict the insulin-sensitizing effect of TZDs on individual patients [12, 55]. We have identified gene expression predictors of TZD responsiveness in SM and AT from IR_d^{all} subjects, i.e., pre-TZD gene expression that correlates with fractional R_d change (R_d2-R_d1/R_d1) (Dataset S3). MLX interacting protein (MLXIP) in SM and major histocompatibility complex class II DR beta 1 (HLA-DRB1) in AT had gene expression signatures that predict insulin sensitization by TZDs. MLXIP is a transcription factor that activates glycolytic genes (including HK2) in SM [56]. Pre-TZD, post-clamp SM expression of MLXIP correlated with fractional R_d change ($r = 0.51$) (Figure 12a). In general, IR_d^{all} subjects with higher SM MLXIP expression before TZD treatment exhibited greater relative insulin-sensitization after TZD treatment (pre-TZD MLXIP expression in IR_d+ subjects was 2.6-fold greater than in IR_d^- subjects ($\alpha_{Bonf}=0.05$)). Adipose tissue HLA-DRB1 expression was negatively correlated with fractional R_d change ($r = {}^-0.48$). HLA-DRB1 plays a central role in antigen presentation and is expressed mainly in antigen presenting cells (APCs). Expression of HLA-DRB1 was 3.4-fold higher in IR_d^- subjects compared to IR_d+ subjects (Figure 12b). Thus, patients who expressed less HLA-DRB1 in AT before TZD treatment experienced greater relative increases in insulin-sensitivity after TZD treatment.

D. Discussion

The multi-dimensionality of our human gene expression dataset allows us to investigate fundamental questions about insulin resistance and TZD-induced sensitization in an unbiased and statistically-robust manner. Our results delineate new mechanistic differences between normal and insulin-resistant subjects and uniquely identify gene expression signatures that characterize TZD-mediated insulin sensitization and predict TZD responsiveness in insulin resistant subjects. Notably, physiologic and individual proteomic data in the literature support many of the differentially expressed, coordinated pathway models generated by our statistical data analyses. Our findings demonstrate that insulin resistance is characterized by altered basal and insulin-induced expression of genes in skeletal muscle. The fasting-to-feeding transition altered the expression of many genes in insulin sensitive subjects including key regulators of glycolysis and other metabolic pathways. Interestingly, insulin-regulation of many genes was significantly blunted in the insulin-resistant subjects. Our data support the notion that over-nutrition insulin resistance is associated with impaired metabolic flexibility in response to insulin [57]. For example, defective insulin-induced regulation of HK2 and PDK4 in insulin resistant subjects (Figure 9c) would result in decreased glycolytic flux. TZD-induced insulin sensitization in responder (IR_d+) subjects was associated with improved insulin-regulated gene expression. Defective insulin-regulated HK2 and PDK4 expression was ameliorated in TZD-treated responder subjects, concomitant with insulin sensitization, but not in TZD-treated non-responder (IR_d^-) subjects who did not become more insulin

sensitive. Thus, insulin sensitization in the responder subjects was likely associated with improved glycolytic flux and overall metabolic flexibility.

Surprisingly, elevated intramuscular adipocyte marker gene expression in the insulin resistant subjects further increased after TZD treatment. This effect was most significant in responder subjects which suggests that TZD-enhanced insulin sensitization in muscle is related to increased intramuscular adipocytes. Intramuscular adipocytes have the potential to improve myocyte sensitivity through paracrine signaling and alleviating local hyperlipidemia by storing excess fatty acids (Fig. S3). For example, TZD-induced elevation of adiponectin secretion would increase AMPK activation and lipid oxidation, which is observed in skeletal muscle of TZD-treated subjects [58]. Thus, presence of adipocytes in skeletal muscle of insulin resistant subjects may not be a causal factor mediating insulin resistance, but an adaptation that accommodates for excess energy storage.

Chronic low-grade inflammation is associated with and can cause insulin resistance. Macrophages infiltrate adipose tissue of obese animals and humans where they secrete cytokines that interfere with insulin signaling [43, 59]. Our pathway analysis results indicate that immunoregulatory genes function together in a network to orchestrate transendothelial migration and antigen presentation in resident leukocytes in adipose tissue from insulin resistant subjects. We found that the activation of pro-inflammatory pathways correlated with the degree of insulin resistance in our subjects. Furthermore, TZD-mediated repression of inflammatory genes in adipose tissue was relative to TZD-induced insulin sensitization of the subjects, i.e., TZD-induced repression was greater in responder than in non-responder subjects. Notably, markers of

macrophage infiltration were most robust in non-responder subjects before TZD treatment and may play a role in making insulin-resistance more refractory to TZD treatment.

Decreased mitochondrial capacity, gene expression, and mass are observed in adipose tissue from insulin resistant humans and rodents and are improved after TZD treatment [45, 57, 60-63]. Our studies of subcutaneous adipose tissue extend previous findings and show that fatty acid and BCAA oxidation, TCA cycle, and oxidative phosphorylation pathways are down-regulated in proportion to insulin resistance, i.e., TZD-induced insulin sensitization was positively correlated with expression of genes regulating mitochondrial activity. Our findings are evidence that the magnitude of insulin resistance in insulin resistant individuals is mechanistically linked to the magnitude of dysfunctional mitochondrial capacity driving pathogenic lipotoxicity, futile triacylglycerol cycling, and generation of reactive oxygen species.

Clinical or transcriptional signatures that differentiate insulin-resistant TZD responder and non-responder subjects have not heretofore been characterized. We have identified novel distinctions between TZD responders and non-responders and have identified gene expression predictors of TZD-mediated insulin sensitization. In skeletal muscle, insulin resistant responder subjects exhibited greater post-TZD normalization of insulin-induced glycolytic flux than insulin resistant non-responder subjects, indicating that responders recover metabolic flexibility as they become more insulin sensitive. This may be due to their higher pre-TZD expression level of MLXIP which was predictive of post-TZD insulin sensitization. MLXIP is a metabolic sensor that shuttles between mitochondria and the nucleus where it is a transcription factor activating HK2 and other

glycolytic target genes [56]. In adipose tissue, pre-TZD HLA-DRB1 expression was correlated with improved insulin sensitivity after TZD treatment. Expression of HLA-DRB1, an antigen-presenting cell gene, might be mechanistically involved in determining the dichotomous anti-inflammation and insulin sensitization responses exhibited by TZD-treated responder and non-responder subjects in our study.

In conclusion, this study brings new light to system-wide mechanistic differences between normal and insulin-resistant subjects and uniquely identifies transcriptional signatures that differentiate insulin-resistant TZD responder from non-responder subjects.

E. Methods

Human subject studies

Our subject cohort includes subjects from three clinical studies. The pioglitazone study included eight NR_d subjects (age 42 ± 5 [SE] yr, BMI 23.1 ± 0.6 [SE] kg/m^2) and 17 IR_d subjects (age 51 ± 2 yr, BMI 36.4 ± 1.5 kg/m^2). The rosiglitazone study included 19 IR_d subjects (age 52 ± 2 yr, BMI 35.6 ± 1.4 kg/m^2). The troglitazone study included 11 NR_d subjects (age 48 ± 2 yr, BMI 25.8 ± 1.2 kg/m^2) and 17 IR_d subjects (age 50 ± 2 yr, BMI 34.4 ± 1.3 kg/m^2). At baseline, each subject underwent a 5 hr 60-80 mU/m^2/min hyperinsulinemic-euglycemic clamp (23,29). After completing the baseline studies, all subjects were treated for 12 wk with pioglitazone (45 mg daily), rosiglitazone (4 mg twice daily), or troglitazone (600 mg daily). Needle biopsies of abdominal subcutaneous adipose tissue were taken in the basal state, before each clamp. Needle biopsies of vastus lateralis skeletal muscle were taken in the basal state (before each clamp) and the insulin-stimulated state (immediately before termination of each hyperinsulinemic-euglycemic

clamp). Biopsies were flash-frozen in liquid nitrogen and stored at -80^{o}C. A schematic of the biopsy, clamp, and TZD treatment study design is shown in Figure 8a. The experimental protocol was approved by the by the Institutional Review Board for Human Subjects of the University of California, San Diego. The methods used for hyperinsulinemic-euglycemic clamps were performed as described previously (29-32). All subjects were volunteers, generally healthy with normal liver and kidney function. Exclusion criteria were active cardiac, liver, or renal disease or long-term complications from diabetes. None of the non-diabetic subjects were taking medications that alter glucose tolerance. Diabetic subjects taking anti-diabetes medications (sulfonylurea or metformin) were asked to discontinue their medications for at least 2 wk prior to initiating their baseline studies. None were previously receiving TZD therapy. All subjects received nutrition counseling regarding diet regulation during the studies.

Hyperinsulinemic-euglycemic clamps

Baseline blood samples were drawn and hyperinsulinemic-euglycemic clamps were performed in the morning after a 10 hr overnight fast, as previously described [64, 65]. The rates of total glucose appearance and disposal (R_d) were calculated from the tracer [3-^{3}H]-glucose data using the non–steady-state equations of Steele [66]. A distribution volume of 0.19 L/kg and pool fraction of 0.5 were used in the calculations [67]. Exogenous glucose infusion (Ginf) rates were used as an approximation for R_d for 10 subjects (five NR_d and five IR_d) because a defective tracer batch prevented calculation of R_d. Ginf rates are approximately equal to R_d when greater than 6 mg/kg/min (8 of these 10 subjects) and slightly over-estimate R_d when very low (2 of these 10 subjects).

Plasma FFA levels were determined using an acyl-CoA oxidase–based colorimetric kit (NEFA-C; Wako, Richmond, VA) with intra- and inter-assay coefficients of variation (CVs) of 2.4 and 3.3%, respectively. Plasma insulin was measured by a double-antibody technique [68]. The intra- and inter-assay CVs were 3.7 and 9.2%, respectively.

Microarray studies

We generated gene expression profiles from tissue biopsy RNA using Affymetrix Human Genome U133 Plus 2.0 oligonucleotide microarrays (Affymetrix, Inc., Santa Clara, CA). RNA from 364 adipose tissue and skeletal muscle biopsies was isolated and gene expression patterns in each sample were determined using Affymetrix Human Genome U133 Plus 2.0 oligonucleotide microarrays (Affymetrix, Inc., Santa Clara, CA) which include >47,000 transcript features. Total RNA samples were isolated and processed as recommended by Affymetrix, Inc. (Affymetrix GeneChip® Expression Analysis Technical Manual) from 50-100mg of tissue using TRIzol Reagent (Invitrogen Corp., Carlsbad, CA). RNA concentrations were adjusted to a final concentration of 1.25 μg/μL. Further RNA processing and microarray analyses were conducted at the UCI DNA & Protein MicroArray Facility, University of California, Irvine. RNA samples were quality assessed prior to beginning target preparation/processing steps by running out a small amount of each sample (typically 25-250 ng/well) onto a RNA Lab-On-A-Chip (Caliper Technologies Corp., Mountain View, CA) that was evaluated on an Agilent Bioanalyzer 2100 (Agilent Technologies, Palo Alto, CA). Single-stranded, then double-stranded cDNA was synthesized from the poly(A)+ mRNA present in the isolated total RNA (typically 10 μg total RNA starting material each sample reaction) using the

SuperScript Double-Stranded cDNA Synthesis Kit (Invitrogen Corp.) and poly (T)-nucleotide primers that contained a sequence recognized by T7 RNA polymerase. A portion of the resulting ds cDNA was used as a template to generate biotin-tagged cRNA from an *in vitro* transcription reaction (IVT), using the Affymetrix GeneChip® IVT Labeling Kit. 15 μg of biotin-tagged cRNA was fragmented (average length 100 bases, range 35-200 bases) following prescribed protocols (Affymetrix GeneChip® Expression Analysis Technical Manual). 10 μg of fragmented target cRNA was hybridized (45°C with rotation for 16 hr, Affymetrix GeneChip® Hybridization Oven 640) to probe sets present on an Affymetrix Human Genome U133 Plus 2.0 array. The GeneChip® arrays were washed and stained (SAPE, streptavidin-phycoerythrin) on an Affymetrix Fluidics Station 450, then scanned on a GeneChip® Scanner 3000. Hybridization results were quantified and analyzed using GCOS 1.2 software (Affymetrix, Inc.) using default values (Scaling, Target Signal Intensity = 500; Normalization, All Probe Sets; Parameters, all set at default values). Gene expression levels, expressed as average difference scores, were determined using Affymetrix MAS 5.0 software. Semi-quantitative RT-PCR evaluation of several differentially expressed genes correlated with validated microarray expression data (r_{avg}=0.83, r_{range}=0.68-0.98).

Statistical analyses

Clinical characteristics data were analyzed using Student's t test (paired and unpaired, as appropriate) and a statistical cutoff of $p<0.05$. We applied our Variance Modeled Posterior Inference with Regional Exponentials (VAMPIRE) [25] microarray analysis web suite [22] to the gene expression data to identify significant differences

between gene expression profiles from the subject groups. We identified statistically enriched of Gene Ontology (ver. 200704) functional annotation terms in expression data sets using GOby [22]. We used variance-balanced regression and Pearson correlation coefficients to conduct our regression analyses. Variance-balanced regression is a weighted least squares method where the weights are based on the inverse of the estimate of variance, as computed by VAMPIRE. We conducted two regression line comparisons using the F-test statistic for coincidence of two regression lines [69]. We used the Chi-square test statistic where indicated. We corrected for family-wise error associated with multiple comparisons (accounting for the number of probe sets or genes examined) using the stringent Bonferroni correction at a 5% significance level cutoff (α_{Bonf} =0.05).

F. Acknowledgements

We acknowledge Dr. J. Denis Heck, Sriti Misra, and Lana Bordcosh at the UCI DNA & Protein MicroArray Facility, University of California, Irvine for conducting the RNA microarray analyses and Jerrold Olefsky for support in the study, interpretation and manuscript preparation. Funding was provided by NIH NIDDK K01-DK62025 (DDS), the Eunice Kennedy Shriver NICHD/NIH cooperative agreement [U54-HD012303] as part of the Specialized Cooperative Centers Programs in Reproduction and Infertility Research (JMO, JGY, CHC), NIH P01-DK074868 (DDS, JMO, JGY, CHC), NIH R01-DK033651 (JMO, JGY, CHC), NHLBI R33-HL087375 (SS), NIGMS U54-GM69338(SS), NIDDK P01-DK074868(SS), and the University of California Discovery Program Project #bio03-10383 with matching funds from Pfizer, Inc. (DDS, JGY, CHC, SS).

This chapter, in full, is a reprint of the material as it appears in Proceedings of the National Academy of Sciences of the United States of America 2009, Sears, Dorothy D.; Hsiao, Gene; Hsiao, Albert; Yu, J.G.; Courtney, C.H.; Ofrecio, Jachelle M.; Chapman, Justin; Subramaniam, Shankar. "Mechanisms of human insulin resistance and thiazolidinedione-mediated insulin sensitization", Proc. Natl. Acad. Sci. USA 2009 Nov 3;106(44):18745-50. Epub 2009 Oct 19. The dissertation author was the second author on this work, responsible for developing the statistical methodology, data analysis and curation, pathway and network analyses and manuscript preparation.

G. Appendix

Dataset S1: Clinical characteristics.

Dataset S2: Differential gene expression in skeletal muscle; Insulin-induced gene expression in skeletal muscle; Differential expression of adipocyte genes in skeletal muscle

Dataset S3: Correlations between pre-TZD gene expression and R_d or R_dFrac

Dataset S4: Differential gene expression in adipose tissue; Macrophage-associated genes overexpressed in adipose tissue and repressed after TZD-treatment; Inflammation-associated genes overexpressed in non-responders (IR_d-) but not responders (IR_d+) after TZD-treatment

Dataset S5: Comprehensive differential gene expression table

Dataset S6: Adipose tissue GOby reports

Dataset S7: Correlations between adipose tissue gene expression and R_d

Figure S1: Overall down-regulation of insulin signaling pathways by insulin-induced gene expression changes in skeletal muscle.

Figure S2: Post-TZD inflammatory marker over-expression in adipose tissue of non-responder insulin resistant (IR_d-) subjects.

Figure S3: A model of skeletal muscle adiposity in IR_d+ subjects.

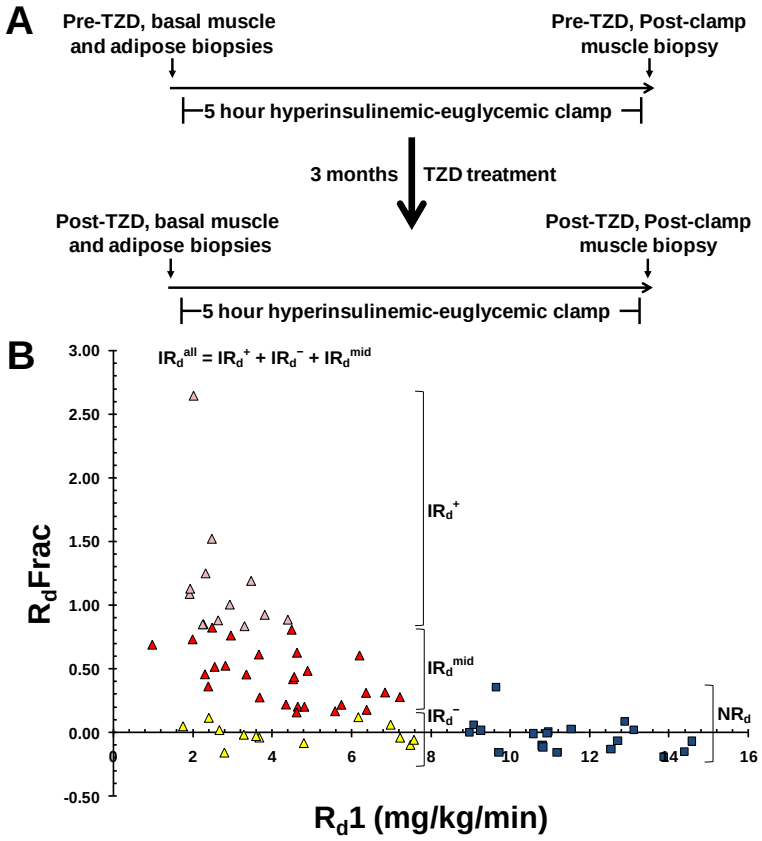

Figure 8: Study design and subject insulin sensitivity distribution.
(a) Schematic of human insulin-resistance study. (b) Distribution of baseline insulin sensitivity and TZD-mediated insulin sensitization response of study subjects. NR_d (insulin sensitive subjects with normal R_d, >8mg/kg/min, blue square symbols), IR_d^{all} (insulin resistant subjects with impaired R_d, <8mg/kg/min, triangle symbols), IR_d+ (subgroup of insulin resistant subjects that are TZD responders, in upper quartile of post-TZD fractional R_d change, pink triangles), IR_d^- (subgroup of insulin resistant subjects that are TZD non-responders, in bottom quartile of post-TZD fractional R_d change, yellow triangles), IR_d^{mid} (subgroup of insulin resistant subjects in the middle two quartiles of post-TZD fractional R_d change, red triangles). R_dFrac – fractional R_d change $[(R_d2- R_d1)/ R_d1]$.

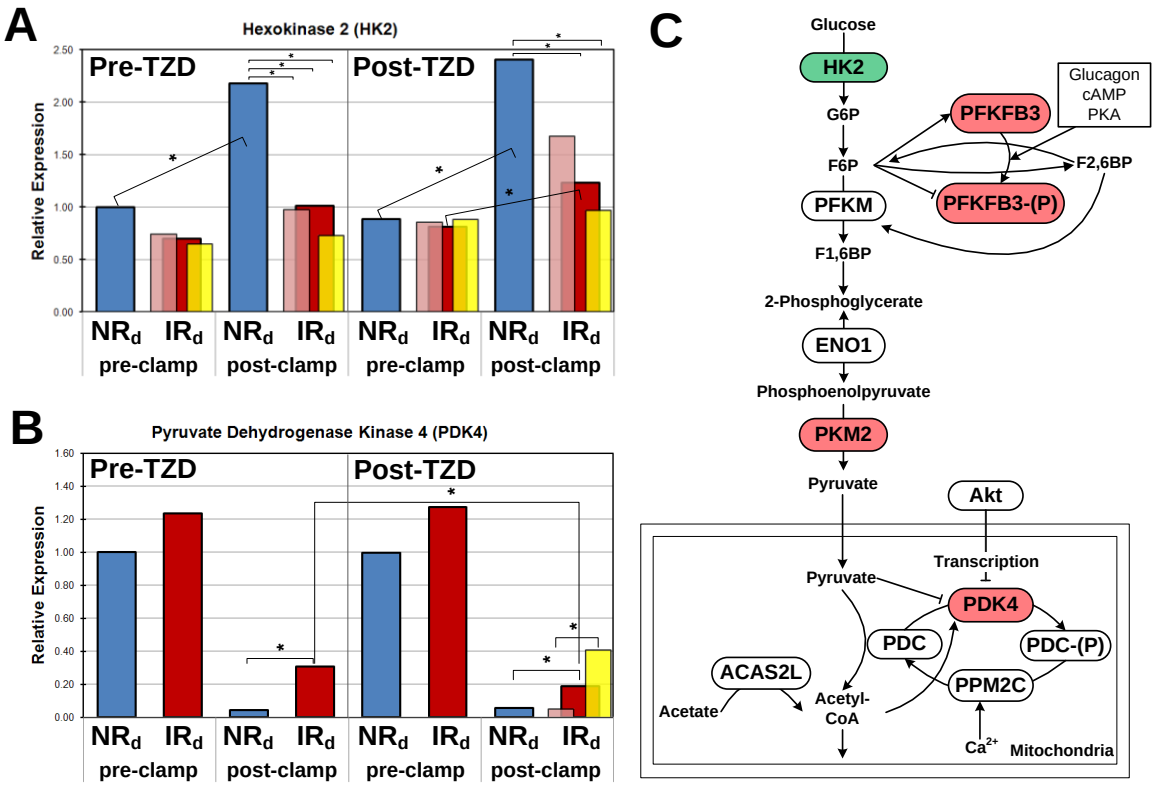

Figure 9: Differential expression of glucose metabolism genes in skeletal muscle. (a)-(b) Pre- and post-clamp HK2 and PDK4 expression data from the subject groups before and after TZD treatment are shown. (a) Insulin-activated expression of HK2 in NR_d subjects was completely blocked in IR_d^{all} subjects. After TZD-treatment, this defect was improved in IR_d^{all} subjects, normalized in IR_d+ subgroup subjects and unaffected in IR_d^- subgroup subjects. (b) Insulin-induced repression of PDK4 expression in NR_d subjects was blunted in IR_d^{all} subjects. After TZD-treatment, this defect was improved in IR_d^{all} subjects, normalized in IR_d+ subgroup subjects and unaffected in IR_d^- subgroup subjects. NR_d (blue), IR_d^{all} (red), IR_d+ subgroup (pink), IR_d^- subgroup (yellow). (c) Glycolysis schematic highlighting defectively regulated genes by insulin in IR_d^{all} subjects compared to NR_d subjects before TZD treatment. Green fill indicates significantly blunted insulin-induced expression in IR_d^{all} subjects, resulting in low post-clamp expression. Red fill indicates significantly blunted insulin-repressed expression in IR_d^{all} subjects, resulting in high post-clamp expression. *Indicates statistically significant difference between bracketed groups (α_{bonf}=0.05).

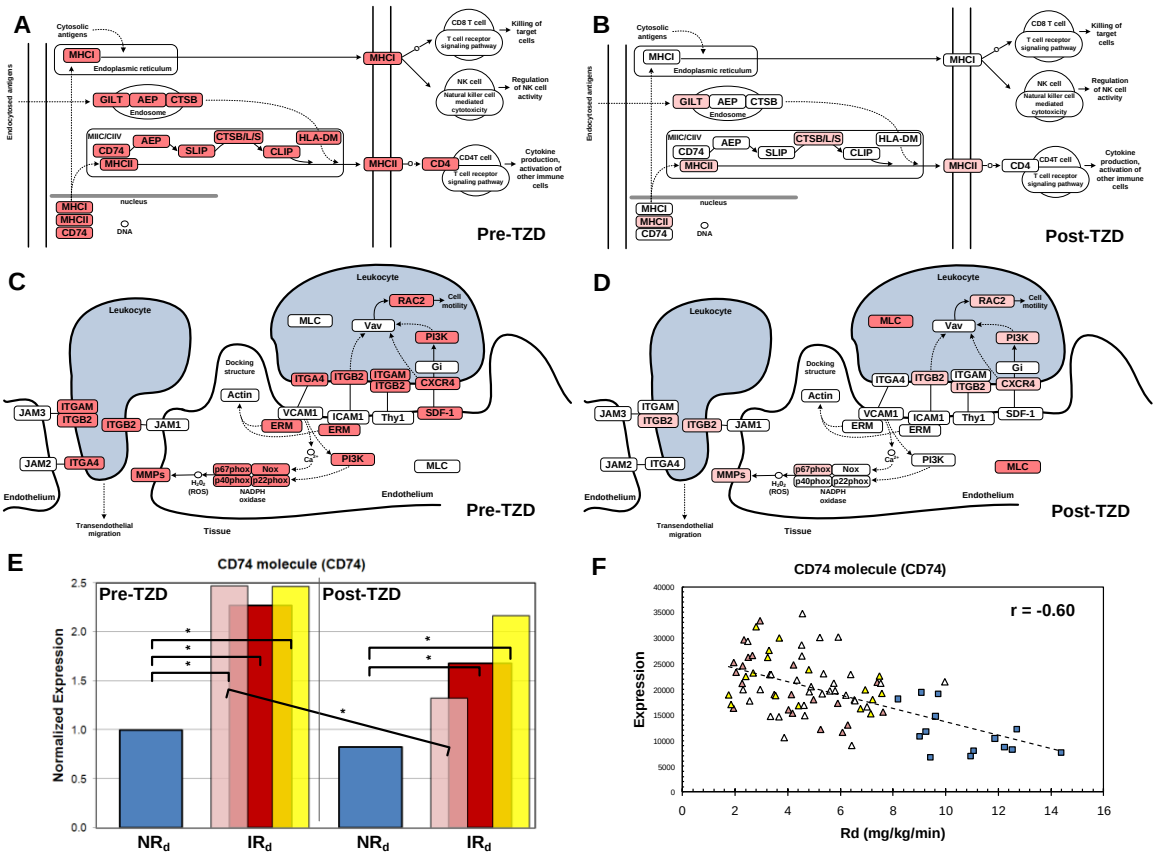

Figure 10: Inflammatory marker expression in adipose tissue of insulin resistant subjects. (a-b) Schematics of the antigen processing and presentation pathway highlighting genes that are (a) over-expressed in IR_d^{all} subjects before TZD treatment and (b) down-regulated in IR_d+ subjects after TZD treatment. (c-d) Schematics of the leukocyte transendothelial migration pathway that highlight genes that are (c) over-expressed in IR_d^{all} subjects before TZD treatment and (d) down-regulated in IR_d+ subjects after TZD treatment. White ovals -- genes not differentially expressed between NR_d and IR_d^{all} (a&c) or IR_d+ (b&d) subjects. Red ovals -- genes significantly over-expressed between NR_d and IR_d^{all} (a&c) or IR_d+ (b&d) subjects. Pink ovals -- genes still significantly over-expressed in IR_d+ subjects compared to NR_d subjects, but are significantly down-regulated compared to pre-TZD levels. Schematics are adapted from KEGG. (e) CD74 was significantly over-expressed in all IR_d subject groups compared to NR_d subjects. After TZD treatment, CD74 expression was significantly down-regulated in IR_d+ subgroup subjects (pink), but not in IR_d^{all} subjects (red) or IR_d^- subgroup subjects (yellow). *Indicates statistically significant difference between bracketed groups (α_{bonf}=0.05). (f) Negative correlation between CD74 expression and Rd (r=-0.59). Graph includes pre- and post-TZD treatment data. IR_d^{all} subjects (pink, red, and yellow triangles). IR_d+ subgroup subjects (pink), IR_d^- subgroup subjects (yellow), IR_d^{mid} subgroup subjects (red).

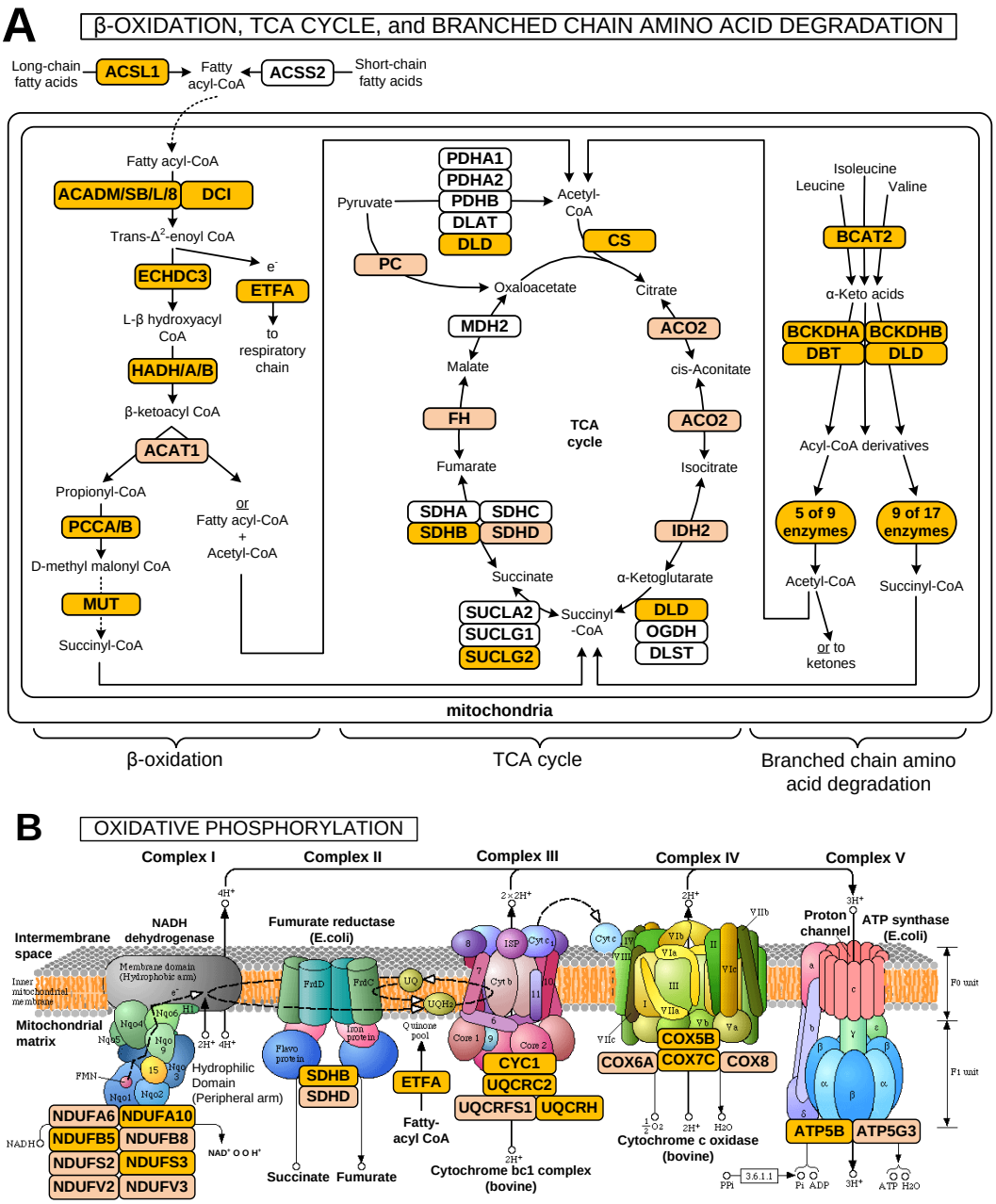

Figure 11: Mitochondrial metabolic function in adipose tissue is correlated with insulin sensitivity.

Schematics of mitochondrial metabolic pathways highlighting genes whose adipose tissue expression (before and after TZD treatment) was positively correlated with R_d. (a) β-oxidation of fatty acids, TCA cycle, and branched chain amino acid degradation. (b) Oxidative phosphorylation. Dark orange ovals -- genes with expression vs. R_d correlations of $r > 0.5$. Light orange ovals -- genes with expression vs. R_d correlations of $r = 0.45 – 0.50$.

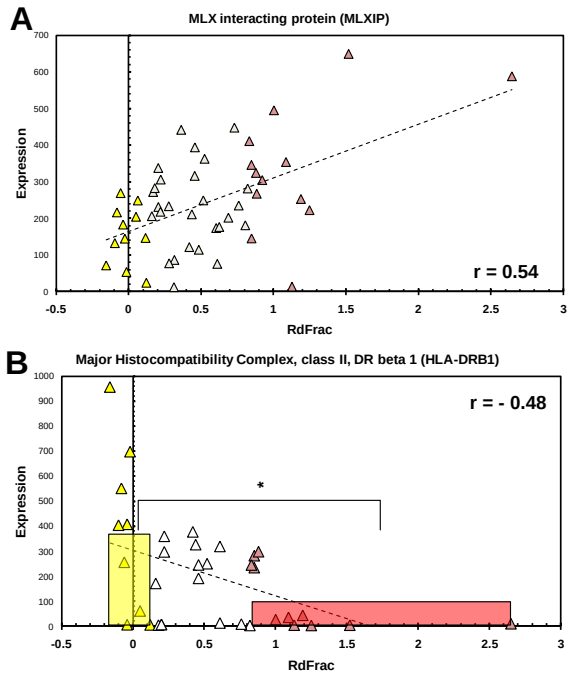

Figure 12: Gene expression predictors of TZD-mediated insulin sensitization.
(a) Expression of MLXIP in pre-TZD skeletal muscle was positively correlated with fractional R_d change in IR_d^{all} subjects (r=0.54) and significantly higher in IR_d+ vs IR_d^- subjects. (b) Expression of HLA-DRB1 in pre-TZD, basal adipose tissue was negatively correlated with fractional R_d change in IR_d^{all} subjects (r=-0.47) and significantly lower in IR_d+ vs IR_d^- subjects. Bars indicate the expression mean and range of fractional R_d change for the IR_d+ (red) and IR_d^- (yellow) subject groups. IR_d^{all} subjects (pink, red, and yellow triangles), IR_d+ subgroup subjects (pink), IR_d^- subgroup subjects (yellow), IR_d^{mid} subgroup subjects (red).

Dataset S1: Clinical characteristics.

Values are mean±SEM. R_d, rate of glucose disposal. NR_d, normal rate of glucose disposal, insulin sensitive subjects. IR_d, impaired rate of glucose disposal, insulin resistant subjects. IR_d^{all}, all insulin resistant subjects. IR_d+, insulin resistant TZD responder subgroup subjects. IR_d^-, insulin resistant TZD non-responder subgroup subjects. R_dDiff, differential improvement in R_d (R_d2- R_d1). R_dFrac, fractional R_d change (R_d2- R_d1/ R_d1). A1c, glycosylated hemoglobin. FPG, fasting plasma glucose. FFA, fasting plasma free fatty acids. * significant (t-test) vs. NR_d subjects. † significant (t-test) vs. IR_d^- group. ‡ significant (paired t-test) vs. post-Rx levels. Rx – TZD treatment.

Characteristics	Subject group			
	NR_d	IR_d^{all}	IR_d+	IR_d−
Gender (male/female)	16/3	44/9	9/4	11/2
Age (years)	45 ± 3	51 ± 1*	53 ± 2*	49 ± 2
Rd1, pre-Rx (mg/kg/min)	11.4 ± 0.4	4.0 ± 0.2*	2.8 ± 0.2*†	4.6 ± 0.6*
Rd2, post-Rx (mg/kg/min)	11.0 ± 0.4	5.6 ± 0.3*‡	5.8 ± 0.4*‡	4.6 ± 0.6*
RdDiff (mg/kg/min)	-0.41 ± 0.31	1.59 ± 0.19*	3.06 ± 0.29*†	-0.07 ± 0.11
RdFrac (unitless)	-0.03 ± 0.03	0.50 ± 0.07*	1.16 ± 0.14*†	-0.01 ± 0.02
A1c, pre-Rx (%)	5.3 ± 0.1	7.2 ± 0.2*	6.9 ± 0.2*	7.3 ± 0.5*
A1c, post-Rx (%)	5.5 ± 0.1‡	7.3 ± 0.3*	6.7 ± 0.3*	7.4 ± 0.4*
BMI, pre-Rx (kg/m^2)	24.6 ± 0.8	35.5 ± 0.8*	38.1 ± 1.4*	35.1 ± 1.5*
BMI, post-Rx (kg/m^2)	24.9 ± 0.9	35.8 ± 0.9*	38.8 ± 1.4*‡	35.9 ± 1.7*
FPG, pre-Rx (mg/dL)	88.6 ± 1.4	158.1 ± 8.8*	160.0 ± 14.1*	171.4 ± 20.7*
FPG, post-Rx (mg/dL)	86.7 ± 1.3	133.1 ± 6.6*‡	124.6 ± 10.1*‡	145.2 ± 14.4*‡
Insulin, pre-Rx (mU/mL)	8.3 ± 1.4	20.5 ± 1.6*	21.1 ± 1.9*	19.0 ± 2.6*
Insulin, post-Rx (mU/mL)	7.6 ± 1.6	14.8 ± 1.2*‡	14.4 ± 1.8*‡	16.8 ± 3.0*
FFA, pre-Rx (mmol/L)	0.38 ± 0.03	0.57 ± 0.03*	0.66 ± 0.06*	0.50 ± 0.05*
FFA, post-Rx (mmol/L)	0.39 ± 0.03	0.49 ± 0.03‡	0.58 ± 0.05*†‡	0.39 ± 0.03‡

Values are Mean ± SEM. Rd, rate of glucose disposal.
NRd, normal rate of glucose disposal, insulin sensitive subjects.
IRd, impaired rate of glucose disposal, insulin resistant subjects.
IR_d^{all}, all insulin resistant subjects.
IR_d+, insulin resistant TZD responder subgroup subjects.
IR_d-, insulin resistant TZD non-responder subgroup subjects.
RdDiff, differential improvement in Rd (Rd2 - Rd1).
RdFrac, fractional Rd change (Rd2 - Rd1/ Rd1).
A1c, glycosylated hemoglobin.
FPG, fasting plasma glucose.
FFA, fasting plasma free fatty acids.
* significant (t test) vs. NRd subjects.
† significant (t test) vs. IRd- group.
‡ significant (paired t test) vs. post-Rx levels. Rx – TZD treatment.

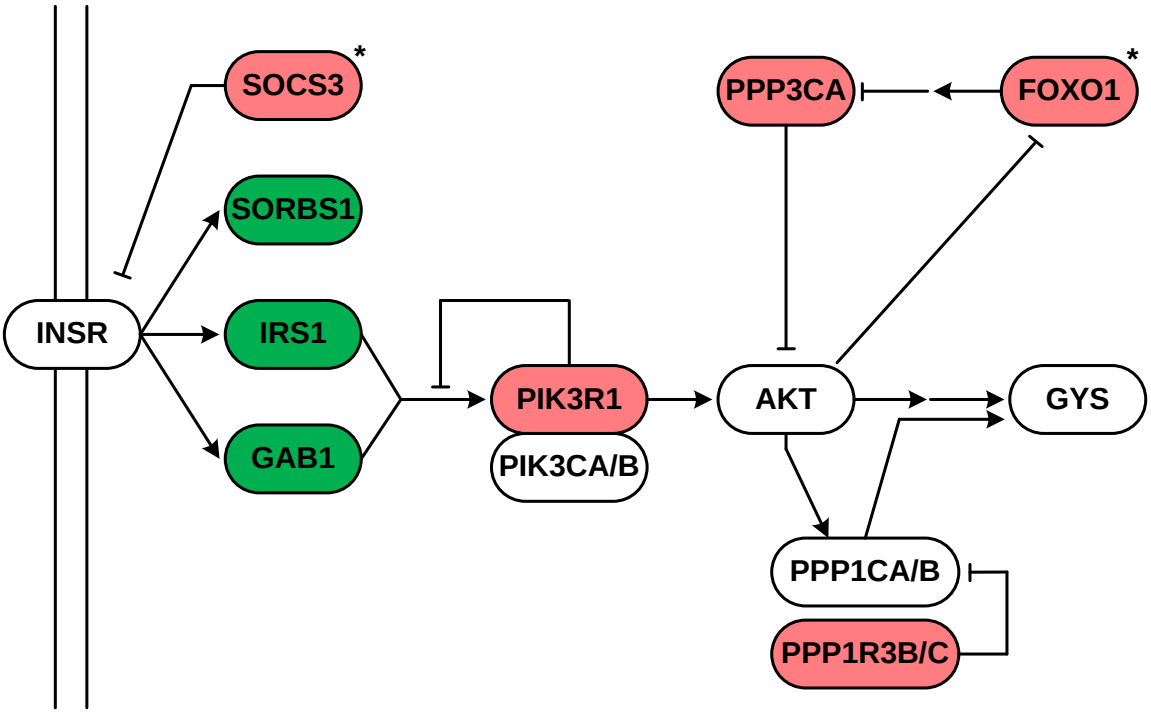

Figure S1: Overall down-regulation of insulin signaling pathways by insulin-induced gene expression changes in skeletal muscle. An abbreviated schematic of insulin signaling is shown. In response to insulin, genes encoding multiple primary substrates of the insulin receptor are down-regulated and inhibitory signaling components up-regulated. Green ovals indicate genes that were repressed after hyperinsulinemic euglycemic clamp, red ovals indicate genes that were activated after hyperinsulinemic euglycemic clamp, white ovals indicate no insulin-induced expression change (α_{bonf}=0.05). Asterisks indicate insulin-induced gene expression changes that were up-regulated but significantly blunted in IR_d^{all} subjects compared to NR_d subjects (α_{bonf}=0.05). Expression patterns of the remaining genes were not significantly different between IR_d^{all} and NR_d subjects.

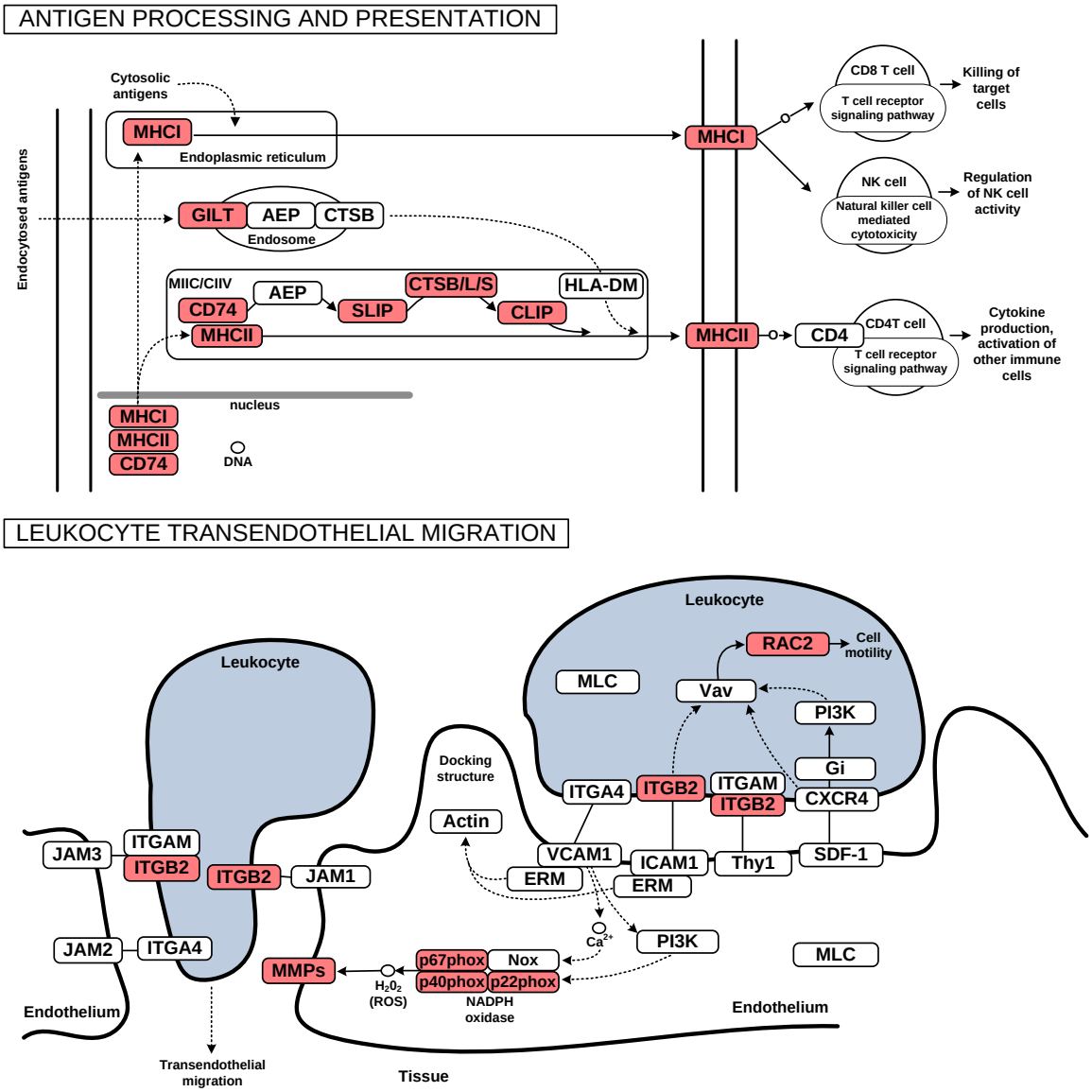

Figure S2: Post-TZD inflammatory marker over-expression in adipose tissue of non-responder insulin resistant (IR_d-) subjects. Schematics of the (a) antigen process and presentation and (b) leukocyte transendothelial migration pathways highlighting genes that are still over-expressed in IR_d- subjects after TZD-treatment. White ovals indicate genes that are not differentially expressed between NR_d and IR_d- subjects. Red ovals indicate genes significantly over-expressed in IR_d- subjects compared to NR_d subjects (α_{bonf}=0.05). Schematics are adapted from KEGG.

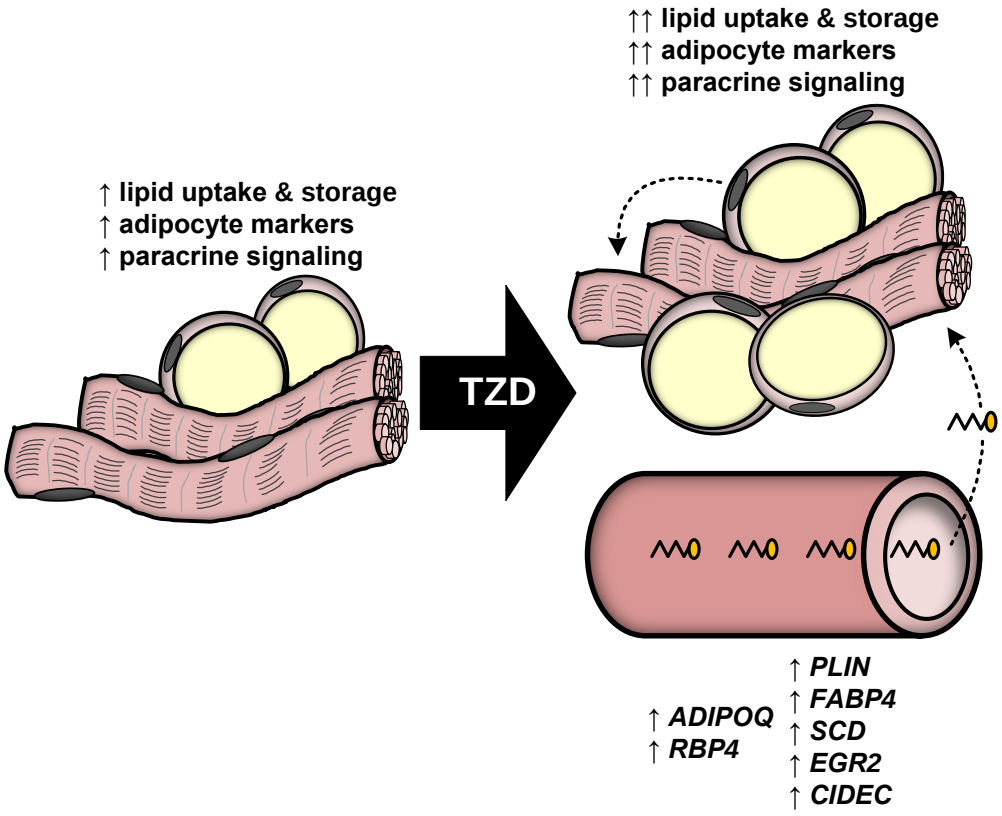

Figure S3: A model of skeletal muscle adiposity in IR_d+ subjects. The transcriptional signature of skeletal muscle from IR_d+ subjects was characterized by over-expression of specific adipocyte markers, including those involved in lipid uptake/storage and paracrine signaling which were coordinately maintained or further enhanced after TZD-mediated insulin sensitization in IR_d+ subjects. These post-TZD changes were significantly blunted in IR_d^- subjects, suggesting that increased lipid uptake/storage and myocyte-adipocyte crosstalk are associated with TZD-mediated insulin sensitization.

IV.

Multi-tissue, selective PPARγ modulation of insulin sensitivity in obese rats

A. Abstract

Peroxisome proliferator-activated receptor gamma (PPARγ) ligands, including the insulin-sensitizing thiazolidinedione drugs, transcriptionally regulate hundreds of genes. Little is known about the relationship between PPARγ ligand-specific modulation of cellular mechanisms and insulin sensitization. We characterized the insulin sensitivity and multi-tissue gene expression profiles of lean and insulin resistant, obese Zucker rats untreated or treated with one of four PPARγ ligands (pioglitazone, rosiglitazone, troglitazone, and AG035029). We analyzed the transcriptional profiles of adipose tissue, skeletal muscle, and liver from the rats and determined whether ligand insulin-sensitizing potency was related to ligand-induced alteration of functional pathways. Ligand treatments improved insulin sensitivity in obese rats, albeit to varying degrees. Adipose tissue profiles revealed ligand-selective modulation of inflammatory and branched chain amino acid (BCAA) metabolic pathways which correlated with ligand-specific insulin-sensitizing potency. Skeletal muscle profiles showed that insulin resistance was associated with increased expression of adipocyte and slow-twitch fiber markers, a pattern that was augmented similarly in all the ligand-treated groups. Although PPARγ ligand treatments heterogeneously improved dysregulated expression of cholesterol and fatty acid biosynthetic pathways in obese rat liver, these alterations were not correlated with ligand insulin-sensitizing potency. PPARγ ligand-specific insulin-sensitizing potency correlated with modulation of adipose tissue inflammatory and BCAA metabolic pathways, suggesting a functional relationship between these pathways and whole-body

insulin sensitivity. Other PPARγ ligand-induced functional pathway changes were detected in adipose tissue, skeletal muscle and liver profiles but were not related to degree of insulin sensitization.

B. Introduction

Insulin resistance is a pathophysiological state in which the intracellular signaling actions of insulin are blunted. It is manifested in multiple insulin target tissues, including adipose tissue, skeletal muscle, and liver. Each tissue must respond to insulin with specific metabolic outcomes in order to maintain normal glycemia and lipidemia. Altered expression of cellular components that ensure insulin's tissue-specific metabolic outcomes is known to affect insulin sensitivity, however, the exact changes in gene expression that induce insulin resistance are unknown. Thiazolidinediones (TZDs) are clinically potent insulin sensitizing drugs. These compounds are ligands of and alter gene transcription via the nuclear receptor peroxisome proliferator-activated receptor gamma (PPARγ). PPARγ and its ligands are transcriptionally active in insulin target tissues (liver, adipose, muscle, macrophages). Studies of tissue-specific PPARγ knockout mice and in insulin resistant, obese Zucker fa/fa rats show that PPARγ regulates metabolism and insulin action in each of these tissues [70]. Although hundreds of TZD target genes have been identified, it is unclear which TZD-induced gene expression changes specifically induce insulin sensitization. The coordinated functional and metabolic pathway changes that occur as a consequence of gene expression change during insulin sensitization have also not been characterized.

Insulin target tissues depend on PPARγ for their proper metabolic functions. Ordinarily, this is modulated by tissue-specific endogenous ligands and transcriptional regulators, resulting in tissue-specific PPARγ-regulated expression profiles. Thus, tissue-specific PPARγ target gene regulation is coordinated to maintain whole body insulin sensitivity and normal metabolic homeostasis. PPARγ can bind to and is differentially regulated by many synthetic and natural ligands. Binding of various ligands induces ligand-specific 3-dimensional structures to PPARγ, conferring ligand-specific interactions of PPARγ with transcriptional regulators and DNA, and imparting ligand-specific transcriptional activity [5-8]. This concept is described by the SPPARM (selective PPAR modulator) model [47]. Some insulin-sensitizing PPARγ ligands are full agonists, activating transrepression and transactivation [71], some are primarily partial agonists, e.g., activating transrepression only [72].

We have shown in insulin resistant human subjects that TZDs improve dysregulated expression of genes involved in specific skeletal muscle and adipose tissue metabolic pathways and, further, that some of these pathway changes correlate with improved insulin sensitivity [73]. We now report similar studies in insulin resistant, obese, non-diabetic Zucker rats (*fa/fa*). Additionally, we show that the SPPARM concept can be manifested *in vivo*, demonstrating for the first time that ligand-selective PPARγ modulation of insulin sensitivity correlates with ligand-selective alteration of inflammatory and branched chain amino acid metabolic pathway expression in adipose tissue.

C. Materials and Methods

Animal studies.

Male Zucker fatty (fa/fa) and lean (fa/+) rats (Charles River, Wilmington, MA) were received at 6 weeks of age, housed individually under controlled light (12:12 light:dark) and climate conditions, and had free access to food and water. All procedures were performed in accordance with the *Guide for Care and Use of Laboratory Animals* of the National Institutes of Health and were approved by the University of California, San Diego, Animal Subjects Committee. Fatty rats were weight-matched upon arrival and randomly divided into one of five experimental groups. The fatty rat groups varied by the type of chow they were fed - normal chow alone or with a PPARγ ligand admixture: normal chow (fatty control, FC), rosiglitazone-treated (2 mg/kg/day), pioglitazone-treated (10 mg/kg/day), troglitazone-treated (200 mg/kg/day), or AG035029-treated, (10 mg/kg/day). Drug doses are all in the lower range of efficacy in humans and rodents models. AG035029 [74] is an experimental PPARγ-specific ligand obtained from Pfizer, Inc., La Jolla, CA. Lean control (LC) rats were all fed normal chow. Rats groups were maintained on the diets for 21 days (12-15 rats per group), after which half of each group was subjected to clamp and tissue harvest (below) and the other half was used for tissue harvest only.

Hyperinsulinemic-euglycemic clamp and microarray studies.

We evaluated the insulin sensitivity of rats from each experimental group using the hyperinsulinemic euglycemic clamp procedure, as previously described [75]. Clamps were conducted at nine weeks of age. Four days prior to clamp, rats were anesthetized with inhaled isoflurane (to allow rapid recovery since little anesthetic is stored in fat

tissue), then cannulated in the jugular vein for infusion of glucose, tracer, and insulin (dual cannula; Dow Corning; silastic, ID=0.03 cm) and the carotid artery (PE-50; Clay Adams) for blood sampling. Cannulas were tunneled subcutaneously, exteriorized at the back of the neck, and encased in silastic tubing (0.2 cm ID) sutured to the skin [75]. Rats were given four days to recover from surgery prior to undergoing clamp procedure. They continued to receive their assigned study chow during the recovery and were fasted 12 hr prior to the clamp procedure. Ninety minutes before the clamp, rats were weighed and placed in a modified metabolic chamber. Basal blood samples were drawn at –60 and 0 min. After the –60 min sampling, a priming dose of 5 μCi D-[3-^{3}H] glucose (New England Nuclear, Boston, MA) was administered. This was followed by a constant infusion of radioisotope tracer of 0.16 μCi/min. After 60 min of tracer equilibration, blood samples were again obtained (t=0 min) and a variable infusion of glucose (50% dextrose; Abbott Laboratories) was begun along with insulin (25 mU x kg^{-1} x min^{-1}, Novlin R; Novo Nordisk, Copenhagen) and continued infusion of tracer (0.16 μCi/min). Blood samples (0.2 ml) were drawn at 10 min intervals and immediately analyzed for glucose throughout the duration of the glucose clamp. Whole blood glucose concentrations were measured in duplicate. Larger blood samples were taken for determining tracer specific activity. Plasma was frozen for subsequent analysis of insulin, free fatty acids (FFA), and glucose at –60 min, 0 min, and upon completion of the clamp experiment. Rats were then administered a lethal injection of sodium pentobarbital (100 mg/kg; Nembutal; Abbott Laboratories), and tissues were excised, flash-frozen in liquid nitrogen, and stored at -80^{o} C for subsequent *in vitro* analyses.

Biochemical analyses.

Whole blood glucose concentrations were determined using the HemoCue™ glucose analyzer (Angelholm, Sweden). Plasma insulin was measured via radioimmunoassay kit (Linco Research, St. Charles, MO). Plasma glucose specific activity was measured in duplicate after deproteinization with zinc sulfate and barium hydroxide. Plasma FFA levels were measured enzymatically using a commercially available kit (NEFA C; Wako Chemicals USA, Richmond, VA). Hepatic glucose output (HGO) and glucose disposal rate (GDR) at steady state were calculated using Steele's equation [66].

Microarray studies.

Adipose tissue, skeletal muscle (gastrocnemius), and liver from unclamped rat groups (euthanized as described above) were harvested, frozen and stored as described above. Tissue RNA was isolated using Qiagen RNeasy kits (Qiagen, Inc., Valencia, CA). Biotinylated-cRNA made from pooled RNA preparations (RNA from two rats per preparation) was used to probe Affymetrix Rat Expression 230A GeneChips (Affymetrix) as per the Invitrogen protocol (Invitrogen, Inc., Carlsbad, CA), three arrays per group. Briefly, cDNA was synthesized with the SuperScript Choice system using a T7-$(dT)_{24}$ oligomer (Ambion). Biotin-labeled cRNA probes were *in vitro* transcribed using the BioArray High Yield RNA Transcript Labeling Kit (Enzo Life Sciences). Gene expression levels, expressed as average difference scores, were determined using Affymetrix MAS 5.0 software. Data files are deposited in the Gene Expression Omnibus (GEO) database as series GSE21329.

Statistical analyses.

Biochemical characteristics were analyzed using analysis of variance (ANOVA), Tukey's post hoc test, and a statistical cutoff of $p<0.05$. We applied our Variance Modeled Posterior Inference with Regional Exponentials (VAMPIRE) [25] microarray analysis web suite [22] to the gene expression data to identify statistically significant differences between rat group gene expression profiles. Variance-stabilized ANOVA (using variance estimates computed by VAMPIRE) was used to identify ligand-selective modulation of gene expression. Spearman rank correlation coefficients (ρ) were calculated to identify genes whose ligand-specific expression was correlated with the ligand's insulin-sensitizing potency. We identified significantly enriched Gene Ontology (ver. 200704) and KEGG pathway annotation terms in gene expression data sets using GOby [22]. We corrected for family-wise error associated with multiple comparisons (accounting for the number of probe sets or genes examined) using the stringent Bonferroni error rate cutoff of 5%, i.e., significance level cutoff, $\alpha_{Bonf}=0.05$.

D. Results

Characterization of lean, obese and PPARγ ligand-treated obese rats

We analyzed the whole body insulin sensitivity and tissue-specific transcriptional profiles of six age-matched Zucker rat groups – lean control (LC) rats fed normal chow and fatty rats fed normal chow (fatty control, FC) or chow containing one of four insulin-sensitizing PPARγ ligands, AG035029, pioglitazone, rosiglitazone or troglitazone, for 21 days (Methods). Physical characteristics of the rat groups are shown in Table 4. The FC

rats had significantly higher body weight, hyperinsulinemia, hypertriglyceridemia than the LC rats. Body weight of the PPARγ ligand-treated fatty rats was not significantly different from that of the FC rats. Both hyperinsulinemia and hypertriglyceridemia were significantly blunted in all the PPARγ ligand-treated groups compared to the FC rats. In fact, fasting insulin and triglyceride (TG) levels in the PPARγ ligand-treated groups were not significantly different from the LC group, although they tended to be higher. Fasting glucose levels in the FC rats tended to be higher than but were not significantly different from the LC group. AG035029- and troglitazone-treated rats exhibited significantly decreased fasting glucose levels compared to the FC group. Basal free fatty acid (FFA) levels were significantly different between the groups, with the pioglitazone- and AG035029-treated groups having the lowest average levels.

We determined the whole body insulin sensitivity of the rat groups using hyperinsulinemic euglycemic clamp studies (Table 4 and Figure 13). Both insulin-stimulated glucose disposal rate (IS-GDR) and total GDR were markedly impaired in the FC rats indicating skeletal muscle insulin resistance (compare to the LC group). Skeletal muscle insulin resistance in fatty rats was ameliorated to varying degrees by PPARγ ligand-treatment. AG035029 was significantly more potent than all the other ligands in improving insulin sensitivity in muscle and rosiglitazone had the weakest effect. Insulin sensitivity in the liver was impaired in the FC rats and was near-normal in the PPARγ ligand-treated groups. Although, basal and insulin-suppressed hepatic glucose output was not significantly different in the groups, insulin-induced suppression of TG levels at steady state during the clamp was severely blunted in the FC rats compared to the LC group. Insulin-induced TG suppression was improved and steady state TG levels

significantly reduced in each of the ligand-treated groups. Insulin-induced FFA suppression, a marker of insulin sensitivity in adipose tissue, was significantly different between the groups. Each ligand-treated group exhibited better average FFA suppression than the FC group with the AG035029-treated group exhibiting significant improvement.

Although all the PPARγ ligand treatments improved aspects of insulin resistance in the fatty rats, they did not exhibit uniform potency. We generated ligand potency rankings for each physiological characteristic by comparing the average values for each PPARγ ligand treatment (Table 4). The AG035029 treatment was the most potent modulator of every characteristic shown; the rosiglitazone treatment was the least potent for most. We sought to determine whether the insulin-sensitizing potency of the ligands was related to their transcription-altering potency in insulin-target tissues. We generated genome-wide, microarray gene expression profiles from epididymal white adipose tissue, liver, and gastrocnemius skeletal muscle harvested from each of the experimental groups. We generated lists of genes that were differentially expressed between the FC, LC, pooled PPARγ ligand treatment (Rx), and individual treatment (AG, Pio, Rosi, Tro) profiles. Next, we identified enriched gene ontology and KEGG pathway annotations associated with the differentially expressed genes. This functional analysis enabled our identification of condition-associated, transcriptional alterations in specific biochemical pathways. In addition, we identified ligand-selective modulation of gene expression in the PPARγ ligand-treated groups using an analysis of variance (ANOVA). Table 5 shows a list of each analysis' comprehensive results. Differential expression, annotation enrichment and ligand selectivity were all determined using stringent statistical tests of significance (see Methods).

Selective PPARγ ligand modulation of inflammatory markers in adipose tissue correlates with insulin sensitization

We compared adipose tissue expression profiles from lean and fatty control rats (LC vs. FC) and identified 471 differentially expressed genes (Supplementary 1.AT). Our functional analysis of this gene set identified significantly enriched biochemical pathway terms including the immune-related ontology terms "immune system process," "leukocyte mediated immunity," and others (Supplementary 2.AT). Many (47/78) of the immune-related genes were up-regulated in the FC group including activated leukocyte cell adhesion molecule (**Alcam**, 2.6-fold), **Cd24** (10.4-fold), **Cd40** (7.4-fold), protein tyrosine phosphatase receptor (**Ptprc** aka **Cd45**, 1.9-fold), and sialophorin (**Spn** aka **Cd43**, 2.6-fold). The enrichment of immune system-related genes indicates the presence of antigen-presenting cells in adipose tissue from the insulin resistant, obese rats. PPARγ ligand treatment of the obese rats induced the differential expression of 732 genes in adipose tissue. Genes down-regulated by ligand treatment included immune cell markers (**Cd68** and **Cd74)** and genes involved in macrophage transendothelial infiltration (chemokines **Ccl6, Cxcl1, Cxcl12, Cxcl14**, **Spp1**), cell adhesion (**Cd24**, **Cd44, Icam1, Lsp1**), and matrix remodeling (Mmp2) (examples in Figure 14). Over-expression of nearly all (43/47) the immune-related genes in FC rats was decreased in the ligand-treated rats. Of these 43 genes, 36 were normalized to LC group levels (examples in Figure 14, all data in Supplementary 3).

We compared the individual ligand-treated expression profiles to identify PPARγ ligand-selective gene and pathway regulation. More than 700 genes were selectively

modulated by the individual ligands (Supplementary 1.AT & Supplementary 4), meaning that their transcriptional responses to the different ligands were significantly different from one another. Functional analysis of this gene set revealed enrichment of many inflammation-related terms including the KEGG pathway term "cell adhesion molecules" and the ontology term "immune system process" (Supplementary 5), showing that the PPARγ ligand treatments modulated these biochemical pathways to varying degrees. Next, we correlated the individual ligand-treated expression profiles with their matched insulin-sensitizing potency rankings with respect to GDR and FFA suppression (Supplementary 6). We subjected the top positively and negatively correlated genes (Spearman, $|\rho|>0.79$) from each correlation to functional analysis. Immune-related ontology and KEGG terms were enriched in the list of genes negatively correlated with GDR and FFA suppression (Supplementary 7), i.e., expression of immune-related genes negatively correlated with ligand insulin-sensitizing potency. Thirty-one percent (29/93) of the immune-related genes over-expressed in FC adipose tissue and selectively-modulated by the ligands were most potently down-regulated by AG035029, the most effective muscle and adipose tissue insulin-sensitizer. Rosiglitazone, the least effective muscle and adipose tissue insulin-sensitizer, was the weakest ranking transcriptional regulator for 57% (53/93) of these genes. Single gene examples of this pattern are shown in Figure 14 (**Cd74**, **Cxcl14**, and **Spp1)**. These results suggest a functional relationship between ligand-specific insulin-sensitizing potency and modulation of inflammation-related biochemical pathways. Further, there seems to be a functional relationship between the degree of adipose tissue inflammation and the degree of insulin resistance in muscle and adipose tissue.

PPARγ ligands increase adipose tissue expression of mitochondrial metabolic pathways and modulate branched-chain amino acid metabolism with ligand-specificity

Whereas expression of immune-related genes was predominantly decreased in the adipose tissue of PPARγ ligand-treated rats, expression of genes involved in mitochondrial metabolic pathways was mostly increased (Supplementary 8). Functional analysis of the genes differentially expressed between FC and PPARγ ligand-treated rats (Supplementary 2.AT) revealed enrichment for the term "oxidative phosphorylation" (OXPHOS), represented by 33 up-regulated electron transport chain genes (Figure 15A). The terms "citrate cycle (TCA cycle)," represented by 25 genes, and "valine, leucine, isoleucine degradation" (branched chain amino acid, BCAA, degradation), represented by 22 genes, were also enriched (most of the pathway genes are represented in Figure 15B). Interestingly, none of the genes annotated with the terms OXPHOS, TCA cycle, and/or BCAA degradation (except for Me1) were differentially expressed between FC and LC rats. These pathway genes were only differentially expressed after PPARγ ligand treatment, resulting in levels exceeding those observed in LC rats (Supplementary 8).

Most PPARγ ligand-regulated genes associated with TCA cycle and OXPHOS pathways (54 of 58) were similarly modulated by the individual ligands. Only five genes were ligand-selectively modulated, one in TCA cycle and four in OXPHOS (Supplementary 8; see also three yellow-outlined ovals in Figure 15A). In contrast, the BCAA degradation pathway was markedly enriched with ligand-selectively modulated genes, 10 of 22 genes (Supplementary 8, including yellow-outlined ovals in Figure 15B),

i.e., the PPARγ ligand treatments modulated this pathway to varying degrees (see also Supplementary 8). Six of the 10 selectively-regulated, BCAA-annotated genes (**Acadsb**, **Aldh1a7**, **Aldh6a1**, **Ehhadh**, **Ivd**, and **Pcca)** were most potently regulated by AG035029, the most potent insulin-sensitizer; rosiglitazone, the least effective insulin-sensitizer, was the least potent regulator for four of the 10 genes (**Echs1**, **Ehhadh**, **Hmgcs1**, and **Pcca)**. Induction of **Ehhadh** and **Pcca** expression was perfectly correlated to ligand- specific insulin-sensitizing potency (Spearman, $\rho=1$) (Figure 15C, all correlations shown in Supplementary 6). Thus, our data show that ligand-selective induction of the BCAA pathway is correlated with ligand potency and suggests that increased flux though this pathway is related to PPARγ ligand-induced insulin-sensitization. Although $1/3^{rd}$ (148/454) of the ligand-induced adipose tissue genes were annotated with mitochondria-related terms, we think it unlikely that PPARγ ligand treatment simply increases overall mitochondrial density. The TCA cycle and OXPHOS pathways were uniformly induced, not correlated with insulin sensitization, and the BCAA pathway was ligand-selectively induced and correlated with insulin sensitization.

Elevated expression of adipocyte and type-I (slow twitch) fiber genes in insulin resistant skeletal muscle is enhanced after PPARγ ligand treatment

We identified 33 differentially regulated genes in skeletal muscle expression profiles from the FC and LC groups (Supplementary 1.SM). Interestingly, expression of insulin-like growth factor (**Igf1**) and PPARγ (**Pparg**) was significantly blunted in FC rats. These two genes are important modulators of insulin sensitivity in skeletal muscle [76-78]. Several over-expressed genes in skeletal muscle of the FC rats are adipocyte

markers (Table 6), including Cd36, fatty acid synthase (Fasn), and stearoyl-Coenzyme A desaturase (**Scd1**), which have roles in fatty acid trafficking and synthesis. Eighty-nine genes were differentially expressed in skeletal muscle from PPARγ ligand-treated compared to FC rats. We used functional analysis to identify muscle biochemical pathway alterations associated with PPARγ ligand treatment. Several lipid metabolism ontology categories were enriched (Supplementary 2.SM). All the genes annotated with lipid metabolism-related terms, as well as other related genes, were up-regulated by ligand treatment (37 genes). Most of these are adipocyte-associated genes (25/37, shown in Table 6) including acetyl-coenzyme A carboxylase alpha (**Acaca**), a fatty acid elongase (**Elovl6**), fatty acid binding proteins (**Fabp4**, **Fabp5**), hormone-sensitive lipase (**Lipe**), lipoprotein lipase (**Lpl**), and retinol binding proteins (**Rbp4**, **Rbp7**). **Pparg**, highly expressed in adipocytes, was also increased (5.6-fold) after ligand treatment. Interestingly, genes over-expressed in FC vs. LC rats (**Angptl4, Cd36**, **Fasn**, and **Scd1)** were further over-expressed in the PPARγ ligand-treated rats. Muscle tissue expression of adipocyte markers was induced by all the PPARγ ligand treatments and all the genes exhibited ligand-specific modulation, except for **Pparg** (Supplementary 1.SM). Remarkably, ligand-specific expression of the adipocyte markers did not correlate with ligand-induced insulin sensitization (Supplementary 6). For example, troglitazone was the most potent inducer of adipocyte marker expression but was significantly less effective than AG035029 as an insulin-sensitizer. These results suggest that PPARγ ligand-induced alterations in adipocyte markers and lipid metabolic pathways may be necessary but are not sufficient for mediating degree of insulin-sensitization.

PPARγ ligands also induced expression of slow-twitch muscle fiber markers in skeletal muscle profiles (Table 6), including the three troponin subunits specific for slow-twitch skeletal muscle (**Tnnc1**, **Tnni1, Tnnt1**) and the slow-twitch type-I fiber type-specific myosin heavy chain 7 (**Myh7**) [79]. Two genes involved in calcium transport and binding in the sarcoplasmic reticulum of slow-twitch fiber types (**Atp2a2**, **Casq2**) were also up-regulated after PPARγ ligand treatment. The slow-twitch muscle markers tended to be over-expressed in the FC vs. LC rats, but this did not exceed our stringent significance thresholds. **Tnnc1** and **Tnni1** exhibited ligand-selective modulation which was not correlated with ligand insulin-sensitizing potency. Overall, our observations in skeletal muscle profiles suggest that insulin resistance is associated with moderate remodeling of the skeletal muscle involving increased adiposity and slow-twitch muscle fibers, and that this remodeling is further amplified after PPARγ ligand treatment.

PPARγ ligand treatment normalizes over-expression of liver lipogenic genes associated with insulin resistance

Comparison of liver expression profiles revealed 126 genes differentially expressed between the FC and LC groups (Supplementary 1.L). This gene set was enriched for annotation terms including the "biosynthesis of fatty acids" and "biosynthesis of steroids" (Supplementary 2.L). All genes annotated with "biosynthesis of fatty acids" were up-regulated (**Acaca**, **Acsl5**, **Fasn**) as were other related genes (**Elovl6**, **G6pdx**, **Me1**, **Scd1**). Correspondingly, expression of sterol regulatory element binding transcription factor 1 (**Srebf1**) was over-expressed 2.3-fold in FC rats (Figure 16A). Srebf1 encodes Srebp1, a transcription factor that positively regulates fatty acid

synthesis [80] and directly regulates the expression of all the aforementioned genes [81, 82]. In contrast, genes involved in cholesterol synthesis were under-expressed in FC rats. **Srebf2** encodes Srebp2, a transcription factor that preferentially regulates cholesterol and steroid biosynthesis genes [80]. Srebf2 expression was slightly blunted in FC rats (fold=0.879). Although down-regulation of Srebf2 itself did not meet our stringent statistical threshold, expression of several Srebf2 target genes (**Cyp51**, **Idi1**, **Sc4mol**, **Sqle** [80]) was significantly decreased. Figure 16B shows the aberrant regulation of Srebf1 and Srebf2 target genes in insulin resistant, obese rats and how this would alter fatty acid and cholesterol synthesis.

Srebf1 expression in PPARγ ligand-treated fatty rats was normalized down to LC levels and was not different between the ligand-treated groups (Figure 16A). Expression of several Srebf1 target genes associated with lipogenesis was also decreased by at least one of the ligands (**Elovl5**, **Fasn**, **G6pdx**, **Me1**, **Scd1**) (green-outlined ovals in Figure 16B, Supplementary 1.L). Of these, **G6pdx** expression was completely normalized to LC levels (Supplementary 1.L). Ligand treatment increased pyruvate dehydrogenase kinase 4 (**Pdk4**) expression. In its active state, **Pdk4** protein inhibits pyruvate dehydrogenase complex conversion of pyruvate into acetyl-CoA, effectively preventing the accumulation of the fatty acid precursors. Blunted cholesterol synthesis gene expression in FC rats was increased by PPARγ ligand treatment (**Cyp51**, **Idi1**, **Sc4mol**, **Sqle**) (red-outlined ovals in Figure 16B, Supplementary 1.L) with **Cyp51**, **Sc4mol**, and **Sqle** expression normalized to LC levels. Improved expression of these genes was selectively modulated by the PPARγ ligand treatments (Figure 16B, asterisks; Supplementary 1.L and Supplementary 4). Using data from each ligand-treated group, we correlated expression of these genes

with indexes of ligand insulin-sensitizing potency (i.e., GDR and TG suppression) (Supplementary 6). Expression of **Fasn** exhibited a perfect negative correlation with ligand potency (Spearman, $\rho = -1$). Expression of **Sc4mol**, a cholesterol synthesis gene, exhibited a perfect positive correlation with ligand potency (Spearman, $\rho = 1$). Expression of most of these genes was not correlated with ligand potency. Troglitazone was the most potent transcriptional regulator for the majority of the selectively modulated genes (7 of 11) but was not the most effective insulin-sensitizer. Thus, PPARγ ligand-induced reversal of elevated fatty acid and blunted cholesterol synthesis pathway expression is unlikely the primary mechanism by which PPARγ ligands modulate insulin-sensitivity, unless mediated by expression changes in the individual genes **Fasn** and **Sc4mol**.

E. Discussion

PPARγ ligands have been used extensively to study physiological and molecular changes affecting insulin sensitivity [83]. Nonetheless, little is known about how PPARγ ligand-specific modulation of cellular mechanisms correlates with gradations of insulin sensitization. Our studies have addressed this question and reveal mechanistic actions shared by PPARγ ligands and, importantly, mechanistic actions that are functionally related to insulin sensitization. Although four different PPARγ ligand treatments improved whole-body insulin sensitivity of obese rats in our study, they did so to varying degrees. The AG035029 treatment ranked the most potent in insulin sensitizing the rats, the rosiglitazone treatment ranked the least potent. Using genome-wide gene expression profiling of adipose, skeletal muscle, and liver tissue, we identified functional pathway

changes that correspond to insulin resistance, PPARγ ligand treatment, and insulin sensitization.

Chronic, low-grade inflammation is associated with and can cause insulin resistance. Macrophages infiltrate adipose tissue of obese animals and humans where they secrete cytokines that interfere with insulin signaling [43, 47]. Our results indicate increased immune cell residence in adipose tissue from obese, insulin resistant rats. PPARγ ligand-induced repression of inflammatory marker genes in adipose tissue correlated with ligand-specific insulin sensitization potency, i.e., PPARγ ligand-induced repression was greatest in response to the most effective insulin sensitizing treatment; repression was weakest in response to the least effective insulin sensitizing treatment. We have also shown that adipose tissue inflammation is inversely proportional to insulin sensitivity in human subjects [73]. These findings assert that suppressing the inflammatory state is central for reversing insulin resistance.

PPARγ ligand-induced mitochondrial capacity, gene expression, and mass have been observed in adipose tissue from insulin resistant humans and rodents [45, 60, 62, 63, 84]. Our studies extend previous findings and show that oxidative phosphorylation, TCA cycle, and BCAA degradation pathways are up-regulated in ligand-treated fatty rats to levels significantly higher than in LC and FC rats. Furthermore, the degree of induction of the BCAA pathway correlated with the degree of PPARγ ligand-induced insulin-sensitizing potency. Together, these results show that PPARγ ligands are not indiscriminately increasing mitochondria-associated metabolic pathways and suggest that insulin sensitivity is mechanistically linked to BCAA pathway flux. We have observed a similar correlation between insulin sensitivity and adipose tissue BCAA degradation

pathway expression in human subjects [73]. BCAAs are elevated in plasma of obese human and rodents, including Zucker fatty rats [85-89], and BCAA degradation pathway components are down-regulated [88]. Reversal of obesity by weight loss ameliorates these defects [88, 90]. BCAAs may inhibit insulin sensitivity in peripheral tissues via activation of mTOR and serine phosphorylation of IRS proteins [86, 91-93]. Our rat and human data suggest that PPARγ ligand-induced BCAA degradation in adipose tissue may serve as a compensatory metabolic shift that relieves BCAA accumulation and their insulin-desensitizing effects in the obese, over-nutritive state.

Skeletal muscle profiles from insulin resistant, obese rats exhibited elevated intramuscular adipocyte marker expression which was further increased after ligand treatment. We observed the same phenotypes in insulin resistant humans [73] and related observations have been reported [94-98]. Intramuscular adipocyte expression of lipid processing genes has the potential to improve myocyte sensitivity by alleviating local lipotoxicity and storing excess fatty acids [97, 99]. Expression of slow-twitch oxidative muscle fiber genes was also increased after PPARγ ligand treatment. Studies have shown that increasing slow-twitch fibers in skeletal muscle can lead to improved insulin sensitivity [70, 100]. In the liver, over-expression of Srebf1 and its target genes support that insulin resistance is characterized by increased hepatic lipogenesis [80]. Liver over-expression of Srebf1 causes increased expression of fatty acid synthesis genes and causes fatty liver [80]. PPARγ ligand treatments in the obese rats uniformly reversed Srebf1 over-expression back to LC levels, simultaneously repressing the lipogenesis program. This effect may be partly indirect due to concurrent lowering of plasma insulin levels, as

Srebf1 is an insulin target gene. However, fasting insulin levels did not correlate with liver expression of Srebf1.

The SPPARM (selective PPAR modulator) model describes the ability of heterogeneous ligands to impart specific 3-dimensional structure and transcriptional activity to PPARγ [8, 73]. We have demonstrated herein that SPPARM effects on gene expression and insulin sensitivity can be observed *in vivo* and in multiple tissues, even between ligands with structural similarity (e.g., rosiglitazone and pioglitazone). These effects vary by gene and tissue and, therefore, cannot be explained by drug dose and/or exposure, e.g., liver **G6pdx** expression was similarly regulated by all the ligands (no SPPARM; see Results and Supplementary 1.L) vs. liver **Fasn** which was differentially expressed and exhibited a perfect negative correlation with ligand insulin-sensitizing potency (SPPARM; see Results, Supplementary 1.L and Supplementary 6). Importantly, we observed that SPPARM effects on adipose tissue inflammatory and BCAA degradation pathways had inverse and direct correlations with insulin sensitization potency, respectively. Although we identified SPPARM effects on skeletal muscle adipocyte and slow-twitch fiber marker expression, these changes did not correlate with ligand insulin-sensitizing potency. In liver, we observed SPPARM effects on improved expression of Srebf1 target genes, however, and this also generally did not correlate with ligand-specific insulin sensitizing potency. These findings in skeletal muscle and liver suggest that these ligand-induced alterations may be necessary, but not sufficient, for PPARγ ligand-induced insulin-sensitization.

In summary, our results reveal functional pathway alterations that correlate with obesity, PPARγ ligand treatment, and insulin sensitization. Interestingly, we only

observed a strong correlation between differentially modulated biochemical pathways and insulin sensitization potency in adipose tissue. We have reported recently that adipocyte-specific PPARγ activation is sufficient to mediate whole body insulin sensitivity [101]. Although we have discerned important functional alterations in the skeletal muscle and liver, it is in the adipose tissue where pharmacological intervention seems to play a more significant role in whole-body insulin sensitization.

F. Acknowledgements

We would like to thank Dr. Albert Hsiao for initially uploading our microarray data and Dr. Jerrold Olefsky for support with the study and manuscript preparation.

Funding support for this research was provided by NIH NIDDK K01-DK62025 (DDS), NIH R01-DK033651 (JMO), NHLBI R33-HL087375 (SS), NIGMS U54-GM69338(SS), NIDDK P01-DK074868(SS), and the University of California Discovery Program Project #bio03-10383 with matching funds from Pfizer, Inc. (DDS, SS).

Disclosure summary/Conflict of Interest information: Support for this research was provided, in part, by the University of California Discovery Program Project #bio03-10383 with matching grant funds provided by Pfizer, Inc (DDS, SS). The terms of this arrangement have been reviewed and approved by the University of California, San Diego in accordance with its conflict of interest policies. JC is an employee and shareholder of Pfizer and participated as a collaborator in sample and data analysis for the project. There are no other issues regarding competing interests known to us.

This chapter, in full, has been submitted for publication of the material as it may appear in American Journal of Physiology Endocrinology and Metabolism, 2010, Hsiao,

Gene; Chapman, Justin; Ofrecio, Jachelle M.; Wilkes, Jason; Resnik, Jamie L.; Thapar, Divya; Subramaniam, Shankar; Sears, Dorothy D. "Multi-tissue, selective PPARγ modulation of insulin sensitivity and metabolic pathways in obese rats." The dissertation author was the sole first author on this paper.

G. Supporting Information

Supplementary 1: Differential gene expression in AT, SM, and L

Supplementary 2: GOby reports of the differential gene expression in AT, SM, and L

Supplementary 3: Immune-related genes overexpressed in FC AT which are decreased in ligand-treated rats

Supplementary 4: Ligand-selectively modulated genes in AT, SM, and L

Supplementary 5: GOby reports of the ligand-selectively modulated genes in AT, SM, and L

Supplementary 6: Gene expression correlations with GDR, %FFA suppression, and %TG suppression

Supplementary 7: GOby reports from the list of genes from AT whose expression levels correlate with GDR and/or %FFA suppression

Supplementary 8: Differentially regulated genes in AT involved with mitochondria-associated metabolism. Oxidative phosphorylation, citric acid (TCA) cycle, branched-chain amino acid degradation.

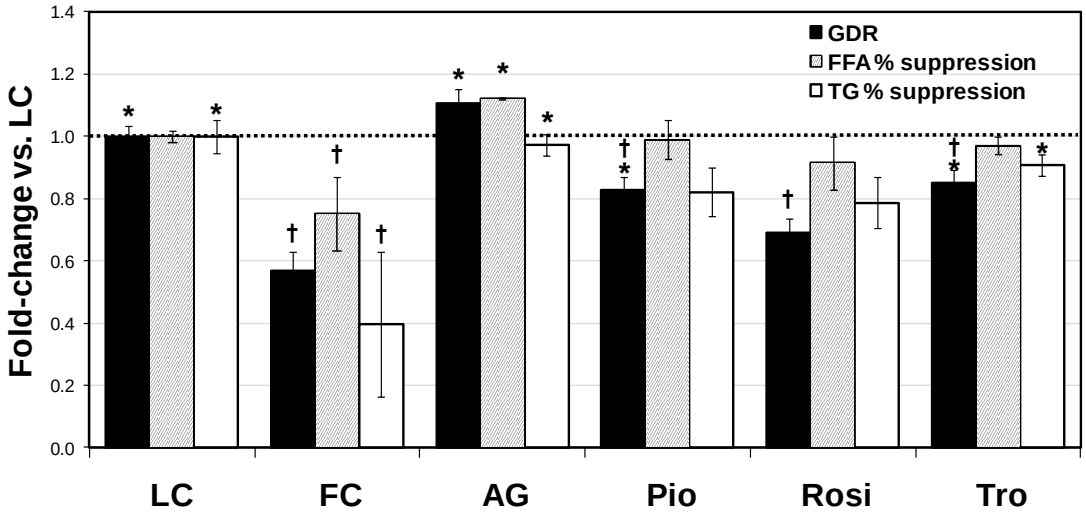

Figure 13: PPARγ ligand treatments improve parameters of insulin sensitivity.
GDR, FFA percent suppression, and TG percent suppression during the clamp. Data from Table 4 were modified and are shown as averages normalized to lean control (LC) group ± SEM. ANOVA $p<0.05$ for each. * – significant versus fatty control (FC) group in posthoc tests; † – significant versus AG035029-treated group in posthoc tests; GDR – glucose disposal rate, FFA – free fatty acid, TG – triglyceride; AG - AG035029-, Pio – pioglitazone-, Rosi – rosiglitazone-, Tro – troglitazone-treated fatty groups.

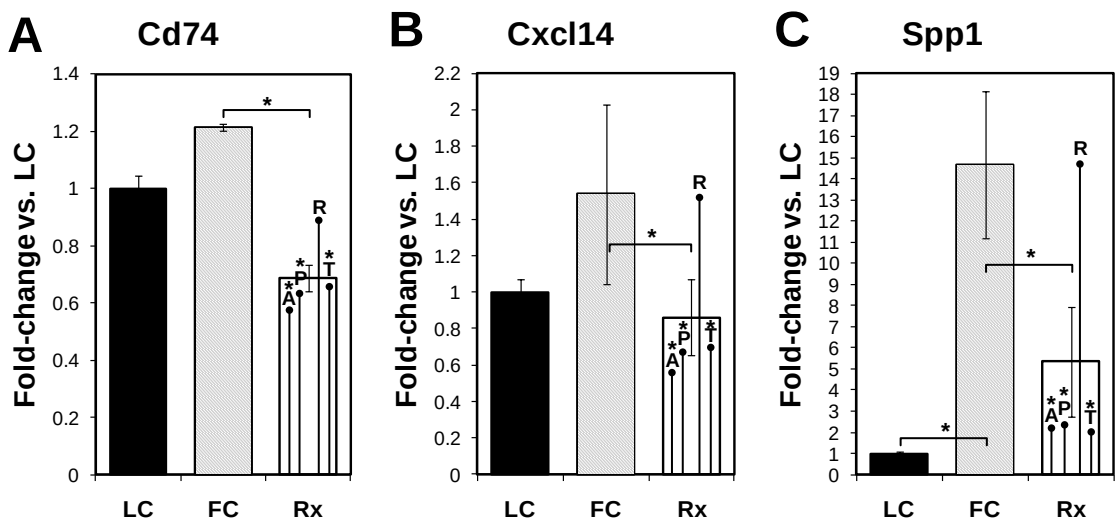

Figure 14: PPARγ ligand-selective modulation of immune cell marker genes in adipose tissue.

A: **Cd74**, a MHC class II gene. *B*: **Cxcl14** and *C*: **Spp1,** both chemokines. Data are averages normalized to LC group ± SEM. ANOVA $p<0.05$ for each. * – $\alpha_{bonf}<0.05$ versus fatty control (FC) group. LC – lean control, FC – fatty control, Rx – pooled data from PPARγ ligand-treated groups, A – AG035029-, P – pioglitazone-, R – rosiglitazone-, T – troglitazone-treated groups.

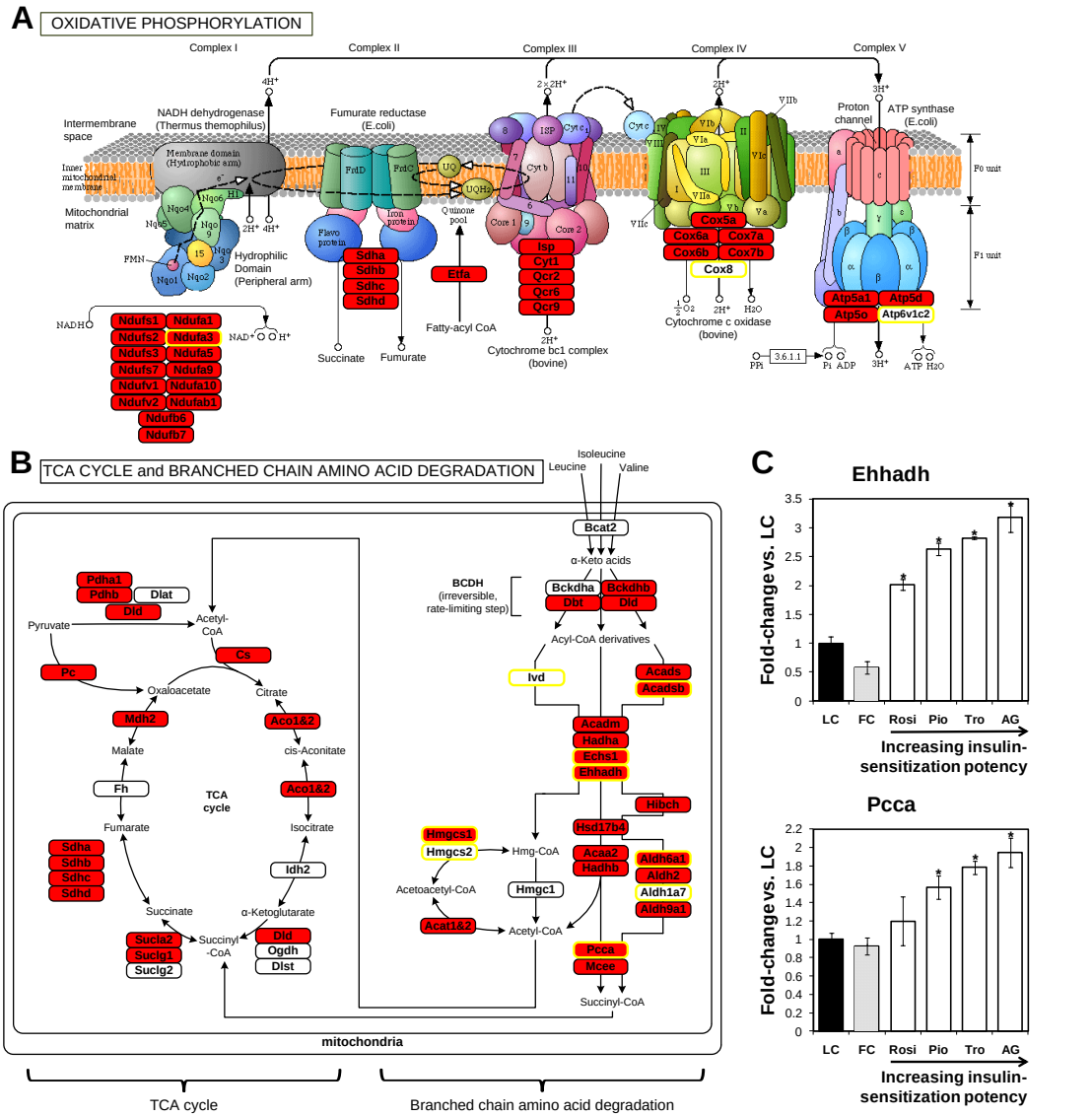

Figure 15: PPARγ ligand treatments increase expression of mitochondria-associated metabolic pathways in adipose tissue.

Selected genes up-regulated in ligand-treated adipose tissue are shown for the oxidative phosphorylation (***A***), TCA cycle and BCAA degradation metabolic pathways (***B***). Red ovals = genes up-regulated in PPARγ ligand-treated vs. FC groups. Unfilled ovals = no gene expression difference comparing ligand-treated and FC groups. Yellow-outlined ovals = genes exhibiting ligand-selective expression patterns (ANOVA, $p<0.05$). Figures adapted from KEGG. ***C*:** Examples of BCAA degradation pathway genes exhibiting ligand-selective expression that perfectly correlates with ligand potency (Spearman, $\rho=1$). Data are averages normalized to LC group ± SEM. ANOVA $p<0.05$ for each. * – $\alpha_{bonf}<0.05$ versus fatty control (FC) group.

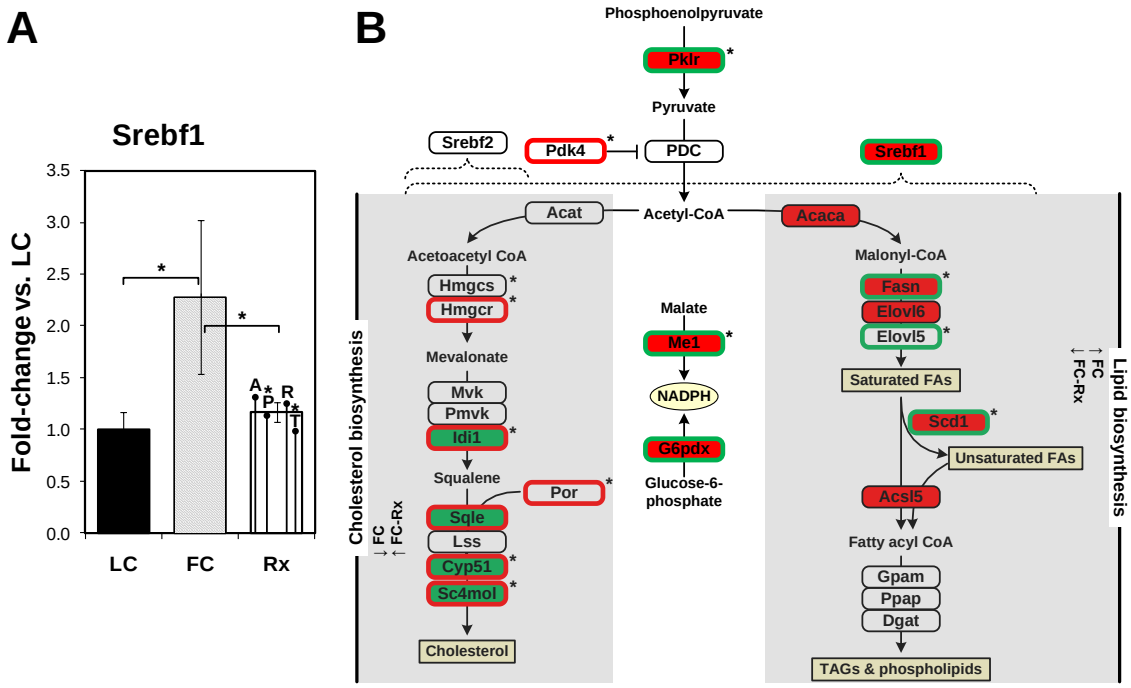

Figure 16: Dys-regulated expression of fatty acid and cholesterol synthesis genes in liver is reversed by PPARγ ligand treatments.

A: **Srebf1** expression. Data are averages normalized to LC group ± SEM. * – α_{bonf}<0.05 versus fatty control (FC) group. FC – fatty control, Rx – pooled data from PPARγ ligand-treated groups, A – AG035029-, P – pioglitazone-, R – rosiglitazone-, T – troglitazone-treated groups. ***B***: Red ovals = genes up-regulated in FC vs. LC rats (involved in fatty acid synthesis). Green ovals = genes down-regulated in FC vs. LC rats (involved in cholesterol synthesis). PPARγ ligand treatment reverses the FC group expression pattern, down-regulating fatty acid synthesis genes (green-outlined ovals) and up-regulating cholesterol synthesis genes (red-outlined ovals). Fill = differentially expressed in FC vs. LC groups; outline = differentially expressed in at least one PPARγ ligand-treated group compared to FC group. Asterisks above ovals indicate genes which exhibit ligand-selective expression (ANOVA, p<0.05). Pathway adapted from Horton *et al [80]*.

Table 4: Rat group characteristics and corresponding rankings of PPARγ ligand potencies.

Data are means ± SEM. ANOVA p values for each characteristic and post-hoc statistics for comparisons to FC & AG are shown. Potency ranking established using average values compared to FC. *Significant versus fatty control (FC) group, $p < 0.05$. †Significant versus AG035029-treated group, $p < 0.05$. GDR - glucose disposal rate, IS-GDR – insulin stimulated GDR during clamp, FFA - free fatty acids, HGO - hepatic glucose output, LC - lean control group, AG - AG035029-, Pio – pioglitazone-, Rosi – rosiglitazone-, Tro – troglitazone-treated fatty groups.

	ANOVA pvalue	LC	FC	AG	Pio	Rosi	Tro	PPARγ-ligand Potency Ranking
Body weight (gm)	0.000	236.6 ± 4.5*	379.4 ± 15.1	402.7 ± 6.1	386.9 ± 13.0	383.3 ± 16.5	379.7 ± 20.0	AG > Pio > Rosi > Tro
Fasting arterial glucose (mg/dl)	0.005	117.8 ± 3.6	136.7 ± 7.2	105.2 ± 2.7*	124.8 ± 3.7	125.5 ± 9.7	111.2 ± 4.2*	AG > Tro > Pio > Rosi
Fasting plasma insulin (ng/ml)	0.000	1.20 ± 0.16*	22.11 ± 4.94†	2.67 ± 0.20*	4.76 ± 1.26*	9.21 ± 3.31*	3.69 ± 1.06*	AG > Tro > Pio > Rosi
IS-GDR	0.000	38.41 ± 2.64*	17.44 ± 2.47†	46.86 ± 2.00*	30.63 ± 2.72*†	24.82 ± 1.70†	36.84 ± 3.04*	AG > Tro > Pio > Rosi
GDR (mg/kg/min)	0.000	52.61 ± 1.77*	29.91 ± 3.09†	58.24 ± 2.31*	43.56 ± 2.27*†	36.30 ± 2.32†	44.76 ± 2.15*†	AG > Tro > Pio > Rosi
Triglycerides (mg/dl)								
Basal	0.000	44.6 ± 4.1*	286.0 ± 47.0†	117.7 ± 8.8*	108.0 ± 14.9*	96.2 ± 11.5*	101.0 ± 7.6*	
Steady-state clamp	0.000	7.4 ± 2.1*	141.4 ± 24.3†	22.5 ± 2.6*	31.0 ± 3.7*	29.8 ± 4.4*	24.6 ± 1.5*	
% suppression during clamp	0.008	82.4% ± 4.4%*	32.8% ± 19.1%†	80.2% ± 2.8%*	67.7% ± 6.5%	64.8% ± 6.7%	74.6% ± 2.8%*	AG > Tro > Pio > Rosi
FFA (μmol/ml)								
Basal	0.043	1.50 ± 0.14	1.68 ± 0.67	0.13 ± 0.02	0.69 ± 0.27	0.82 ± 0.36	1.56 ± 0.39	
Steady-state clamp	n.s.	0.16 ± 0.02	0.35 ± 0.15	0.00 ± 0.00	0.16 ± 0.08	0.19 ± 0.08	0.19 ± 0.02	
% suppression during clamp	0.019	88.6% ± 1.7%	66.6% ± 10.4%	99.4% ± 0.4%*	87.6% ± 5.6%	80.9% ± 7.5%	85.9% ± 2.7%	AG > Pio > Tro > Rosi
HGO (mg/kg/min)								
Basal	n.s.	12.6 ± 2.4	12.5 ± 2.0	11.4 ± 0.7	12.9 ± 1.0	11.5 ± 1.1	9.2 ± 1.0	
Steady-state clamp	n.s.	9.6 ± 0.6	9.7 ± 3.2	5.6 ± 2.4	9.7 ± 1.6	6.2 ± 1.1	5.0 ± 2.0	
% suppression during clamp	n.s.	22.3% ± 6.5%	28.8% ± 11.2%	53.1% ± 20.1%	18.8% ± 18.1%	47.2% ± 5.6%	46.2% ± 18.3%	AG > Rosi > Tro > Pio

Table 5: List of supplemental data.
AT – adipose tissue, SM – skeletal muscle, L – liver.

Supplementary 1	Differential gene expression in AT, SM, and L
Supplementary 2	GOby reports of the differential gene expression in AT, SM, and L
Supplementary 3	Immune-related genes overexpressed in FC AT which are decreased in ligand-treated rats
Supplementary 4	Ligand-selectively modulated genes in AT, SM, and L
Supplementary 5	GOby reports of the ligand-selectively modulated genes in AT, SM, and L
Supplementary 6	Gene expression correlations with GDR, %FFA suppression, and %TG suppression
Supplementary 7	GOby reports from the list of genes from AT whose expression levels correlate with GDR and/or %FFA suppression
Supplementary 8	Differentially regulated genes in AT involved with mitochondria-associated metabolism. Oxidative phosphorylation, citric acid (TCA) cycle, branched-chain amino acid degradation.

Table 6: Expression of adipocyte and slow-twitch fiber genes in skeletal muscle. Statistically significant expression ratios are shown for rat groups (LC – lean controls, FC – fatty controls, Rx – pooled PPARγ ligand-treated fatty rats).

Gene Symbol	EntrezID	Description	FC/LC	Rx/FC	Rx/LC	
Acaca	60581	acetyl-coenzyme A carboxylase alpha		2.38	1.98	predominately expressed in adipocytes
Acly	24159	ATP citrate lyase		4.92	5.44	
Angptl4	362850	angiopoietin-like 4	3.64	2.42	8.83	
Aqp7	29171	aquaporin 7		3.35	5.71	
Cd36	29184	cd36 antigen	1.97	1.79	3.52	
Cfd	54249	complement factor D (adipsin)		2.55	1.98	
Dgat2	252900	diacylglycerol O-acyltransferase 2		2.03	2.55	
Egfl7 | Agpat2	245963 | 311821	EGF-like domain 7 | 1-acylglycerol-3-phosphate O-acyltransferase 2 (lysophosphatidic acid acyltransferase, beta)		2.15	2.58	
Elovl6	171402	ELOVL family member 6, elongation of long chain fatty acids (yeast)		11.16	11.54	
Fabp4	79451	fatty acid binding protein 4, adipocyte		4.22	5.56	
Fabp5	140868	fatty acid binding protein 5, epidermal		3.21	3.44	
Fasn	50671	fatty acid synthase	3.47	7.84	27.18	
G6pdx	24377 | 678700	glucose-6-phosphate dehydrogenase X-linked		1.89	1.78	
Hsd17b12	84013	hydroxysteroid (17-beta) dehydrogenase 12		2.38	1.74	
Lipe	25330	lipase, hormone sensitive		4.74	7.53	
Lpl	24539	lipoprotein lipase		2.13	2.52	
Mgll	29254	monoglyceride lipase		4.36	4.47	
Mgst1	171341	microsomal glutathione S-transferase 1		9.28	11.06	
Pparg	25664	peroxisome proliferator activated receptor gamma	0.16	5.64		
Rbp4	25703	retinol binding protein 4, plasma		8.84	13.02	
Rbp7	362662	retinol binding protein 7, cellular		24.71	43.03	
Retsat	246298 | 360384	retinol saturase (all trans retinol 13,14 reductase)		2.33	3.11	
Scd1	246074	stearoyl-Coenzyme A desaturase 1	3.25	11.18	36.33	
Thrsp	25357	thyroid hormone responsive protein		16.18	12.38	
Tusc5	360576	tumor suppressor candidate 5		6.19	5.56	
Atp2a2	29693	ATPase, Ca++ transporting, cardiac muscle, slow twitch 2			1.59	slow-twitch muscle fiber markers
Casq2	29209	calsequestrin 2			1.64	
Myh7	29557	myosin, heavy polypeptide 6, cardiac muscle, alpha | myosin, heavy polypeptide 7, cardiac muscle, beta			2.19	
Tnnc1	290561	troponin C, cardiac/slow skeletal			1.98	
Tnni1	29388	troponin I, skeletal, slow 1			1.79	
Tnnt1	171409	troponin T1, skeletal, slow			1.59	

V.

Conclusions

In this work, we formulated a sensitive and robust statistical approach for the detection of differentially expressed genes. Microarray experiments present a distinctive statistical design of an inordinately low sample size for the massively high number of simultaneous hypothesis tests. Because of this, accurate gene level variance estimation is essential for sensitive detection of differentially expressed genes with proper error control. We conducted sensitivity analysis of leading microarray statistical testers with receiver operating characteristic curves on various controlled datasets where the true changes are known in advance. We demonstrated that the global variance modeling approach increases detection sensitivity across the range of expression and fold-change levels. Increased sensitivity to detect significantly changing genes at the lower fold-change and higher variance regions are important because these genes can have real biological consequences. We also demonstrated that this gain in sensitivity is consistent across the various controlled datasets, commercial platforms, and experimental designs tested.

Using this defined methodology, we investigated the pathophysiology of insulin resistance and PPARγ ligand-mediated insulin sensitization in human subjects whom respond or do not respond to TZD treatment. We identify pathway alterations in skeletal muscle and adipose tissue which are characteristic of insulin resistance, TZD-induced insulin sensitization, and potential TZD responsiveness. TZD-induced insulin sensitization in responder subjects was associated with improved insulin-regulated gene expression of key regulators of glycolysis and other metabolic pathways in the skeletal

muscle. Also in the skeletal muscle, the elevated intramuscular adipocyte markers in insulin resistant responder subjects before treatment were further increased with TZD. In the adipose tissue of insulin resistant subjects, our results indicate that immunoregulatory genes function together in a network to orchestrate transendothelial migration and antigen presentation in resident leukocytes. With TZD treatment, repression of inflammatory genes was greater in responder than in non-responder subjects. Notably, markers of macrophage infiltration were more prevalent in non-responder subjects before TZD treatment and may play a role in making insulin-resistance more refractory to TZD treatment. Also in the adipose tissue, TZD-induced insulin sensitization was positively correlated with expression of genes regulating mitochondrial activity. We also identified candidate genes in insulin resistant subjects which were linearly predictive of post-TZD insulin sensitization.

In obese insulin resistant Zucker rats, all PPARγ ligands improved insulin sensitivity, albeit to varying degrees. We interrogated adipose tissue, skeletal muscle, and liver gene expression profiles for functional pathways which were necessary and sufficient for effective insulin sensitization. Like our study with insulin resistant human subjects, our results in insulin resistant rats indicated increased immune cell residence in adipose tissue. PPARγ ligand-induced repression of inflammatory markers was greatest in response to the most effective insulin sensitizing treatment; repression was weakest in response to the least effective insulin sensitizing treatment. These findings suggest that suppressing the inflammatory state is central for reversing insulin resistance. Also in the adipose tissue, PPARγ ligands are not indiscriminately increasing mitochondria-associated metabolic pathways, but insulin sensitivity is mechanistically linked to BCAA

pathway flux. Our rat and human data suggest that PPARγ ligand-induced BCAA degradation in adipose tissue may serve to relieve plasma BCAA accumulation and their insulin-desensitizing effects in the obese, over-nutritive state. Like our study in insulin resistant human subjects, the insulin resistant rats exhibited elevated intramuscular adipocyte marker expression which was further increased after ligand treatment. Expression of slow-twitch oxidative muscle fiber genes was also increased after PPARγ ligand treatment. In the liver, over-expression of Srebf1 and its target genes support that insulin resistance is characterized by increased hepatic lipogenesis. PPARγ ligand treatments in the obese rats uniformly reversed Srebf1 over-expression back to LC levels, simultaneously repressing the lipogenesis program. While our findings which exhibited SPPARM (selective PPAR modulator) pattern in adipose tissue correlated with insulin sensitization potency, our findings in skeletal muscle and liver did not. Our observations in skeletal muscle and liver suggest that these ligand-induced alterations may be necessary, but not sufficient, for PPARγ ligand-induced insulin-sensitization. Although we have discerned functional alterations in the skeletal muscle and liver, it is in the adipose tissue where pharmacological intervention seems to play a more significant role in whole-body insulin sensitization.

It is important to note that our observations were inferred from massively parallel genome-wide measurements of gene expression with microarrays. Although, there is correlation between gene expression and protein abundance, there is little substitute for actual measurements of protein and other genomic products. As the reproducibility of mass spectrometry technology improves and its data analysis algorithms mature, proteome, lipidome, and metabolome quantification will offer a more comprehensive

view of cellular mechanisms. Other new technologies, such as high-throughput sequencing, are aimed to revolutionize the way in which investigators approach biological questions. RNA fragments can be sequenced rapidly in parallel, with some methods not even requiring amplification. This technology requires less sample material, can be more sensitive for low abundance transcripts, does not require predefined probes, and does not have the issues that arise from hybridization effects. However, data analysis for these extremely large sequencing datasets is still in its infancy. Accurate *de novo* assembly of short reads and the data warehousing of terabytes of data are just a couple issues which are in active development. Despite the emergence of these new technologies, microarrays are more cost-effective and will continue to be the preferred choice for rapid pathway analysis, disease classification, and screening.

While our studies of insulin resistant human and rat suggest increased immune cell residence in adipose tissue and increased fat markers in skeletal muscle, follow up studies are necessary in order to isolate the mechanisms that are specific to the cell types which are represented within each tissue. Additionally, although we have identified MLXIP and HLA-DRB1 to be predictive of TZD response, further investigation is needed in order to explain if and how TZDs interact directly with these proteins. Our findings presented in this text bring to light new transcriptional biomarkers of insulin resistance and response signatures of PPARγ ligand treatment.

REFERENCES

1. Wallace, T.M. and D.R. Matthews, *The assessment of insulin resistance in man.* Diabet Med, 2002. **19**(7): p. 527-34.

2. Despres, J.P., B. Lamarche, P. Mauriege, et al., *Hyperinsulinemia as an independent risk factor for ischemic heart disease.* N Engl J Med, 1996. **334**(15): p. 952-7.

3. Grundy, S.M., H.B. Brewer, Jr., J.I. Cleeman, et al., *Definition of metabolic syndrome: Report of the National Heart, Lung, and Blood Institute/American Heart Association conference on scientific issues related to definition.* Circulation, 2004. **109**(3): p. 433-8.

4. CDC. *CDC Diabetes At A Glance 2010*. 2010 [cited 2010 May 13, 2010].

5. Berger, J.P., A.E. Petro, K.L. Macnaul, et al., *Distinct properties and advantages of a novel peroxisome proliferator-activated protein [gamma] selective modulator.* Mol Endocrinol, 2003. **17**(4): p. 662-76.

6. Camp, H.S., O. Li, S.C. Wise, et al., *Differential activation of peroxisome proliferator-activated receptor-gamma by troglitazone and rosiglitazone.* Diabetes, 2000. **49**(4): p. 539-47.

7. Fujimura, T., C. Kimura, T. Oe, et al., *A selective peroxisome proliferator-activated receptor gamma modulator with distinct fat cell regulation properties.* J Pharmacol Exp Ther, 2006. **318**(2): p. 863-71.

8. Sears, D.D., A. Hsiao, J.M. Ofrecio, et al., *Selective modulation of promoter recruitment and transcriptional activity of PPARgamma.* Biochem Biophys Res Commun, 2007. **364**(3): p. 515-21.

9. *Standards of medical care in diabetes--2006.* Diabetes Care, 2006. **29 Suppl 1**: p. S4-42.

10. Kahn, S.E., S.M. Haffner, M.A. Heise, et al., *Glycemic durability of rosiglitazone, metformin, or glyburide monotherapy.* N Engl J Med, 2006. **355**(23): p. 2427-43.

11. Viberti, G., S.E. Kahn, D.A. Greene, et al., *A diabetes outcome progression trial (ADOPT): an international multicenter study of the comparative efficacy of rosiglitazone, glyburide, and metformin in recently diagnosed type 2 diabetes.* Diabetes Care, 2002. **25**(10): p. 1737-43.

12. Igarashi, M., Y. Jimbu, M. Kimura, et al., *Effect of pioglitazone on atherogenic outcomes in type 2 diabetic patients: a comparison of responders and non-responders.* Diabetes Res Clin Pract, 2007. **77**(3): p. 389-98.

13. Suter, S.L., J.J. Nolan, P. Wallace, et al., *Metabolic effects of new oral hypoglycemic agent CS-045 in NIDDM subjects.* Diabetes Care, 1992. **15**(2): p. 193-203.

14. Fodor, S.P., R.P. Rava, X.C. Huang, et al., *Multiplexed biochemical assays with biological chips.* Nature, 1993. **364**(6437): p. 555-6.

15. Fodor, S.P., J.L. Read, M.C. Pirrung, et al., *Light-directed, spatially addressable parallel chemical synthesis.* Science, 1991. **251**(4995): p. 767-73.

16. Schena, M., D. Shalon, R.W. Davis, et al., *Quantitative monitoring of gene expression patterns with a complementary DNA microarray.* Science, 1995. **270**(5235): p. 467-70.

17. Shi, L., L.H. Reid, W.D. Jones, et al., *The MicroArray Quality Control (MAQC) project shows inter- and intraplatform reproducibility of gene expression measurements.* Nat Biotechnol, 2006. **24**(9): p. 1151-61.

18. Allison, D.B., X. Cui, G.P. Page, et al., *Microarray data analysis: from disarray to consolidation and consensus.* Nat Rev Genet, 2006. **7**(1): p. 55-65.

19. Tusher, V.G., R. Tibshirani, and G. Chu, *Significance analysis of microarrays applied to the ionizing radiation response.* Proc Natl Acad Sci U S A, 2001. **98**(9): p. 5116-21.

20. Baldi, P. and A.D. Long, *A Bayesian framework for the analysis of microarray expression data: regularized t -test and statistical inferences of gene changes.* Bioinformatics, 2001. **17**(6): p. 509-19.

21. Smyth, G.K., R. Gentleman, V. Carey, et al., *Limma: linear models for microarray data*, in *Bioinformatics and Computational Biology Solutions using R and Bioconductor*. 2005, Springer, New York. p. 397-420.

22. Hsiao, A., T. Ideker, J.M. Olefsky, et al., *VAMPIRE microarray suite: a web-based platform for the interpretation of gene expression data.* Nucleic Acids Res, 2005. **33**(Web Server issue): p. W627-32.

23. Smyth, G.K., *Linear models and empirical bayes methods for assessing differential expression in microarray experiments.* Stat Appl Genet Mol Biol, 2004. **3**: p. Article3.

24. Hsiao, A. and S. Subramaniam, *Bivariate microarray analysis: statistical interpretation of two-channel functional genomics data.* Syst Synth Biol, 2008. **2**(3-4): p. 95-104.

25. Hsiao, A., D.S. Worrall, J.M. Olefsky, et al., *Variance-modeled posterior inference of microarray data: detecting gene-expression changes in 3T3-L1 adipocytes.* Bioinformatics, 2004. **20**(17): p. 3108-27.

26. Rocke, D.M. and B. Durbin, *A model for measurement error for gene expression arrays.* J Comput Biol, 2001. **8**(6): p. 557-69.

27. Ideker, T., V. Thorsson, A.F. Siegel, et al., *Testing for differentially-expressed genes by maximum-likelihood analysis of microarray data.* J Comput Biol, 2000. **7**(6): p. 805-17.

28. Li, C. and W.H. Wong, *Model-based analysis of oligonucleotide arrays: expression index computation and outlier detection.* Proc Natl Acad Sci U S A, 2001. **98**(1): p. 31-6.

29. Choe, S.E., M. Boutros, A.M. Michelson, et al., *Preferred analysis methods for Affymetrix GeneChips revealed by a wholly defined control dataset.* Genome Biol, 2005. **6**(2): p. R16.

30. Pearson, R.D., *A comprehensive re-analysis of the Golden Spike data: towards a benchmark for differential expression methods.* BMC Bioinformatics, 2008. **9**: p. 164.

31. Thompson, K.L., B.A. Rosenzweig, P.S. Pine, et al., *Use of a mixed tissue RNA design for performance assessments on multiple microarray formats.* Nucleic Acids Res, 2005. **33**(22): p. e187.

32. Benjamini, Y. and Y. Hochberg, *Controlling the false discovery rate—a practical and powerful approach to multiple testing.* J. R. Stat. Soc. B, 1995. **57**: p. 289-300.

33. Murie, C., O. Woody, A.Y. Lee, et al., *Comparison of small n statistical tests of differential expression applied to microarrays.* BMC Bioinformatics, 2009. **10**: p. 45.

34. Pine, P.S., M. Boedigheimer, B.A. Rosenzweig, et al., *Use of diagnostic accuracy as a metric for evaluating laboratory proficiency with microarray assays using mixed-tissue RNA reference samples.* Pharmacogenomics, 2008. **9**(11): p. 1753-63.

35. Thompson, K.L. and P.S. Pine, *Comparison of the diagnostic performance of human whole genome microarrays using mixed-tissue RNA reference samples.* Toxicol Lett, 2009. **186**(1): p. 58-61.

36. Kanehisa, M., S. Goto, M. Hattori, et al., *From genomics to chemical genomics: new developments in KEGG.* Nucleic Acids Res, 2006. **34**(Database issue): p. D354-7.

37. *Bioconductor*. 2010.

38. Storey, J.D., *A Direct Approach to False Discovery Rates.* Journal of the Royal Statistical Society. Series B, Statistical Methodology, 2002. **64**(3): p. 479-498.

39. Long, A.D., H.J. Mangalam, B.Y. Chan, et al., *Improved statistical inference from DNA microarray data using analysis of variance and a Bayesian statistical framework. Analysis of global gene expression in Escherichia coli K12.* J Biol Chem, 2001. **276**(23): p. 19937-44.

40. Wettenhall, J.M., K.M. Simpson, K. Satterley, et al., *affylmGUI: a graphical user interface for linear modeling of single channel microarray data.* Bioinformatics, 2006. **22**(7): p. 897-9.

41. Wettenhall, J.M. and G.K. Smyth, *limmaGUI: a graphical user interface for linear modeling of microarray data.* Bioinformatics, 2004. **20**(18): p. 3705-6.

42. Sinha, R., S. Dufour, K.F. Petersen, et al., *Assessment of skeletal muscle triglyceride content by (1)H nuclear magnetic resonance spectroscopy in lean and obese adolescents: relationships to insulin sensitivity, total body fat, and central adiposity.* Diabetes, 2002. **51**(4): p. 1022-7.

43. Hotamisligil, G.S., *Inflammation and metabolic disorders.* Nature, 2006. **444**(7121): p. 860-7.

44. Matsuzawa, Y., *The metabolic syndrome and adipocytokines.* FEBS Lett, 2006. **580**(12): p. 2917-21.

45. Dahlman, I., M. Forsgren, A. Sjogren, et al., *Downregulation of electron transport chain genes in visceral adipose tissue in type 2 diabetes independent of obesity and possibly involving tumor necrosis factor-alpha.* Diabetes, 2006. **55**(6): p. 1792-9.

46. Mootha, V.K., C.M. Lindgren, K.F. Eriksson, et al., *PGC-1alpha-responsive genes involved in oxidative phosphorylation are coordinately downregulated in human diabetes.* Nat Genet, 2003. **34**(3): p. 267-73.

47. Olefsky, J.M., *Treatment of insulin resistance with peroxisome proliferator-activated receptor gamma agonists.* J Clin Invest, 2000. **106**(4): p. 467-72.

48. Lapsys, N.M., A.D. Kriketos, M. Lim-Fraser, et al., *Expression of genes involved in lipid metabolism correlate with peroxisome proliferator-activated receptor gamma expression in human skeletal muscle.* J Clin Endocrinol Metab, 2000. **85**(11): p. 4293-7.

49. Desvergne, B., L. Michalik, and W. Wahli, *Transcriptional regulation of metabolism.* Physiol Rev, 2006. **86**(2): p. 465-514.

50. Arner, P., *The adipocyte in insulin resistance: key molecules and the impact of the thiazolidinediones.* Trends Endocrinol Metab, 2003. **14**(3): p. 137-45.

51. Fruebis, J., T.S. Tsao, S. Javorschi, et al., *Proteolytic cleavage product of 30-kDa adipocyte complement-related protein increases fatty acid oxidation in muscle and causes weight loss in mice.* Proc Natl Acad Sci U S A, 2001. **98**(4): p. 2005-10.

52. Herman, M.A. and B.B. Kahn, *Glucose transport and sensing in the maintenance of glucose homeostasis and metabolic harmony.* J Clin Invest, 2006. **116**(7): p. 1767-75.

53. Toyoshima, Y., O. Gavrilova, S. Yakar, et al., *Leptin improves insulin resistance and hyperglycemia in a mouse model of type 2 diabetes.* Endocrinology, 2005. **146**(9): p. 4024-35.

54. Yamauchi, T., J. Kamon, H. Waki, et al., *The fat-derived hormone adiponectin reverses insulin resistance associated with both lipoatrophy and obesity.* Nat Med, 2001. **7**(8): p. 941-6.

55. Araki, T., M. Emoto, H. Yokoyama, et al., *Insulin resistance index as a predictor for pioglitazone treatment in type 2 diabetes.* Osaka City Med J, 2005. **51**(1): p. 19-25.

56. Sans, C.L., D.J. Satterwhite, C.A. Stoltzman, et al., *MondoA-Mlx heterodimers are candidate sensors of cellular energy status: mitochondrial localization and direct regulation of glycolysis.* Mol Cell Biol, 2006. **26**(13): p. 4863-71.

57. Muoio, D.M. and C.B. Newgard, *Mechanisms of disease: molecular and metabolic mechanisms of insulin resistance and beta-cell failure in type 2 diabetes.* Nat Rev Mol Cell Biol, 2008. **9**(3): p. 193-205.

58. Bandyopadhyay, G.K., J.G. Yu, J. Ofrecio, et al., *Increased malonyl-CoA levels in muscle from obese and type 2 diabetic subjects lead to decreased fatty acid oxidation and increased lipogenesis; thiazolidinedione treatment reverses these defects.* Diabetes, 2006. **55**(8): p. 2277-85.

59. Neels, J.G. and J.M. Olefsky, *Inflamed fat: what starts the fire?* J Clin Invest, 2006. **116**(1): p. 33-5.

60. Bogacka, I., H. Xie, G.A. Bray, et al., *Pioglitazone induces mitochondrial biogenesis in human subcutaneous adipose tissue in vivo.* Diabetes, 2005. **54**(5): p. 1392-9.

61. Choo, H.J., J.H. Kim, O.B. Kwon, et al., *Mitochondria are impaired in the adipocytes of type 2 diabetic mice.* Diabetologia, 2006. **49**(4): p. 784-91.

62. Rong, J.X., Y. Qiu, M.K. Hansen, et al., *Adipose mitochondrial biogenesis is suppressed in db/db and high-fat diet-fed mice and improved by rosiglitazone.* Diabetes, 2007. **56**(7): p. 1751-60.

63. Wilson-Fritch, L., S. Nicoloro, M. Chouinard, et al., *Mitochondrial remodeling in adipose tissue associated with obesity and treatment with rosiglitazone.* J Clin Invest, 2004. **114**(9): p. 1281-9.

64. Frias, J.P., J.G. Yu, Y.T. Kruszynska, et al., *Metabolic effects of troglitazone therapy in type 2 diabetic, obese, and lean normal subjects.* Diabetes Care, 2000. **23**(1): p. 64-9.

65. Yu, J.G., S. Javorschi, A.L. Hevener, et al., *The effect of thiazolidinediones on plasma adiponectin levels in normal, obese, and type 2 diabetic subjects.* Diabetes, 2002. **51**(10): p. 2968-74.

66. Steele, R., *Influences of glucose loading and of injected insulin on hepatic glucose output.* Ann N Y Acad Sci, 1959. **82**: p. 420-30.

67. Wolfe, R.R., *Tracers in metabolic research: radioisotope and stable isotope/mass spectrometry methods.* Lab Res Methods Biol Med, 1984. **9**: p. 1-287.

68. Desbuquois, B. and G.D. Aurbach, *Use of polyethylene glycol to separate free and antibody-bound peptide hormones in radioimmunoassays.* J Clin Endocrinol Metab, 1971. **33**(5): p. 732-8.

69. Glantz, S.A., *Primer of biostatistics*. 6th ed. 2005, New York: McGraw-Hill Medical Pub. Division. 520.

70. Evans, R.M., G.D. Barish, and Y.X. Wang, *PPARs and the complex journey to obesity.* Nat Med, 2004. **10**(4): p. 355-61.

71. Ricote, M. and C.K. Glass, *PPARs and molecular mechanisms of transrepression.* Biochim Biophys Acta, 2007. **1771**(8): p. 926-35.

72. Gregoire, F.M., F. Zhang, H.J. Clarke, et al., *MBX-102/JNJ39659100, a novel peroxisome proliferator-activated receptor-ligand with weak transactivation activity retains antidiabetic properties in the absence of weight gain and edema.* Mol Endocrinol, 2009. **23**(7): p. 975-88.

73. Sears, D.D., G. Hsiao, A. Hsiao, et al., *Mechanisms of human insulin resistance and thiazolidinedione-mediated insulin sensitization.* Proc Natl Acad Sci U S A, 2009. **106**(44): p. 18745-50.

74. Kline, B., Saenz, J., Stankovi N., Mitchell M., *Polymorph and Particle Size Control of PPAR Compounds PF00287586 and AG035029.* Organic Process Research and Development, 2006. **10**(2): p. 203-211.

75. Hevener, A.L., D. Reichart, A. Janez, et al., *Thiazolidinedione treatment prevents free fatty acid-induced insulin resistance in male wistar rats.* Diabetes, 2001. **50**(10): p. 2316-22.

76. Fernandez, A.M., J.K. Kim, S. Yakar, et al., *Functional inactivation of the IGF-I and insulin receptors in skeletal muscle causes type 2 diabetes.* Genes Dev, 2001. **15**(15): p. 1926-34.

77. Hevener, A.L., W. He, Y. Barak, et al., *Muscle-specific Pparg deletion causes insulin resistance.* Nat Med, 2003. **9**(12): p. 1491-7.

78. Kolaczynski, J.W. and J.F. Caro, *Insulin-like growth factor-1 therapy in diabetes: physiologic basis, clinical benefits, and risks.* Ann Intern Med, 1994. **120**(1): p. 47-55.

79. Tajsharghi, H., L.E. Thornell, C. Lindberg, et al., *Myosin storage myopathy associated with a heterozygous missense mutation in MYH7.* Ann Neurol, 2003. **54**(4): p. 494-500.

80. Horton, J.D., J.L. Goldstein, and M.S. Brown, *SREBPs: activators of the complete program of cholesterol and fatty acid synthesis in the liver.* J Clin Invest, 2002. **109**(9): p. 1125-31.

81. Horton, J.D., N.A. Shah, J.A. Warrington, et al., *Combined analysis of oligonucleotide microarray data from transgenic and knockout mice identifies direct SREBP target genes.* Proc Natl Acad Sci U S A, 2003. **100**(21): p. 12027-32.

82. Reed, B.D., A.E. Charos, A.M. Szekely, et al., *Genome-wide occupancy of SREBP1 and its partners NFY and SP1 reveals novel functional roles and combinatorial regulation of distinct classes of genes.* PLoS Genet, 2008. **4**(7): p. e1000133.

83. Yki-Jarvinen, H., *Thiazolidinediones.* N Engl J Med, 2004. **351**(11): p. 1106-18.

84. Toseland, C.D., S. Campbell, I. Francis, et al., *Comparison of adipose tissue changes following administration of rosiglitazone in the dog and rat.* Diabetes Obes Metab, 2001. **3**(3): p. 163-70.

85. Felig, P., E. Marliss, and G.F. Cahill, Jr., *Plasma amino acid levels and insulin secretion in obesity.* N Engl J Med, 1969. **281**(15): p. 811-6.

86. Newgard, C.B., J. An, J.R. Bain, et al., *A branched-chain amino acid-related metabolic signature that differentiates obese and lean humans and contributes to insulin resistance.* Cell Metab, 2009. **9**(4): p. 311-26.

87. Pietilainen, K.H., J. Naukkarinen, A. Rissanen, et al., *Global transcript profiles of fat in monozygotic twins discordant for BMI: pathways behind acquired obesity.* PLoS Med, 2008. **5**(3): p. e51.

88. She, P., C. Van Horn, T. Reid, et al., *Obesity-related elevations in plasma leucine are associated with alterations in enzymes involved in branched-chain amino acid metabolism.* Am J Physiol Endocrinol Metab, 2007. **293**(6): p. E1552-63.

89. Herman, M.A., P. She, O.D. Peroni, et al., *Adipose tissue branched-chain amino acid (BCAA) metabolism modulates circulating BCAA levels.* J Biol Chem, 2010.

90. Lien, L.F., A.M. Haqq, M. Arlotto, et al., *The STEDMAN project: biophysical, biochemical and metabolic effects of a behavioral weight loss intervention during weight loss, maintenance, and regain.* Omics, 2009. **13**(1): p. 21-35.

91. Krebs, M., M. Krssak, E. Bernroider, et al., *Mechanism of amino acid-induced skeletal muscle insulin resistance in humans.* Diabetes, 2002. **51**(3): p. 599-605.

92. Tremblay, F., C. Lavigne, H. Jacques, et al., *Role of dietary proteins and amino acids in the pathogenesis of insulin resistance.* Annu Rev Nutr, 2007. **27**: p. 293-310.

93. Um, S.H., D. D'Alessio, and G. Thomas, *Nutrient overload, insulin resistance, and ribosomal protein S6 kinase 1, S6K1.* Cell Metab, 2006. **3**(6): p. 393-402.

94. Hallakou, S., F. Foufelle, L. Doare, et al., *Pioglitazone-induced increase of insulin sensitivity in the muscles of the obese Zucker fa/fa rat cannot be explained by local adipocyte differentiation.* Diabetologia, 1998. **41**(8): p. 963-8.

95. Hausman, G.J., M.V. Dodson, K. Ajuwon, et al., *Board-invited review: the biology and regulation of preadipocytes and adipocytes in meat animals.* J Anim Sci, 2009. **87**(4): p. 1218-46.

96. Nadeau, K.J., L.B. Ehlers, L.E. Aguirre, et al., *Discordance between intramuscular triglyceride and insulin sensitivity in skeletal muscle of Zucker diabetic rats after treatment with fenofibrate and rosiglitazone.* Diabetes Obes Metab, 2007. **9**(5): p. 714-23.

97. Poulos, S. and G. Hausman, *Intramuscular adipocytes- potential to prevent lipotoxicity in skeletal muscle.* Adipocytes, 2005. **1**(2): p. 79-94.

98. Vettor, R., G. Milan, C. Franzin, et al., *The Origin of Intermuscular Adipose Tissue and Its Pathophysiological Implications.* Am J Physiol Endocrinol Metab, 2009.

99. Lelliott, C. and A.J. Vidal-Puig, *Lipotoxicity, an imbalance between lipogenesis de novo and fatty acid oxidation.* Int J Obes Relat Metab Disord, 2004. **28 Suppl 4**: p. S22-8.

100. Ryder, J.W., R. Bassel-Duby, E.N. Olson, et al., *Skeletal muscle reprogramming by activation of calcineurin improves insulin action on metabolic pathways.* J Biol Chem, 2003. **278**(45): p. 44298-304.

101. Sugii, S., P. Olson, D.D. Sears, et al., *PPARgamma activation in adipocytes is sufficient for systemic insulin sensitization.* Proc Natl Acad Sci U S A, 2009. **106**(52): p. 22504-9.